Reconfigurable Satellite Constellations for Mobile Target Tracking

by

Sarah J. Morgan

B.S., University of Virginia (2019)

Submitted to the Department of Aeronautics and Astronautics
in partial fulfillment of the requirements for the degree of

Master of Science in Aeronautics and Astronautics

at the

MASSACHUSETTS INSTITUTE OF TECHNOLOGY

June 2021

Author .....
Department of Aeronautics and Astronautics
May 18, 2021

Certified by .....
Olivier de Weck
Professor of Aeronautics and Astronautics and Engineering Systems
Thesis Supervisor

Certified by .....
Ciara McGrath
Research Associate, Department of Electronic and Electrical Engineering, University of Strathclyde
Thesis Reader

Accepted by .....
Zoltan Spakovszky
Professor, Aeronautics and Astronautics
Chair, Graduate Program Committee

Reconfigurable Satellite Constellations for Mobile Target Tracking

by

Sarah J. Morgan

Submitted to the Department of Aeronautics and Astronautics
on May 18, 2021, in partial fulfillment of the
requirements for the degree of
Master of Science in Aeronautics and Astronautics

Abstract

Current storm monitoring satellites offer unsatisfactory coverage of ongoing storms, either obtaining low spatial resolution, persistent coverage or high spatial resolution coverage with low temporal sampling. A reconfigurable constellation of satellites (ReCon) offers a way to augment these data sources with higher resolution coverage and improved temporal sampling. A ReCon can respond dynamically to different objectives throughout its mission lifetime, offering a more responsive, adaptable alternative to traditional Earth-observing satellite constellations. In the ReCon concept of operations, the constellation is nominally positioned to obtain global coverage. If an event of interest occurs at a particular latitude and longitude location, satellites can be maneuvered to obtain more frequent accesses of this target than otherwise achieved in the nominal configuration. While this architecture has been primarily explored with static ground targets in mind, for more dynamic events of interest, such as hurricanes, an additional layer of responsiveness can be added. A method of mobile target tracking through planning a series of low-thrust maneuvers holds promise. This method has been shown to improve the coverage characteristics of a single satellite in a hurricane case study when compared to a non-maneuvering satellite. This thesis explores and expands upon this concept, reviewing the existing work and applying an alternative approach. Throughout this thesis, procedures for adaptive reconfigurable maneuver planning are laid out and used for two hurricane case studies. This more flexible approach finds solutions for a single satellite case study observing Typhoon Megi using around 2 m/s delta-V, in comparison to similarly performing solutions previously found of around 13.5 m/s delta-V. The inclusion of an optimizer in maneuver planning enhances the prior work, exploring a continuous design space of possible maneuver options. This reveals alternative solutions and a more complete view of the entire design space. This optimization approach also allows a future user to explore the objectives of increased storm access time, closer flyovers, and total delta-V cost of maneuvers. For example, in a single satellite maneuvering case, total target access time can be doubled in comparison to a non-maneuvering case with the use of only around 2.5 m/s delta-V. Overall, this approach has resulted

in the exploration of key tradeoffs between these objectives. For example, increased access time or closer passes each come at the cost of increased delta-V requirements; solutions that provide the same total access time require greater delta-V to achieve closer passes and vice versa. When considering the inclusion of multiple maneuvering satellites, diminishing returns of maneuverability are observed, with greater natural accesses occurring with a greater number of satellites in the constellation. Additionally, the concept of executing this method in real time with uncertain targets based upon hurricane forecasts is explored. This reveals the need to incorporate robustness into this optimization. Finally, the prospect of executing this theoretical concept with a ReCon demonstrator is evaluated, including taking into account potential errors in maneuver planning.

Thesis Supervisor: Olivier de Weck
Title: Professor of Aeronautics and Astronautics and Engineering Systems

Thesis Reader: Ciara McGrath
Title: Research Associate, Department of Electronic and Electrical Engineering
University of Strathclyde

Acknowledgments

First, I would like to say thank you to the support of my advisor, Dr. Oli de Weck, and co-advisor, Dr. Ciara McGrath. I would not have been able to complete this research without their guidance. Oli, thank you so much for offering me a place in the lab in 2019, a research assistantship that allowed me to attend MIT, your endless curiosity, and supporting my pursuit of this research topic early on. Ciara, thank you for your inspirational drive and support. Thank you for meeting with me so frequently and supporting me as I worked to understand and build upon your impressive work; your kindness and support has been vital to my progress in this research. Thank you both.

I also want to express my gratitude for the financial support that enabled this work throughout throughout my two years of research assistantship. In my first year, this was split between the MIT-KACST (Sponsor Code 001104) CCES program and the ReCon project. While I grew to focus on ReCon, this program allowed me to develop technical skills in machine learning I would have never otherwise achieved and I appreciate their support. In my second year, I was supported by the Aerospace Corporation (Contract Number 4600006932). Through the ReCon and ROAMS (ReCon demonstrator) projects, I was able to continue my research and mentor students in the 16.851 and 16.89 courses as they also worked on the ROAMS project. I cannot say thank you enough to Aerospace for the support. The ReCon team was great to be a part of, and I really appreciate those I have met through the project. This was a great experience and I am so thankful to the entire team.

Thank you to my friends I've made at MIT - all the members of the ESL and AeroAstro as a whole have been so friendly and kind. Thank you to a lovely group of pals, without which I would have never visited Canada! To all those I've ever worked with on homework, projects, research, and more- thank you for helping me along the way. I want to also express my thanks to my more distant friends for their support over text, video chat, and calls over my time here.

Finally, thank you so much to my family who supported me throughout my time

at MIT. I want to express my gratitude especially to my parents. Mom and Dad, thank you for your love and support throughout my journey at MIT - the supportive phone calls, encouraging texts, and so much more. You've believed in me even when I haven't. I'm so thankful to you.

Contents

List of Figures

List of Tables

Nomenclature

Abbreviations

LEO Low Earth Orbit

GEO Geosynchronous Equatorial Orbit

TC Tropical Cyclone

SSP Subsatellite Point

FOV Field of View

CONOPS Concept of Operations

SAR Synthetic Aperature Radar

GOM Global Observation Mode

SSO Sunsychronous Orbit

ROM Regional Observation Mode

RGT Repeat Ground Track

MOO Multi-Objective Optimization

RCO Repeat Coverage Orbit

STK Systems Tool Kit (Software from Analytical Graphics, Inc)

BRKGA Biased Random Key Genetic Algorithm

MORDM Many-Objective Robust Decision Making

ADACS Attitude Determination and Control System

Symbols

a Semi-Major Axis

e Eccentricity

i Inclination

Ω (or $RAAN$) Right Ascension of Ascending Node

ω Argument of Perigee

θ True Anomaly

M Mean Anomaly

u Argument of Latitude

J_2 Second Zonal Harmonic Coefficient of the Earth

$\mu_\oplus$ Gravitational Parameter of the Earth

R Radius of the Earth

ΔV (or delta-V) Change in Velocity

I_{sp} Specific Impulse

g_0 Gravitational Constant at the Earth's Surface

Chapter 1

Introduction

1.1 Motivation

Hurricanes, or tropical cyclones, are the deadliest natural disasters to affect the United States and have cost nearly 1 trillion dollars and thousands of peoples lives from 1980 to 2020 [74]. Due to an apparent increase in the intensity of these tropical storms, with more tropical cyclones reaching category 4 or 5 in recent decades (and generally increasing storm intensity occurring specifically in the North Atlantic and Southern Pacific and Indian oceans), effectively monitoring and forecasting these natural forces is all the more important [33]. Additionally, storm surges resulting from storms are becoming more impactful with rising sea levels due to global warming [33]. Individual storms in the past two decades, such as Hurricane Katrina (2005), Harvey (2017) (Figure 1-1), and Maria (2017) cost around 100 billion USD each and destroyed thousands of lives [74].

Since the 1970s, satellite remote sensing methods have been used to inform hurricane forecasting with the use of a variety of instruments [54]. Storm track forecasts have improved significantly since the 90s, due to improvements in modelling and compilation of various data sources [68]. However, there has not been a similarly significant improvement in storm intensity forecasting; this can be attributed to poor storm data sampling and the inability of current instruments to penetrate the precipitation of the eye wall and inner bands of the storm to measure wind speeds and gather

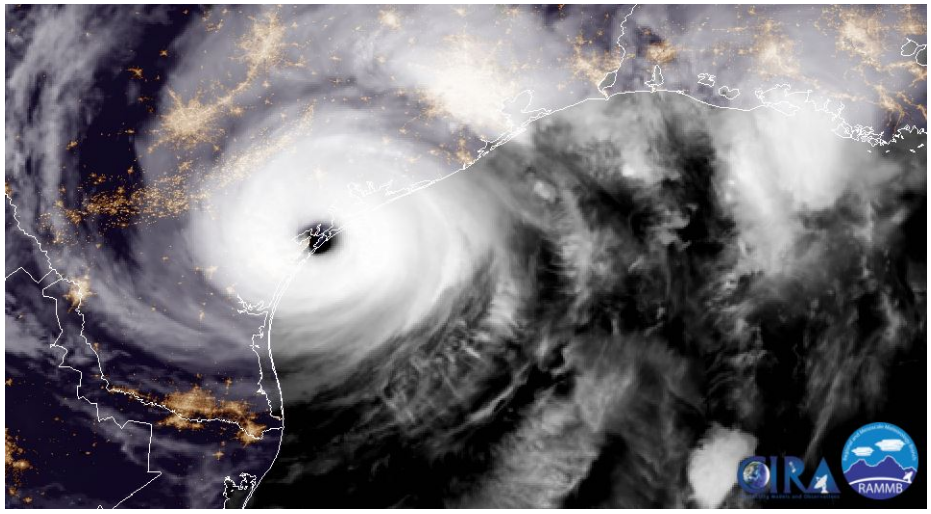

Figure 1-1: An image from GOES-16 of Hurricane Harvey making landfall in Texas (8/25/2017)[2].
The Category 4 storm effects caused the destruction of 200,000 homes and businesses and displaced over 30,000 people [74]

other data around the inner core [68]. Such measurements are integral to predicting storm intensity.

Hurricane forecasting currently draws from two main satellite sources. These are satellites in GEO (geosynchronous equatorial orbit), which view swaths of the Earth continuously but with low-medium spatial resolution, and mostly polar-orbiting LEO (low Earth orbit) satellites, which provide higher spatial resolution but with varying temporal resolution [1]. The GEO satellites offer overall awareness of tropical storm activity, while the LEO satellites provide supplemental, localized information when a pass of a storm is achieved.

A conceptualized architecture of a reconfigurable constellation, also termed *ReCon*, presents an interesting opportunity to augment these data sources to attempt to fill this gap in available data [59, 39, 60, 58, 50, 76, 38]. The essence of the ReCon concept is maneuvering satellites to alter their orbits in response to changing mission interests, having greater flexibility than typical Earth-observing constellations. Typically targets of interest explored in the literature for ReCon have included static latitude and longitude points [39, 76, 59]. However, there is an opportunity to add to the flexible architecture of the ReCon concept by further maneuvering satellites to

dynamically respond to mobile targets, which can likewise address the existing gap in the remote sensing of tropical storms. A ReCon in LEO focused on gathering storm data would be able to improve temporal resolution while providing the superior spatial resolution data achieved in LEO. By maneuvering, the satellite may achieve more consistent and accurate passes than may be otherwise achieved by existing 'static' satellites and obtain vital storm eye accesses [50]. This method could help improve tropical cyclone (TC) intensity forecasting by allowing more high-resolution accesses of the storm, especially in the early stages of tropical storm formation [68]. This technique can also allow for targeting specific regions of the TC for data collection, like the eye, which, as mentioned prior, is frequently valuable for hurricane intensity forecasting.

In general, applying the ReCon architecture to this problem of mobile target tracking presents interesting areas for exploration, with challenges including examining the general logistics of maneuver planning (type, timing, etc.), planning from uncertain forecasted track data, selecting which satellites of the constellation should maneuver, and prioritizing quality or quantity of data accessed. An investigation of these topics and others will enhance the concept of mobile target tracking with ReCon and provide a valuable basis for future missions to utilize these techniques to obtain much-needed TC data and allow for further research into other applications.

1.2 Literature Review

To better characterize the challenges of implementing mobile target tracking with ReCon and specify the kinds of research questions to be explored, a literature review has been conducted. Topics will include a review of orbital motion and constellation design, a survey of current storm monitoring satellites and constellations, a review of existing work done (especially at MIT) on the ReCon concept along with a brief overview of multi-objective optimization, and an investigation of a potential mobile target tracking technique which utilizes the ReCon architecture.

1.2.1 Satellite Orbits and Constellations: Background

Keplerian Orbits

First of all, some basic properties of orbits and their relationship to the Earth will be defined; characterizing satellite orbits, viewing geometry, and maneuvers is vital to the ReCon concept. Keplerian orbital elements will be primarily used throughout this thesis. These can be defined as follows: the semi-major axis (a) and eccentricity (e), which define the shape of the orbit; the inclination (i) and right ascension of the ascending node (RAAN or Ω), which define the orientation of the orbital plane; the argument of perigee (ω), which defines the orientation of the orbit in its plane; and finally the true anomaly (θ), which describes the location of the object in its orbit. The analogous mean anomaly (M) may be used in place of true anomaly for the convenience of calculations. The mean anomaly is defined by the position of a fictitious body moving on an ellipse with constant velocity $n = 2\pi/T$ where T is the period of the true orbit [16]. In the case of a circular orbit, M and θ will be equivalent. Likewise, an alternative orbital element to describe the location of the object in orbit is the argument of latitude (u), defined as the true anomaly (θ) plus the argument of perigee (ω) [64]. These quantities together can be used to describe the location of a satellite and its orbit. These are shown in Figure 1-2 and Table 1.1. Keplerian orbits are used as a basis for defining motion based on these parameters; Keplerian propagation simply assumes gravity is the only force on the object of interest, modelled with a spherically symmetric central body, significantly more massive than the orbiting object, with no third body effects [86].

Perturbations

However, in reality, when dealing with orbits around the Earth, the effects of orbital perturbations must be taken into account in addition to the force of gravity. There are many sources of orbital perturbations, both cyclic effects (perturbation effects which have short term periodic effects that do not impact the average orbital motion) and secular effects (perturbation effects which build up over time) [86]. In the case of

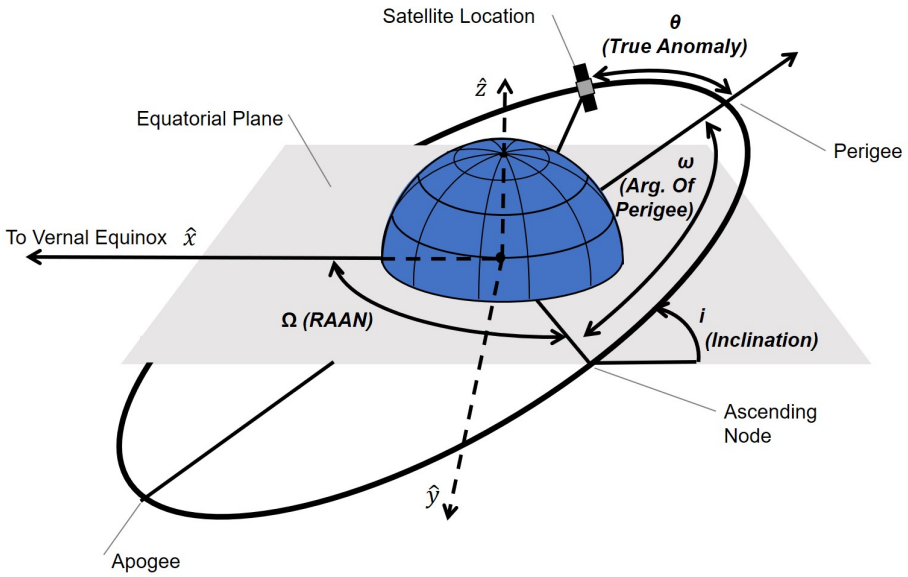

Figure 1-2: Keplerian orbital elements depicted, with GCI (Geocentric Inertial Reference Frame) shown by unit vectors. $\hat{x}$, $\hat{y}$, and $\hat{z}$

Table 1.1: Keplerian Orbital Elements

Parameter	Symbol	Definition
Semi-Major Axis	a	half the long axis of an ellipse (equivalent to the radius of a circular orbit)
Eccentricity	e	defines the shape of an orbit; describes the elongation of an enclosed orbit ($e = 0$ for circular orbits, $0 < e < 1$ for elliptical orbits)
Inclination	i	the angle of the orbital plane and the equatorial plane of the Earth
RAAN	Ω	the angle in the equatorial plane of the ascending node (measured from the vernal equinox)
Argument of Perigee	ω	the angle in the orbital plane that measures from the ascending node to the perigee point of the orbit
True Anomaly	θ	describes the angular position of the satellite in its orbit from the perigee point

LEO satellites, typically the most significant perturbation is the effect of the Earth's oblateness, also called the J_2 effect caused by the non-spherical mass distribution of the Earth [86]. Over long time scales, therefore, secular J_2 effects should be taken into account for more accurate orbital motion modelling, with the remaining zonal harmonic terms J_n considered to be negligible as these are 10^3 times smaller than J_2 or more [16]. The J_2 effect causes orbital precession, creating a rate of change in RAAN and argument of perigee of the satellite according to the following equations [16] [46]:

$$\dot{\Omega} = \frac{3}{2}\frac{\sqrt{\mu_\oplus}J_2R^2}{(1-e^2)^2a^{\frac{7}{2}}}\cos i \tag{1.1}$$

$$\dot{\omega} = \frac{3}{2}\frac{\sqrt{\mu_\oplus}J_2R^2}{(1-e^2)^2a^{\frac{7}{2}}}\left(\frac{5}{2}\sin^2 i - 2\right) \tag{1.2}$$

$$\dot{M} = \frac{-3}{4}\frac{\sqrt{\mu_\oplus}J_2R^2}{(1-e^2)^2a^{7/2}}\left(3\sin^2 i - 2\right)\sqrt{1-e^2} \tag{1.3}$$

where $\mu_\oplus$ is the gravitational parameter of the Earth and R is the radius of the Earth.

Other perturbations that impact LEO satellites include atmospheric drag, third-body effects, and solar radiation pressure [86]. Atmospheric drag is typically the most significant of these, however, the relative significance of these perturbations depend upon the specific orbit and satellite. Relativistic effects and incidental forces (i.e. a leak on the spacecraft) are considered mostly negligible for LEO satellites [86]. Typically, these smaller-order perturbations are all accounted for inherently in satellite design by assuming the need for some station-keeping measures.

Earth Observation

When focused on ground targets it is convenient to also track the sub-satellite point (SSP) in addition to the Keplerian orbital elements. The SSP is the latitude and longitude location on the Earth which corresponds to the intersection of the satellite's nadir vector with the surface of the Earth. If a satellite is always pointing nadir, the SSP will be identical to its target point (where the satellite is actually 'looking') on the surface of the Earth. A field of view (FOV) can be defined for particular sensors

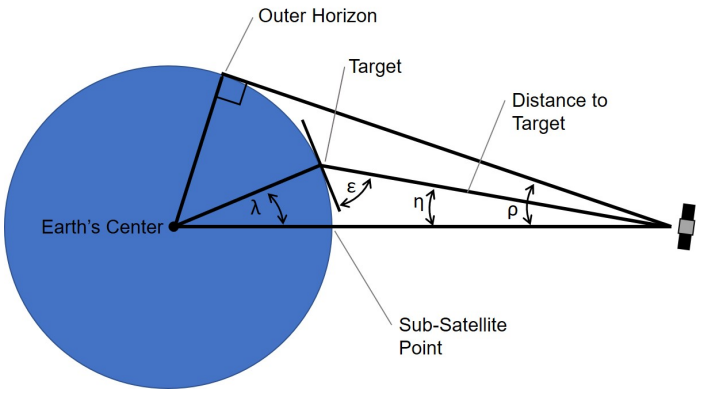

Figure 1-3: Viewing geometry.
Here, the target is different from the satellite's SSP. This creates angle η, the nadir angle between the nadir direction and target. λ is the Earth central angle, ρ is the Earth's angular radius, and ϵ is the satellite elevation angle as viewed from the target point on Earth's surface and looking up.

to describe the area around the target point that is captured by the satellite. For a satellite pointing off-nadir, more complex viewing geometry must be taken into account, as shown in Figure 1-3 [86].

Maneuvers

Once satellites have been deployed in their initial orbits, propulsive capability is required to maintain that orbit (station-keeping) and execute any changes to their initial orbital elements, aside from those induced by perturbations (maneuvers). Propulsion systems may also be used to execute de-orbit or reentry burns at the conclusion of the mission lifetime. Depending on the mission concept of operations (CONOPS), not every satellite requires propulsive capability, but propulsion is certainly needed for reconfigurability and maintenance of orbits in the relatively high-drag environment of LEO [86].

To perform a maneuver, a change in velocity, or delta-V is required. The delta-V requirements will drive propulsion system requirements, and propulsion system mass [86]. The delta-V capability of a given system can be defined by the rocket equation:

$$\Delta V = I_{sp} g_0 \ln \frac{M_0}{M_f} \tag{1.4}$$

where I_{sp} is the specific impulse of the propellant, g_0 is the gravitational constant at the Earth's surface, M_0 is the initial mass, and M_f is the final mass after executing one or several burns [86]. The total propellant mass is therefore $M_0 - M_f$ is the propellant mass [86].

Propulsion systems in satellites are generally of two types: high-thrust or low-thrust propulsion systems. High-thrust systems enable nearly impulsive maneuvers, generating high-thrust over a small amount of time, enabled by chemical propulsion systems [86]. Low-thrust systems build up velocity over time, generating thrust over time through the use of electric propulsion [86]. The variety of maneuvers that can be performed by each of these systems therefore differs greatly in time span and performance. For example, typical Hohmann transfers, which efficiently raise or lower a satellite's orbital altitude, require impulsive burns at two points in the transfer orbit. Low-thrust propulsion systems can conduct maneuvers to reach the same end state (in fact with less delta-V for particular changes in orbital altitude) but at much longer timescales, by continually increasing or decreasing a satellite's altitude in a spiraling motion.

1.2.2 Current Storm Monitoring Satellites: The Challenge

In 1900, a hurricane hit the Gulf Coast unexpectedly, with storm surges killing at least 8000 people in the United States [80]. This immense loss of life, greater than all the combined hurricane-caused deaths in the United States since 1980 [74], was caused by incorrect predictions from the Weather Bureau, incorrectly assuming the system was curving toward the south-east [80]. This event remains the deadliest natural disaster in US history [43]. With the advent of remote sensing with satellites in the 1970s, TCs have been consistently monitored since, making it possible to avoid any disastrous surprises such as the Galveston Hurricane in 1900. Advances in hurricane forecasting in modern times has prevented about 66-90% of hurricane-related deaths in the US that would have otherwise resulted if techniques from the 1950s were used [87]. There is certainly still room for improvement. Hurricane Katrina cost a relatively small amount of lives, attributed to consistent forecasts and persistent

warnings distributed to the affected population, but was the most costly TC since 1980 [65]. This is primarily due to extensive property and infrastructure damage caused by the combination of wind-induced damage and flooding. On the other hand, the high cost of Hurricane Harvey, the second most costly TC since 1980, can be partially attributed to the failure of various models (sourced from NOAA and European forecasts) to predict its rapid intensification prior to landfall [65].

Modern TC track forecasts ([65], 2009) have reduced in error by about 50 percent in comparison to forecasts in 1990 (for 24-72 hour predictions). Improvements in modelling and increased resolution of data sources were key to improved track prediction throughout the 1990s [65]. Data sources have included geostationary satellite data with good temporal resolution and LEO data from usually polar orbiting satellites [20]. Visible, IR (Infared), Next-Generation radar and microwave remote sensing methods have all been used to inform models, with polar LEO data creating significant improvement to prediction accuracy from 1997 to 2000 [65]. The consensus of these data sources with different models has generally improved TC track forecasts [65].

Despite all of these data sources and improvements in data assimilation, forecasts of TC intensity have exhibited almost no improvement since 1990 [65]. Predicting TC intensity remains one of the greatest challenges in TC forecasting, especially anticipating rapid intensification. In 1990, there was no objective guidance for predicting storm intensity and, even in modern times, objective guidance has not yet caught up with human forecasters subjective estimates for TC intensity [20]. Techniques such as the Dvorak method developed in 1980s for predicting hurricane intensity are still used today [20] and while model accuracy has been improving throughout the 2000s, dynamical models are still no better than statistical models (i.e. SHIPS, Statistical Hurricane Intensity Prediction System) (2009) [65]. One of the key reasons for this failure to improve intensity forecasts is due to the particular data required. High-resolution inner core observations, such as the surface windspeed and sea level pressure near the center of the TC, are required to more accurately predict intensification, however, these are difficult pieces of data to capture depending on the

instrument used as heavy precipitation can obscure measurements [65]. Data from aircraft can help, as these measurements are generally of sufficient resolution, however this can be difficult data to gather as only 30% of intensity estimates in the North Atlantic are guided by aircraft reconnaissance [69].

More data from microwave instruments, new radiance instruments such as those on the GOES-R satellite, and use of SAR (synthetic aperture radar) can help augment existing data sources [65],[84]. Currently, microwave instruments are mostly on LEO polar-orbiting satellites which do not offer persistent coverage of the tropics, and geostationary satellites do not always offer high resolution coverage [68]. Therefore, there is an opportunity for remote sensing satellites to obtain data coverage of the inner core of TCs and aid in the improvement of TC intensity forecasting. Likewise there is an opportunity to improve data assimilation. One method includes utilizing deep learning to assist with hurricane track prediction through the use of convolutional neural networks (CNNs) and generative adversarial networks (GANs) based on historical data [63], [70]. These data-hungry processes would likewise be improved with increased data collection, and offer an interesting area for further data processing downstream from the data pipeline from Earth-observing satellites.

A constellation called CYGNSS (Cyclone Global Navigation Satellite System) of 8 microsatellites seeks to fill this gap through the use of GPS reflectrometry to obtain inner core wind speeds with higher revisit times than achievable with other LEO satellites such as QuikScat or ASCAT polar orbiting satellites equipped with scatterometers [68]. The overarching concept is to achieve more consistent TC core coverage through the use of this low-cost constellation than otherwise achievable with other LEO weather-monitoring satellites [68]. Effectively using this data can achieve accurate surface wind speed characteristics [54]. Indeed, when implemented, a review of the experimental constellation shows that the baseline requirement of an average 12 hr revisit time is successfully achieved, while covering the majority of relevant latitude bands (-35 deg to 35 deg) over the course of 24 hours [69]. The ground tracks for the CYGNSS constellation are shown in Figure 1-4. Beyond this, other LEO small-satellite constellations may prove an attractive option to monitor TCs. Of course,

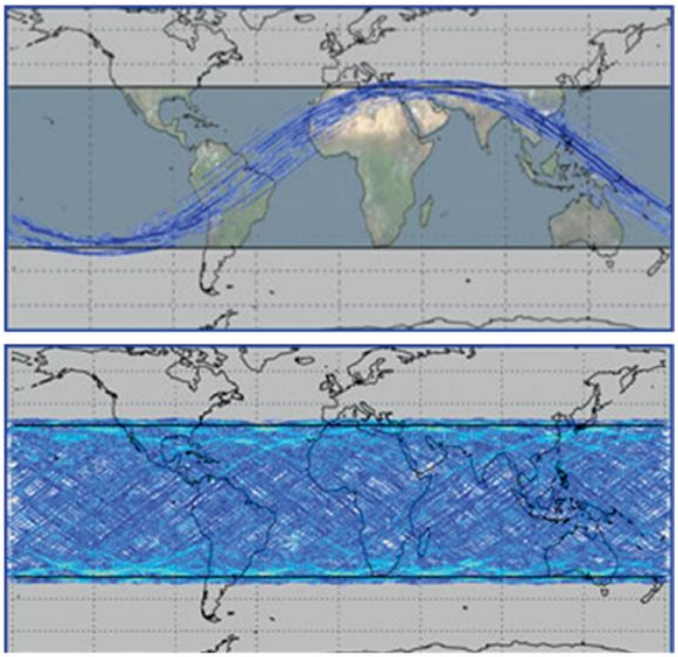

Figure 1-4: CYGNSS ground tracks [69].
The upper image shows a single orbit of the CYGNSS constellation (generated over around 95 mins) and the lower image shows ground tracks over an entire 24-hour period.

with a sufficient number of satellites, one can obtain near constant coverage of desired latitude bands, but this can be costly.

1.2.3 Reconfigurable Constellations: A Potential Solution

Typical Earth-observing satellite missions, such as those described in Section 1.2.2 for TC monitoring, utilize static orbits, which usually do not change throughout the mission lifetime, apart from perturbations and traditional station-keeping maneuvers to counteract these perturbations. In essence, these satellites are deployed at the start of their mission and do not deviate significantly from that initial orbit. Reconfigurablility can be added to these satellites, allowing the mission to evolve with time. The satellites' orbits can be modified with time as mission focus shifts, so coverage can be changed on-demand. With this approach, mission cost savings can be achieved in comparison to an equivalently performing static satellite architecture [39]. Work on such a concept of a reconfigurable constellation of satellites, ReCon,

has been discussed in the literature [24, 17, 29, 44, 27] including a large effort at MIT [59, 39, 76]. Reconfigurable constellations have been implemented on a small scale, including the ERS 1 and 2 satellites maneuvered to new orbits of different repeat cycles (analogous to the repeat ground track options discussed below) and the Keyhole constellation also utilized maneuvers [58, 9]. The premise of previous work conducted at MIT has largely focused on the use of larger Earth Observation constellations to obtain global coverage and, if an event of interest occurs, to reconfigure to observe particular latitude and longitude points. For example, in work by Paek, and following work by Legge and Straub [59, 39, 76], the nominal, global-coverage mode of the constellation, known as Global Observational Mode (GOM), has the satellites positioned in a typical global-coverage pattern. This allows for the satellites to obtain even coverage of the Earth in the default state of the constellation. The latitudes of the Earth covered will depend upon the inclination of the orbits, and the constellation will achieve complete coverage over this latitude band every 24 hrs [76]. The time of each observation may vary each day, unless the satellite is in a sun synchronous orbits (SSO). Note that this prior work has focused on all orbits used by the constellation to be circular orbits. This simplifies mission and maneuver planning with consistent orbital altitude for observations for each stage of the mission, as well as simplifying the calculations to be performed.

If an event of interest occurs over which a user would like more persistent coverage, a subset of the satellites can be maneuvered to new orbits, independent of the larger constellation. Reconfiguration into this Regional Observational Mode (ROM) is achieved by allowing the satellites to go through a series of maneuvers [39]. The first maneuver works to raise or lower a satellite's apogee into a drift orbit. This drift orbit allows the satellite to take advantage of the relative difference in J_2 perturbation due to the altitude change and move out of its location in the constellation, drifting its RAAN and mean anomaly [39]. The satellite is then again raised or lowered to a different altitude into what is known as a repeating ground track orbit (RGT) [39]. RGT orbits, as the name indicates, repeat their ground track after a particular number of orbits. The particular frequency of repetition may be chosen, but for typical

low Earth orbit (LEO) altitudes, one can expect repeated ground tracks, in terms of SSP passage, after less than a day or so. A typical RGT frequency is 15:1, meaning that the satellite completes fifteen orbits during one full rotation of Earth around its axis. After these 15 orbits the satellite will pass exactly over the same latitude and longitude target point SSP as it did during the first orbit. After the event has concluded or sufficient observations have occurred, the satellite can then maneuver back to its original place in the constellation and resume GOM [39]. Alternatively the satellite could not return to GOM, but directly transition to a new repeating ground track target.

Figure 1-5 displays the difference between sample GOM and ROM ground tracks for a constellation. Understanding the basic principles of this concept of operations, including the constellation design and particular steps of the satellite maneuvers, is vital for extending this mission concept. In the following sections, literature will be reviewed on ReCon to develop this foundation.

Constellation Design and Optimization Summary

Key to the foundation of much of the ReCon work done at MIT, which this thesis builds upon, is the concept of concurrent design and optimization. For example, in Paek's work the satellites and their mission design are optimized simultaneously through methods of multidisciplinary design optimization [60]. This method also ensures that the GOM configuration of the constellation is designed with the potential maneuvers required to move to ROM in mind, while remaining agnostic to the targets that must be viewed.

Constellation design, especially for global coverage is a topic extensively covered in research; there are many potential solutions to the problem of global constellation coverage. Now, critically, there is no set process for constellation design, and many performance characteristics do not vary smoothly with the constellation characteristics as would be intuitive [86]. The GOM configuration of a ReCon constellation may be any of these potential solutions from a typical symmetric, evenly distributed pattern to something a bit more complex. In previous works on ReCon, typical tradi-

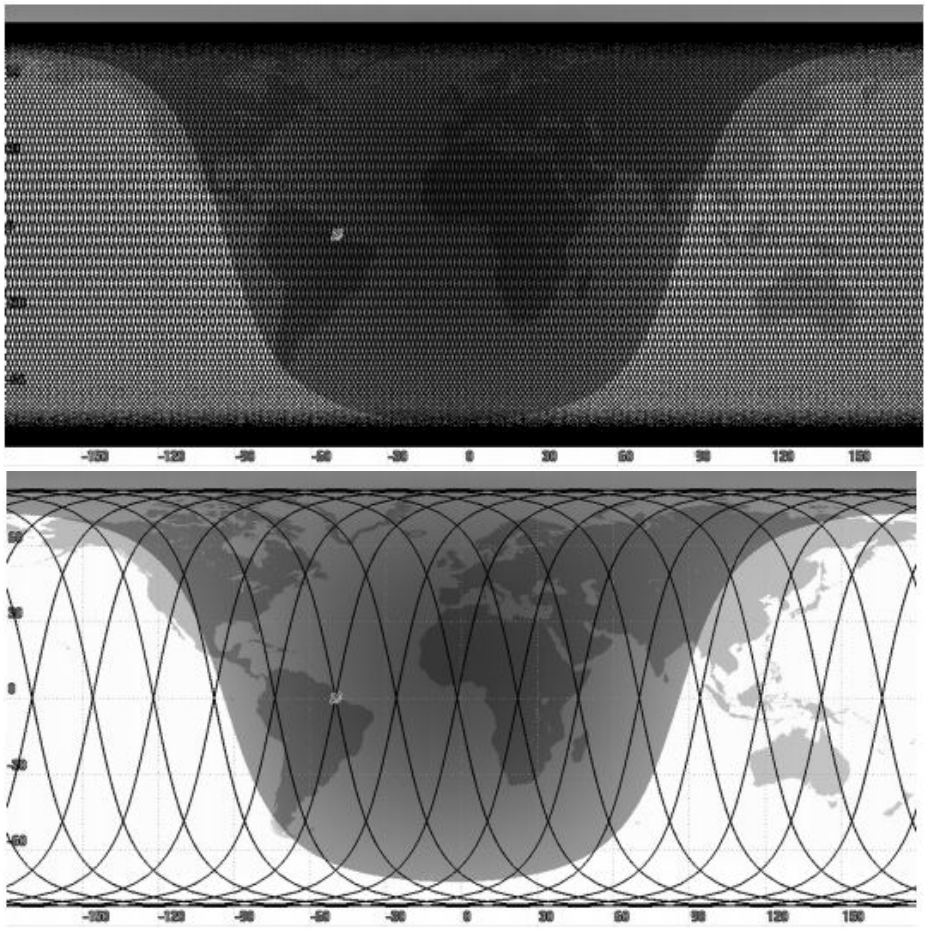

Figure 1-5: Concept of operations for ReCon [60].
The upper ground track plot displays a nominal global observation mode (GOM) for a ReCon constellation, displaying even coverage of the Earth. The lower ground track plot displays a regional observation mode (ROM) for a constellation where all satellites have reconfigured into RGTs. The target is marked by a grey dot- it is clear that this is targeted in ROM with ascending and descending RGT ground tracks covering the target.

tional symmetric static constellation designs such as Walker, streets-of-coverage, and flower constellation patterns have been considered as prevalent methods of obtaining continuous global coverage [39]. These patterns may have satellites on several orbital planes, distributed by RAAN or inclination, and separated within their planes by true anomaly. For example, commonly-used Walker patterns contain satellites all orbiting at a particular inclination, with the planes of the constellation separated by a RAAN spacing, and each plane containing satellites distributed evenly by a true anomaly spacing [86]. Legge explored the GOM constellation design space of a variety of such patterns including layered patterns (which involves two simultaneous Walker patterns at different inclinations), asymmetric patterns (with common inclination and semi-major axis only), and asymmetric Walker patterns [39]. All eligible designs were analyzed for their coverage performance characteristics for both the static constellation and reconfigurable constellation case; ultimately in the cases evaluated for maximum performance and minimum cost, asymmetric patterns worked best for the reconfigurable constellation design [39].

Other works focus on the use of Walker Delta patterns [76]. While a variety of global coverage constellation architectures may be suitable depending on the application, the key point of this analysis for the ReCon concept is the consideration of the entire mission performance in the original constellation design.

Given that there are many different options for constellation design, and there is not a simplistic process of connecting constellation parameters to desired performance characteristics, it is not uncommon to utilize optimization methods to find potential solutions [25, 13, 3]. This method allows for an automated search of the solution space, varying design variables which form the design space, and finding solutions which minimize or maximize particular characteristics. The performance of each design is evaluated with an objective function, which can represent multiple characteristics to be minimized or maximized [18]. Constraints and bounds can be set for the design variables to further characterize the problem and restrict the design space. Multi-objective optimization (MOO) methods allow for several objectives to be minimized or maximized at once, allowing for consideration of several performance characteristics

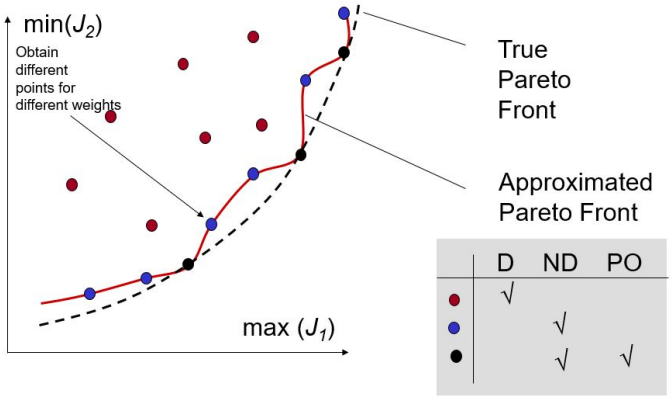

Figure 1-6: Approximated and true Pareto fronts for sample MOO problem for objectives J_1 and J_2 [18].
Non-dominated (ND) solutions are shown to form part of the Pareto optimal (PO) solutions, but not all non-dominated solutions create the true Pareto front. Dominated (D) solutions exist behind the Pareto front.

at once [18]. For example, cost may be minimized, mass may be minimized, and coverage of the Earth may be maximized all at once.

The output from an optimization problem may include solutions that perform better in one objective than another. A solution set, termed the non-dominated set, would include all solutions which cannot perform better in one objective without performing worse in at least one other [18]. A solution is dominated if a solution exists which performs strictly better than it in an objective than another solution without performing worse in any of the others. The best possible solutions in the space create the Pareto front, and the set of non-dominated solutions can approximate this Pareto front (Figure 1-6).

Typically, these problems can also be cross-disciplinary, spanning across fields like satellite engineering, astrodynamics, cost-modelling, etc. [5]. This has been a powerful method of designing ReCon satellites and the constellation as a whole [39, 59] There are several methods of performing this optimization, including heuristic methods such as genetic algorithms and simulated annealing, which are widely used to solve NP-hard combinatorial problems [58]. These methods model natural processes of passing along genes to offspring or the gradual cooling of materials to a minimum energy state in metallurgy, respectively. These use characteristics of the processes

such as mutation rate or cooling rate to search the design space [18]. This procedure of MOO, especially the use of heuristic methods, has been used in much of the ReCon prior work, especially at MIT, and is a valuable method of exploring a space with solutions that are not easily found.

Orbit Selection: ROM

In the concept of operations for ReCon, once an event of interest occurs, a subset of satellites will reconfigure from GOM to ROM. The ROM orbits are selected with the goal of obtaining better revisit characteristics over the target area of interest, including more frequent passes than otherwise obtained by the constellation when in GOM to achieve greater persistence. Previous works have focused on the use of repeating ground tracks (RGTs). These orbits, as their name indicates, having repeating ground tracks after a particular integer number of days. This is achieved by taking advantage of orbital precision and lining this rate up with the Earth's rotation; these provide consistent persistent target viewing and are an attractive option for static targets. These orbits are defined by a N_o/N_d ratio, where every N_o integer orbits the ground track will be repeated, with the N_o orbits being completed an integer number of sidereal days, N_d. For example, an RGT defined by $N_o/N_d = 15/1$ means 15 orbits are completed over the course of one sidereal day. To achieve this resonance, the rotation rate of the Earth must be matched with the orbital motion, including necessary perturbations. The period of the orbit is found by the following [55]:

$$T = \frac{2\pi N_d}{\omega_\oplus N_o}(1 + 2\xi\frac{n}{\omega_\oplus}\cos i)^{-1}\chi \tag{1.5}$$

Where:

$$\chi = 1 + \xi \left[4 + 2\sqrt{1-e^2} - \left(5 + 3\sqrt{1-e^2} \right) sin^2 i \right] \tag{1.6}$$

$$\xi = \frac{3R_{\oplus}^2 J_2}{4a^2(1-e^2)} \tag{1.7}$$

$$T = \frac{2\pi}{n} = 2\pi\sqrt{\frac{a^3}{\mu_{\oplus}}} \tag{1.8}$$

And $\omega_{\oplus}$ is the rotation rate of the Earth. This is a second order relation, through which eligible semi-major axes for a given eccentricity and inclination can be found which fit a particular N_o/N_d integer ratio. This order of precision is sufficient for propagating over a few weeks of simulation and includes the most significant J_2 perturbation. To find the exact RGT that should be used to pass over a particular latitude/longitude point on the Earth, a relationship between the shift in longitude of the ground track, Λ and the N_o/N_d ratio can be obtained [55]:

$$\Lambda = N_o\Omega + N_d M \tag{1.9}$$

So, to shift the longitude of the ground track to line up with a particular target, either M or Ω of the orbit need to be altered. If Ω is shifted in a particular manner, it would be possible to achieve both an ascending and descending pass of the target location [39]. Potential repeat ground tracks near LEO are shown in Figure 1-7.

Alternative opportunities for ROM orbits were considered over the course of this literature review, opening up the trade space of potential ROM orbits to those outside of RGTs, as some missions could benefit from alternative applications. For example, RGT orbits focus on particular latitude and longitude points, and if an event of interest is one that covers a larger area, an RGT orbit should prioritize more spatial coverage. One possible option is the use of Repeat Coverage Orbits (RCO), which are typically used in rapid launch architectures. These aim to target a small geographical region with the ground track of several satellites, offering coverage of multiple successive orbits of particular latitudes [85]. However, these could require an inclination

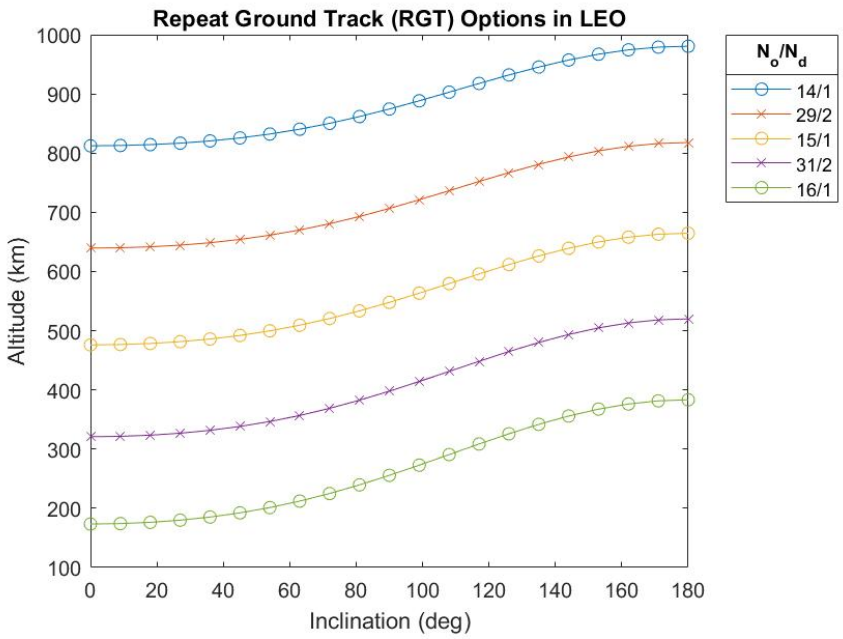

Figure 1-7: Inclination vs altitude of a subset of repeat ground track options in LEO.

change depending on the target area of interest which is typically cost prohibitive in the ReCon architecture [85]. Other options such as SSOs may be more attractive; while these require near polar orbits, some GOM architectures involve near polar inclinations for the constellation [59, 61]. These allow a consistent sun angle for data, which may not be required for all missions but could be useful for particular kinds of data gathering. Elliptical orbits were also considered; in fact there exist elliptical RGTs; however these likewise require a particular inclination (critical inclination) to ensure the perigee does not shift with time [39]. A changing perigee would change the distance to the target and change where the longer dwell time might be located on the surface of the Earth, eliminating consistency in the target passes. Again, this may be achievable for some ROM architectures but not all given the inclination restriction [39]. Another consideration is to have the satellite in a non-specialized orbit, where the ground track of the satellite would drift across the surface with time as is the case for typical satellites. If one can align the shift of this so-called drift orbit with the rate of a moving target, there is a potential for better accesses. This would require extensive knowledge of the moving target speed and direction of travel

Table 1.2: Example categorization of ReCon targets and associated ROM orbits

Target	Characterization	Orbit
Hurricane	Dynamic	Drift or adaptable
Wildfire	Dynamic area with static central point	RCO or RGT orbits covering an area
City	Static	RGT

to be able to pre-plan this orbit and is therefore not realistic for most applications, but serves as an area for future exploration. An alternative to this is an *adaptable* orbit that naturally has good revisit over the starting point (and otherwise no special characteristics) can be adjusted with time, as will be discussed through work by McGrath et al. [50]. These alternatives offer opportunities for possible niche studies, but may not be universally applicable for the entire ReCon space; for example, one might consider a series of RGT orbits to simulate something like an RCO to create an area of coverage for a large area target (Table 1.2).

Maneuver Procedure: GOM to ROM

Particular satellites from the constellation are selected to maneuver to ROM from GOM when an event of interest occurs. This assignment process takes into account the delta-V required for the maneuver, if the resulting configuration will meet the desired revisit characteristics, and if any maneuvers are simply infeasible or otherwise restricted. Then, the process of maneuvering from GOM to ROM can be achieved in a number of methods. This includes a typical Hohmann transfer into an intermediate orbit, called a drift orbit, and a second Hohmann transfer into the final ROM orbit, typically an RGT. So, a total of four burns are required, two for each Hohmann transfer, as shown in Figure 1-8. This drift orbit allows for control over the aforementioned longitude shift to place the ground track over the target. The four steps of this maneuver are described: an initial burn shifts a satellite out of its GOM orbital slot and into a transfer ellipse, the second burn moves the satellite from this transfer ellipse to the drift orbit where the satellite will stay until the designated orbital elements are achieved to properly place the sub-satellite point. The satellite

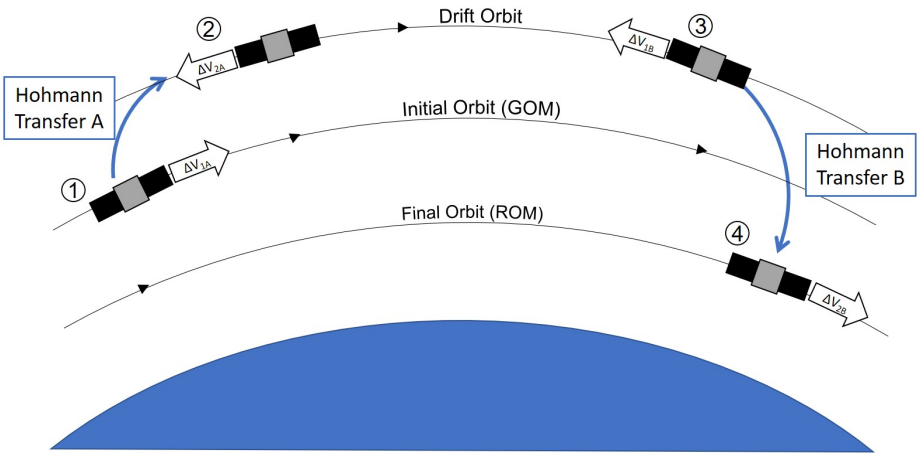

Figure 1-8: Example Process for Maneuver from GOM to ROM.

then performs a second Hohmann transfer, moving into and out of a transfer ellipse, to finally be placed in the RGT orbit. To extend this example, see Table 1.3, for a sample series of maneuvers to move from GOM to ROM, which displays a typical characteristic of these maneuvers; typically the satellite spends the longest time in the drift orbit. The Hohmann transfers themselves typically take less than an hour in LEO, and time spent in the drift orbit is usually on the order of days. Note that the use of low-thrust systems with spiral transfers has also been considered by [76], but may be less mass-efficient and require longer duration than high-thrust systems.

Applications of ReCon

Previously studied applications of ReCon have frequently included natural disasters; such an application benefits from the rapid, flexible response capability of the concept architecture. If a natural disaster occurs, a subset of the constellation may reconfigure to observe the area of interest, with the ability to respond to any target in the latitude band of the constellation. Previously this investigation of this application has been generalized; a historical data set of natural disaster locations was used to generate a probability density function (PDF) for future events across the globe [39] [22]. Sites were then chosen from this data set based upon the PDF and used as hypothetical targets for the constellation. Other case studies have also been conducted using the ReCon architecture, including the 2020 wildfires of Australia for example [76].

Table 1.3: Sample GOM to ROM transition

Burn	Maneuver Description	Delta-V Required (m/s)	Duration (hours)	Altitude (km)
1	Hohmann Transfer A ΔV_{1A} GOM to transfer orbit	13.9	0.78	500
2	Hohmann Transfer A ΔV_{2A} Transfer orbit to drift orbit	13.9		
	Drift Period	0	156	450
3	Hohmann Transfer B ΔV_{1B} Drift orbit to transfer orbit	13.1	0.78	
4	Hohmann Transfer B ΔV_{2B} Transfer orbit to ROM	13.1		497
		Total Delta-V: 53.9 m/s	Total Duration: 157.6 hours	

Other targets of interest include oil spills and hurricanes; all of these aforementioned events would benefit from responsive remote sensing satellite observations due to their dynamic nature. The ERS satellites, an existing example of what can be done with reconfigurability (analogous to a 2-satellite constellation moving from ROM to ROM), also serve as an example of remote sensing of the atmosphere [9, 59]. ReCon can also be used for things other than Earth observation, including serving as communication satellites. This can allow for adaptability that would help deal with unknown demand, something that can be crippling to communication constellation performance [19]. This concept can even be used around other planets, including Mars, to assist with other space missions [56].

1.2.4 Mobile Target Tracking: A Proposed Methodology

A method displayed by McGrath et al. [50] utilizes sequential low-thrust maneuvers to slightly shift satellites in their orbits to provide improved quality of flyovers of a hurricane when compared to a non-maneuvering satellite. The method specifically targets particular latitude/longitude way-points along the hurricane track, each of

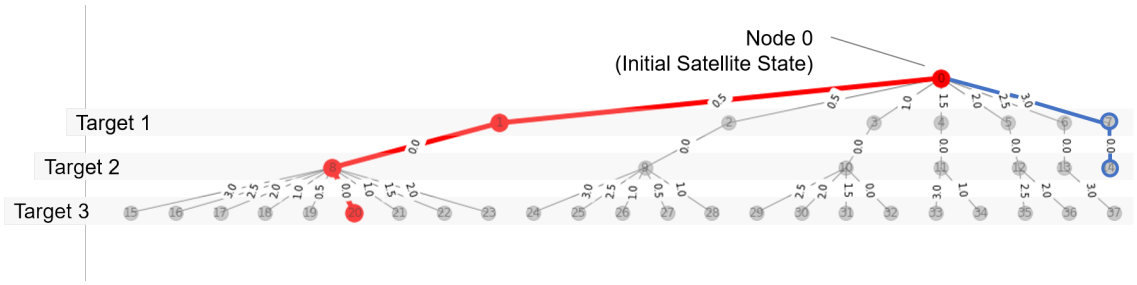

Figure 1-9: Example graph of solutions.

which have a particular associated time window. These way-points and their associated time window will henceforth be called targets.

This method involves selecting a number of targets along the hurricane track and initializing a satellite in an orbit that provides decent passes of the target location. Then, all possible maneuver options, bounded by particular maximum delta-V and duration, are computed for the satellite for each target in succession. These options are then modeled as a graph network whereby each node in the graph represents the satellite parameters at a target flyover and each edge represents the maneuver required to achieve that state. The graph branches out from the origin node and occasionally branches may end if the maneuver required to achieve the next target access is impossible given the delta-V or duration constraints applied. Once the entire graph has been produced, it can then be searched for the lowest delta-V solution using a shortest path solution, as found using something like Dijkstra's algorithm [21]. The space may also be further constrained by only looking for solutions that provide a certain preferred access of the targets- for example, only plotting results which achieve an 80km or closer access of the storm (where the SSP is 80km of closer to the eye latitude/longitude point) [50]. The preferred set of maneuvers can then be selected from the graph and evaluated against other solutions [50].

The network in Figure 1-9 is a sample output from this graph theoretical technique. Each node is numbered and each edge is labeled with the amount of delta-V used (m/s). Node 0 represents the satellite state at epoch, and from there the satellite maneuvers to view target 1 through a variety of delta-V options. Target 2 has no solution, and the satellite simply propagates through the viewing period. The lowest

Table 1.4: Sample GOM to ROM Transition

Burn	Maneuver Description	Delta-V Required (m/s)	Duration (hours)	Altitude (km)
1	Spiral Transfer GOM to transfer orbit	27.8	88.5	500
	Drift Period	0	7.5	450
2	Spiral Transfer Drift orbit to transfer orbit	26.2	83.2	497
		Total Delta-V: 53.9 m/s	Total Duration: 179.2 hours	

delta-V solution is highlighted in red. Early maneuvers have consequences for later target viewings, as can be seen with the solution highlighted in blue, where an early aggressive maneuver results in target 3 not being viewed by the satellite at all. This shows the importance of planning multiple maneuvers in advance to ensure flexibility for future targets.

Inherently, an application of graph theory such as this requires that the search space be discretized, meaning that, in the example in reference [50], the delta-V options for each maneuver are limited by 0.5 m/s intervals. For efficient calculation of a large number of options, a fully analytical method of calculating low-thrust maneuvers which either raise or lower orbital altitude is used [50] [46]. This general perturbation method is a solution to a restricted low-thrust Lambert rendezvous problem with circular in-plane maneuvers, thrusting along the velocity direction only. This allows one to find a target flyover in terms of the RAAN and argument of latitude change of the orbit. The solution is found in the form of a three phase maneuver, similar to the procedure described for drifting to the ROM target orbit described in Section 1.2.3, simply with spiral transfers rather than Hohmann transfers. The same quantitative example as in Table 1.3 is evaluated below in Table 1.4, evaluated with the same total delta-V and drift orbit altitude. Overall, this low thrust method, is generally slower than a high-thrust Hohmann transfer method for large maneuvers like the GOM to ROM transition, as discussed further by [76]. This sample calculation shows this slight difference with increased duration requirement.

The phases are as follows: first the satellite conducts either a lowering or raising

maneuver to change its orbit altitude, thrusting either with or against the velocity vector; then, the satellite drifts in this alternate orbit, termed its 'coast arc'; finally, the satellite returns to its final altitude with a second raising or lowering maneuver. The final altitude may be the same as the starting altitude or could be a different altitude [46].

Secular J_2 effects are included in this calculation, as described earlier, however the higher order effects and third body effects were ignored in the solution. Likewise radiation pressure perturbations were ignored, and drag compensation maneuvers were assumed to occur during the coast arc, but ignored during the maneuver periods to maintain the analytical solution [46]. However, these phases are generally short duration, and in the case of those considered by McGrath et al., these are less than 4 days and require largely negligible delta-V to compensate for drag [46]. Additionally, most operational satellites are already designed with station-keeping capability, so the delta-V cost of drag compensation is not included in the overall delta-V cost for these maneuvers. The results of this analytical solution are generally close to numerical solutions; when compared to a numerical solution (4th and 5th order Runge-Kutta) over the course of 16 days for the evaluated case study, the analytical solution shows a sub-satellite point off by at most 25 km when compared to the numerical solution. This is due to the short periodic J2 and higher-order perturbations not considered in the analytical formulation; longer simulations using this formulation will exhibit greater errors due to these effects [46].

By planning sequential maneuvers using this three-phase formulation found with the analytical solution, there is an opportunity to shift the SSP of a satellite on subsequent orbits to intercept the track of a mobile target. The results from the paper by McGrath et al. show promise in using these kinds of maneuvers, with the options explored through the graph theory method described above [50]. This paper evaluated the use of these sequential low thrust maneuvers to respond to a natural disaster, applying this to a case study of Typhoon Megi, a powerful storm in the Pacific in 2010. Five target flyovers were planned along the storm's track, spaced out at 2.5 day intervals. Note that in this evaluation, the true path of the storm was

used; of course, when planning these maneuvers in real time, the track of the storm will not be precisely known. To simulate this uncertainty and provide some leeway to maneuver planning, each target flyover each had an associated viewing window of +/-20 hours, meaning that the satellite will complete its maneuver at some point over this 40 hour time span, and not begin the next maneuver until the end of the current target time window. The satellite used in this example was a small CubeSat-scale satellite of only 4kg, using electrospray thrusters with maximum thrust values of $0.35mN$. A 200km diameter canonical FOV is assumed, which can be taken as an effective FOV. One thing prioritized in the paper [50] is the importance of capturing the eye of the storm rather than simply capturing the wall; gathering data about the eye of the storm is considered more significant for determining storm strength and predicting possible damage [50]. Specifically, McGrath et al. discusses using a SAR instrument to characterize wind speeds of the TC; this aligns with work discussed, addressing the lack of data about TC center wind speeds, and temperatures, to aid in the prediction of TC intensity [50].

A non-maneuvering satellite was evaluated first for target accesses over the 12.5 day simulation. Then the maneuvering options were evaluated via the graph theoretical technique as described, with possible delta-V options from 0 to 15m/s, spread out by 0.5m/s intervals. A non-maneuvering satellite achieves only one flyover that has the eye of the storm in view. Of the remaining four intended flyovers of targets, only three are achieved in the associated time window. From the graph of possible maneuvering options, two possible maneuvering solutions are identified; one of these solutions is the lowest delta-V option and one is the lowest delta-V solution prioritizing the eye of the storm in view. One solution describes accessing four targets in their associated time window utilizing 13.5m/s delta-V, with the eye fully in view in three of these flyovers. Another solution has the eye fully in view for all five target flyovers utilizing 20.5m/s delta-V, with one of the targets being accessed outside of the associated time window. These results will be discussed in further detail in Chapter 3, when the same case study will be evaluated. [50]

1.3 Summary and Research Questions

Given the background of existing storm monitoring satellites, there exists an opportunity to fill a gap of persistent LEO observations. This can improve existing TC intensity forecasts, which have largely stalled in recent years. One opportunity for addressing this challenge is the use of a ReCon, which has been shown to have better performance than static constellations of the same cost for static ground targets. The application of this concept to TCs, mobile ground targets, may likewise provide better performance than static constellations. This may be achieved through McGrath's method of using low-thrust maneuvers. The following thesis will explore this concept by exploring the following questions:

- Can an adjusted version of McGrath's method be validated?
- What tradeoffs exist in this space of possible maneuver solutions?
- How can this solution space be further characterized?
- How can this method be improved or extended, for single and multiple satellite applications? What other methods exist to search the solution space?
- How does this method perform when used with a ReCon-like constellation?
- How does this method perform with other case studies? What about for non-ideal initial conditions?
- How can this method and the ReCon concept as a whole be realized? What are the yet-to-be-considered real life challenges of implementation?

Overall, a further exploration of McGrath's method will be conducted in Chapter 2, along with an extended methodology that leverages optimization to increase method effectiveness. Then, in Chapter 3, two hurricane case studies will be explored utilizing this extended methodology for single satellite and multiple satellite cases, exploring the resulting solution tradespace, and comparing results to non-maneuvering single and multiple satellite cases. Next, in Chapter 4, there will be a discussion of a

potential demonstrator mission of ReCon: ROAMS. The reality of implementing ReCon, and the kinds of maneuvers proposed for mobile target tracking in this thesis, will be discussed through this proposed mission. Finally, the thesis findings and recommendations will be summarized in Chapter 5 along with a discussion on future work and contributions. These topics are summarized in Figure 1-10.

Figure 1-10: Thesis Flowchart

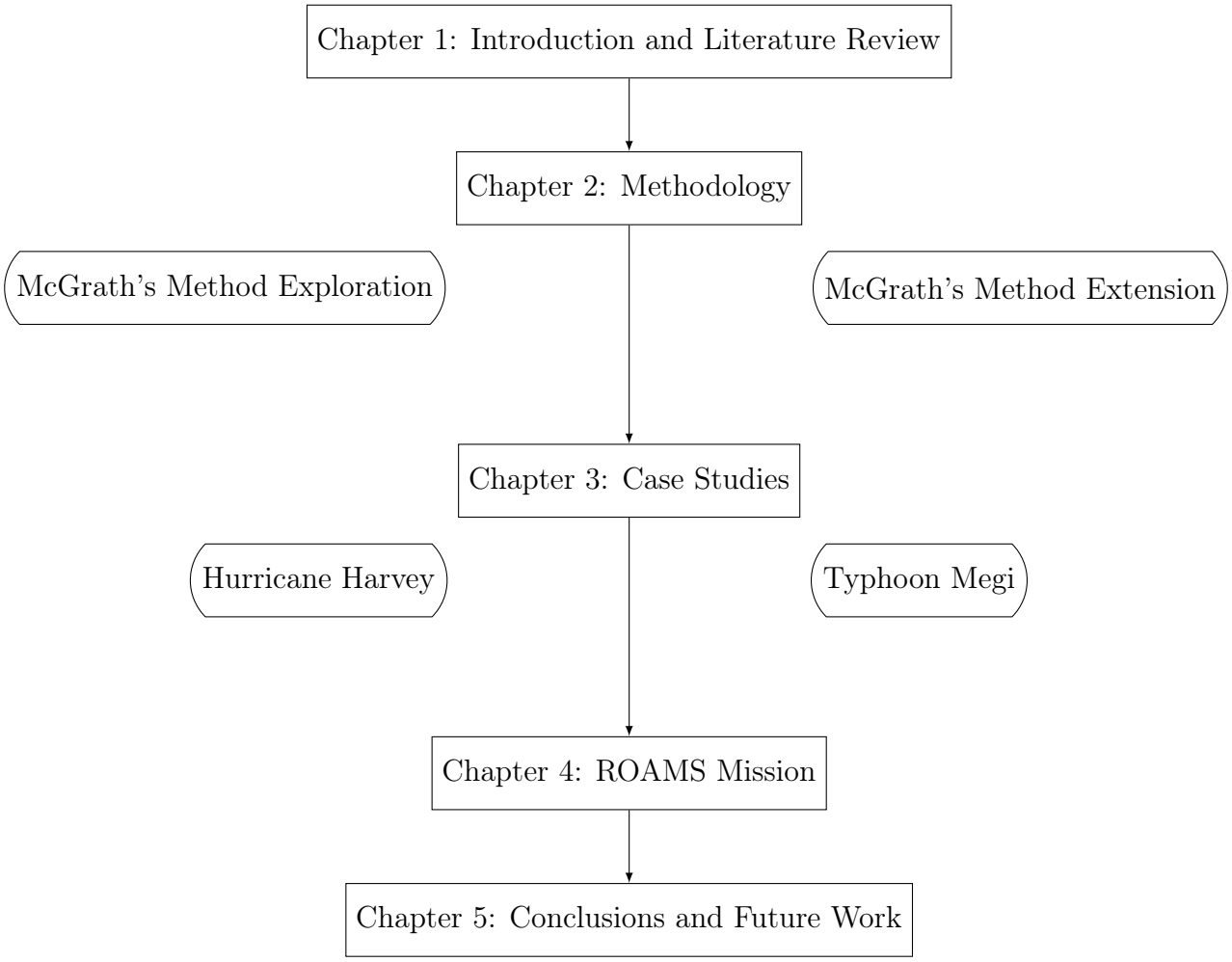

Chapter 2

Methodology

The aforementioned work by McGrath et al. (2019) has shown promise in utilizing a graph theoretical technique to plan low-thrust maneuvers to improve a satellite's view of a moving ground target. To more deeply understand this work, and the solution space being explored, a similar method to this will be explored. An analysis of the same case study, with Typhoon Megi, as presented in [50] will be conducted using a similar graph theory technique to the one described. This includes the use of the general perturbation method for finding possible maneuvers [46]. The solution space of possible maneuver opportunities for target viewing will be explored, compared to results of a numerical propagator (in STK) and compared to the work done by McGrath.

Then, two possible mechanisms of extending this work will be discussed, based upon this preliminary analysis. First, an optimizer will be used to select possible maneuvers rather than finding these through a graph search. Secondly, the use of multiple satellites, both 2- and 3-satellite cases, will also be explored. These options have been explored through a prior paper [53] and this will be expanded upon below. The inclusion of multiple satellites will allow for further viewing opportunities of the targets and more maneuver options, expanding the design space of options and more closely relating this mobile target tracking application to a full ReCon design as described in Chapter 1. The design space will again be explored utilizing an optimizer for more efficient investigation.

Table 2.1: Satellite characteristics and orbit parameters. [50]

Characteristic	Value
Mass (kg)	4
Maximum Thrust (mN)	0.35
Altitude (km)	703
Inclination (i) (deg)	40
RAAN at Epoch (deg)	0
Argument of Latitude (u) at Epoch (deg)	0
Right Ascension of Greenwich at Epoch (deg)	-161
Epoch Date	10/10/2010 12:00 UTC

A final addition is to consider the use of forecasted track data, rather than the true historical TC path, to plan maneuvers. This will be more realistic to how real operations will be conducted, and while the success of this application will mostly depend upon the accuracy of the forecasted track versus actual data, this will present an opportunity to examine the robustness of this method under less ideal circumstances.

2.1 Exploration of McGrath's Graph Theory Method

2.1.1 Adjusted Methodology

For the initial exploration of McGrath's method, a similar graph theory method as used in [50]. This was coded in Python, using the NetworkX [26] package to generate the network of potential maneuver options, as generated by the general perturbation method [46].

To form a comparison to results shown by McGrath et al. the same general problem setup is used as in [50]. The characteristics of the satellites(s) and the initial orbit are shown in Table 2.1; small 3U CubeSats are used with electrospray thrusters [50]. This assumes the use of TILE thrusters developed at MIT, which for a 4 kg spacecraft, can provide a total of around 90 m/s delta-V [47]. These are the parameters of the model. Model constants are likewise shown in Table 2.2 [50].

The same Typhoon Megi case study is used, as in [50] with targets located at the center of the eye of the storm, spaced out at 2.5 day intervals along the typhoon's

Table 2.2: Model Constants [50]

Symbol	Description	Value
$\mu_\oplus$	gravitational parameter of the earth	$3.986 \times 10^14 m^3/s^2$
$R_\oplus$	mean Earth radius	$6371000m$
J_2	coefficient of Earth's gravitational zonal harmonic (2nd degree)	1082.7×10^{-6}
$\omega_\oplus$	Earth's rotation rate	$7.29212 \times 10^{-5} rad/s$
f	flattening factor of the Earth	0.0335281

Table 2.3: Typhoon Megi eye locations at 2.5 day intervals. [31]

Date and Time	Days Since Epoch	Latitude (deg)	Longitude (deg)
13 Oct 2010 00:00 UTCG	2.5	11.9	141.4
15 Oct 2010 12:00 UTCG	5	15.7	135.5
18 Oct 2010 00:00 UTCG	7.5	17.5	123.3
20 Oct 2010 12:00 UTCG	10	18.4	117.2
23 Oct 2010 00:00 UTCG	12.5	23.4	118

track (Table 2.3). A viewing window of 20 hours on either side of each target time was allowed. In the simulation, track data collected at 6 hour time intervals was used [31] and interpolation between these latitude and longitude points was performed to approximate the true storm path. If a potential flyover is slightly before or after the available path data, it is assumed the storm is at the interpolated point. Note that the distance to the target at each access is recorded and whether or not the flyover would include the eye of the storm in view. The eye of Typhoon Megi was around 28km in diameter, so any image that fully contains the eye must have the center of the eye within 14km of the edge of the image [50]. As the eye size changes over time, it is assumed any image that is taken within 80km of the eye will have the eye fully in view.

The overall procedure of the simulation is as follows: after being initialized at epoch (set as 10/10/2010 at 12:00 UTCG for the Typhoon Megi case), the satellite enters the first maneuver period during which a low-thrust maneuver of a particular delta-V is conducted. A key difference between the work presented in [50], as discussed

in Section 1.2.4, and the method presented in this thesis is that the maneuver duration is fixed in this procedure. It is set such that the maneuver is completed at the start of the first viewing window. In the case of these low-thrust maneuvers, this limits the total delta-V that can be generated during each maneuver period. There is an absolute maximum of 6.3 m/s permitted per maneuver, restricted by the maneuver time. In work done by McGrath [50], the maneuver duration was not fixed, but left flexible, and the end maneuver location was fixed, to be reached in a certain time frame. This slight difference in appraoch leads to quite different results, which will be discussed. This means that there is not necessarily a one-to-one comparison to be made between the results presented in this thesis and those generated by McGrath, however, the results presented herein serve as an alternative approach.

These maneuvers are either raising or lowering maneuvers computed via the general perturbation formulation described in section 1.2.4 [46]. The formulas involved calculating the change in RAAN and argument of latitude after a 3-phase maneuver using low-thrust propulsion, from the inputs of satellite maximum acceleration, maneuver duration, maneuver delta-V, initial orbit (a, i, RA_{et}, $RAAN$, u), final orbit semi-major axis, and model constants, are set as shown in the Table 2.1 and Table 2.2. The equations to compute these maneuvers, as provided by McGrath [48], is shown in the appendix. From the post-manuever $RAAN$ and u values, SSP latitude (ϕ) and longitude (λ) can be found:

$$\phi = \tan^{-1}\left(\frac{\tan\left(\sin^{-1}\left(\sin i \sin u\right)\right)}{1 - f(2-f)}\right) \tag{2.1}$$

$$\lambda = \tan^{-1}\left(\frac{\cos i \sin u}{\cos u}\right) - \omega_{\oplus} t + RAAN - RA_{et} \tag{2.2}$$

where t is the time since epoch. RA_{et} is the right ascension of Greenwich at epoch, used to orient the satellite with respect to the surface of the Earth.

The satellite's location in orbit is then propagated using the same formulas with no delta-V or acceleration applied, which includes J2 effects, through the viewing window, during which any accesses of the storm are recorded. An access of the storm

is defined as whenever the eye is within the field of view (FOV) of the satellite. In other words, whenever the eye of the storm is within 100km of the SSP, according to the Haversine distance formula:

$$d = 2R_{\oplus} \arcsin\left(\sqrt{\sin^2\left(\frac{\phi_{SSP} - \phi}{2}\right) + \cos\phi_{SSP}\cos\phi\sin^2\left(\frac{\lambda_{SSP} - \lambda}{2}\right)}\right) \tag{2.3}$$

where ϕ_{SSP} and ϕ are the SSP and target latitudes, respectively, and λ_{SSP} and λ are the SSP longitude and target longitude, respectively.

The orbit propagation steps through time in 10 second intervals. The total number of intervals during which an access of the storm occurs is recorded; this is used as an approximation for total target access time. The distance to the target and date and time of each access is recorded as well. At the end of the first viewing window, the second maneuver period begins, and this process is repeated for all five targets. A flowchart of this tree generation process is shown in Figure 2-1.

This method described differs slightly from [50] as this includes a fixed maneuver duration that ends at the start of each viewing window. However, this only slightly reduces the achievable delta-V and therefore does not significantly impact maneuver options, but may result in different solutions found. In summary, given the delta-V to be applied for each maneuver, the simulation will output all access of the storm during the target viewing windows, including the total access time, distance to the target at each access, and time of each access. If no access of the storm is possible during a given viewing window regardless of the maneuver attempted, the satellite will simply propagate during the maneuver period to conserve delta-V capability. The delta-V will be supplied by a list of possible options set by a minimum, maximum, and interval of delta-V.

To describe a single solution output of this model, a plot in Figure 2-2 shows a potential solution for single satellite maneuvers along with a storm's track. The storm's track in red, marked with five target points along the track. This is overlaid with flyovers from a sample solution to be discussed. The FOV of the satellite at these flyovers is shown by yellow circles, of a 200km diameter. A satellite ground track is

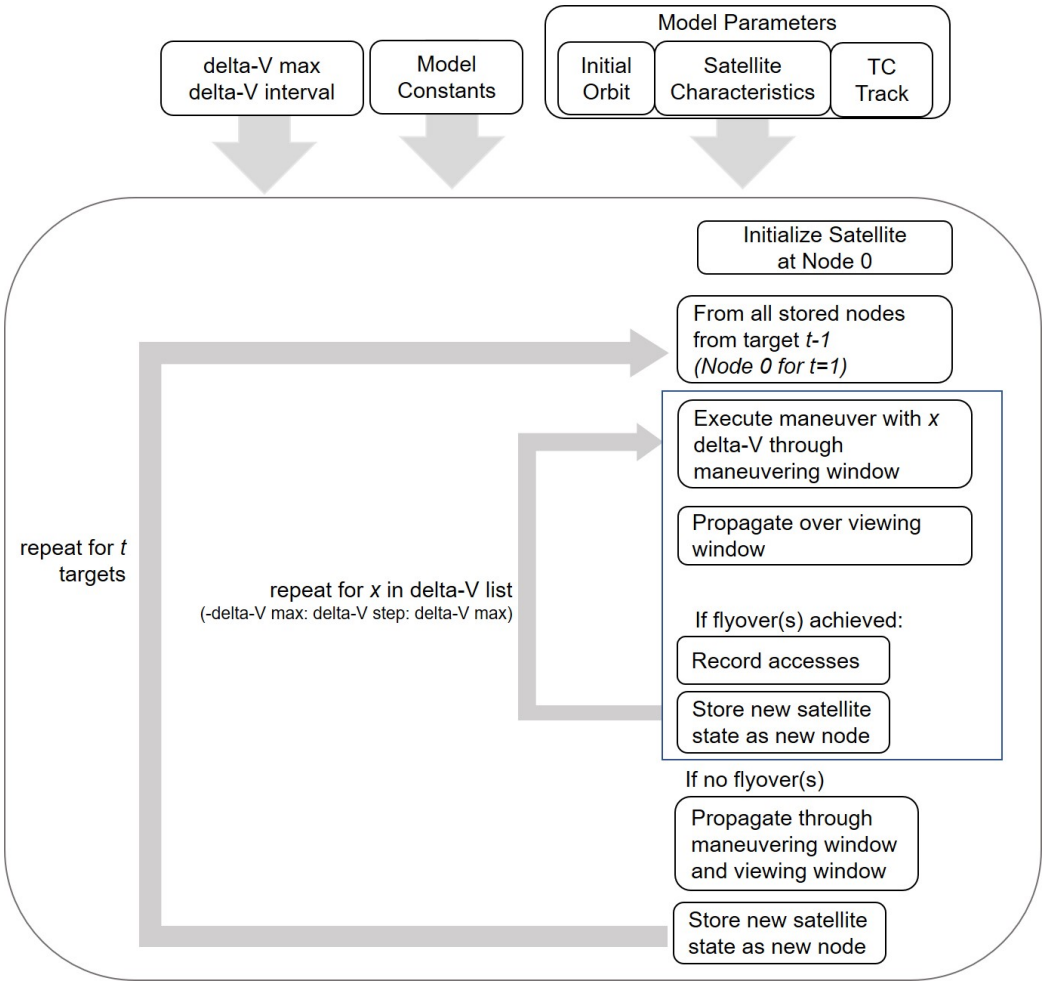

Figure 2-1: Tree generation flowchart.

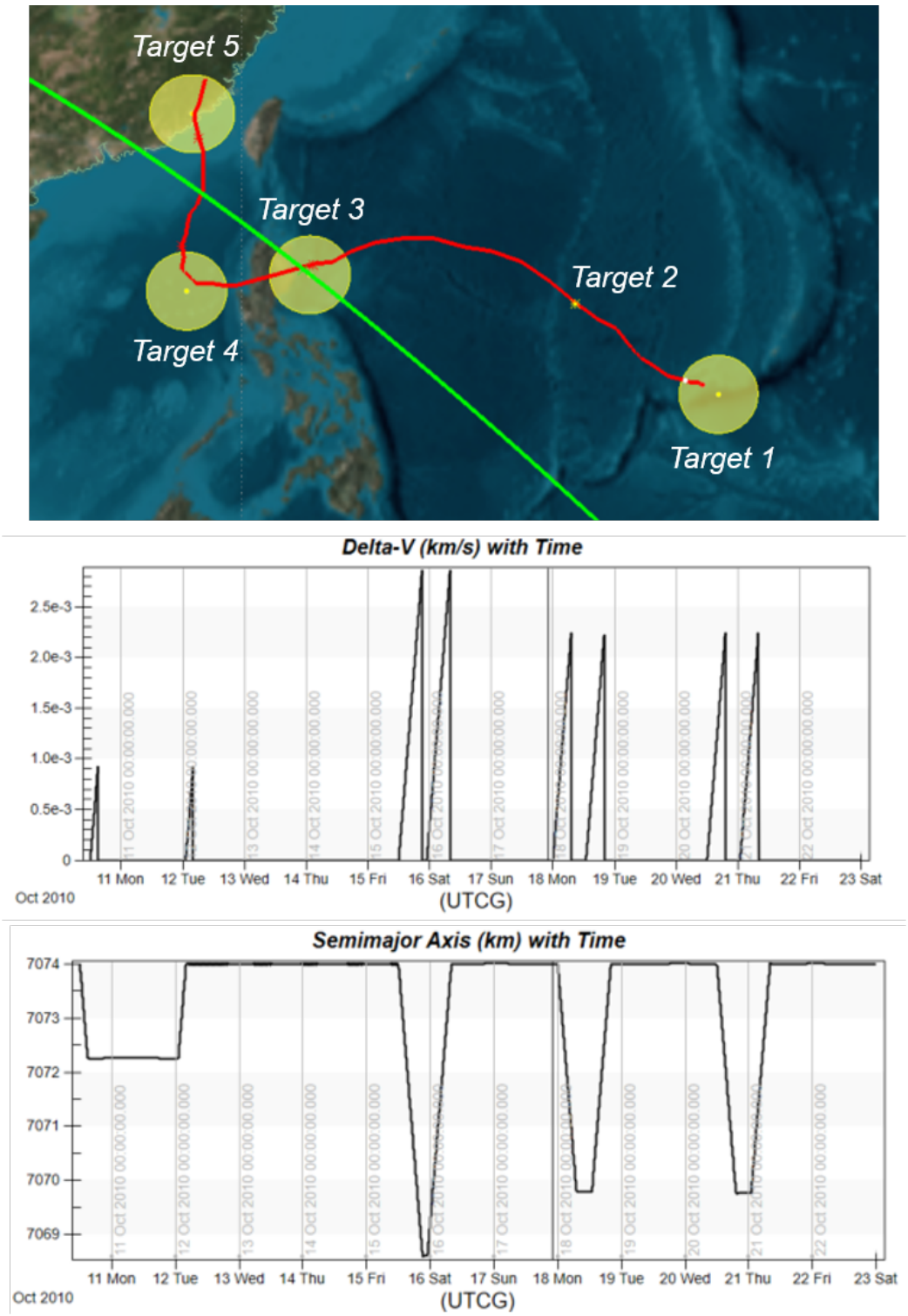

Figure 2-2: Sample single satellite case modelled in STK [6].

shown by the green line across the figure. The maneuvers required to complete these flyovers are shown in the plot below, along with the resulting semi-major axis change over the course of the simulation. As shown, the semi-major axis changes temporarily by only a few kilometers to shift the RAAN and argument of latitude of the orbit and then the satellite returns to the original orbit altitude. These small changes are on order of what can be expected for this exploration, requiring low amounts of delta-V to shift the satellite SSP to achieve better target accesses. These plots in Fig. 2-1 were generated in Systems Tool Kit (STK) from Analytical Graphics, Inc [6].

2.1.2 Results

The described adjusted version of McGrath's method will now be applied to the Typhoon Megi case. Graphs of solutions and potential individual solutions will be evaluated. A sample output from this methodology, a graph of solution options, is shown in Figure 2-3.

This displays the lowest delta-V solution marked in red, with each node representing the satellite state at each time indicated. The edges of the graph are the amount of delta-V used to achieve that satellite state. As can be seen, numerous possible solutions exist shown by each branch in the graph.

The time step for the model was initially set to 60 seconds, however, throughout the process of testing the code it was found that results were sensitive to the time step used. A complete pass over the target area of interest (i.e. the amount of time taken by the satellite at 703 km altitude to travel 200 km ground distance) is very short, only approximately 30 seconds at the intended orbital altitude. This means that the time step for evaluation should be less than 30 seconds to ensure most lengthy potential passes are not missed. Shorter passes may be not captured. For example, if the eye only crosses some of the field of view (i.e. only crossing a chord of the circular FOV rather than the full diameter) this may be missed in this simulation. With the time step adjusted to 15 seconds, a similar graph to the one in Figure 2-3 was generated. This graph is laid out in a circular pattern, beginning from the center initial node, Node 0. This represents the initial satellite state. From there, the satellite maneuvers

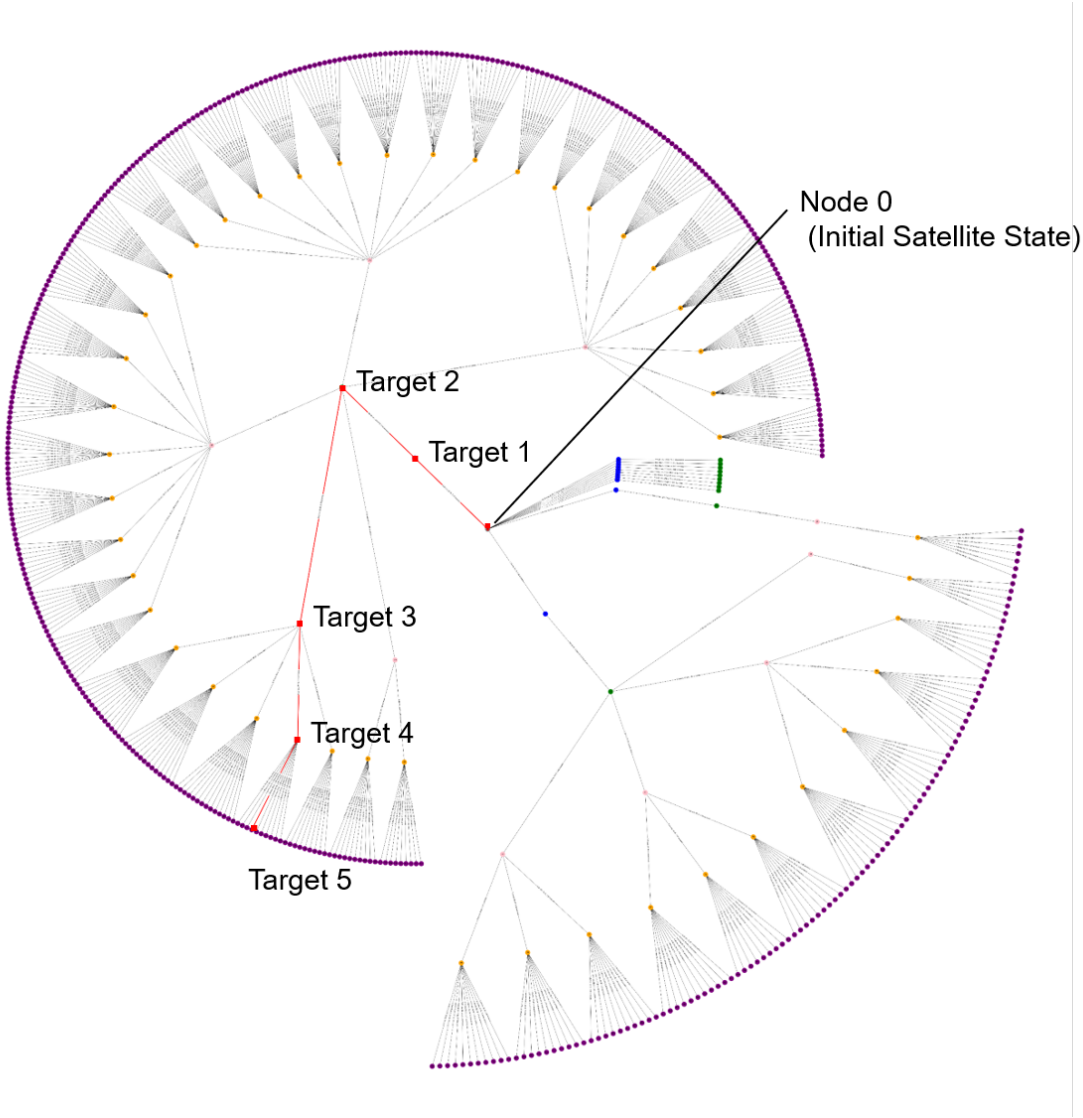

Figure 2-3: Graph theory sample result.

Table 2.4: Non-maneuvering satellite results for Typhoon Megi Case Study by McGrath et al. [50]

Target	Non-maneuvering					
	Date	Time UTCG	Eye Latitude (deg)	Eye Longitude (deg)	Distance from center of FOV to eye (km)	Eye in View?
1	10/12/2010	13:20	11.9	141.4	73	Yes
2	-	-	-	-	-	-
3	10/17/2010	22:01	17.5	123.6	95	No
4	10/19/2010	21:38	17.1	117.4	92	No
5	10/23/2010	19:10	25.0	118.0	83	No

in attempt to view the first target (shown by blue nodes). Each possible maneuver option is shown by an edge to the next node. Then, the next set of edges extending from each of those nodes generated represents the next possible satellite maneuvers to view the second target, and so forth. Third, fourth, and fifth target accesses are shown by green, pink, orange, and purple nodes respectively. It is clear that some branches of this tree do not allow accesses of all targets, as shown by several branches ending at the third node.

This graph was then searched for its shortest (lowest delta-V) path, using Dijkstra's algorithm in order compare to McGrath's work. There were some discrepancies noted. Of course a slightly different method was used, as noted prior, so these differences are not unexpected but worth noting for future work on this case.

Before comparing these solutions with maneuvering satellites, the non-maneuvering satellite solutions will be compared to see any initial differences in propagation. These results generated will then be compared with those given by McGrath [50] for both the non-maneuvering and maneuvering satellite.

Both sets of solutions show no accesses in the associated time window (as shown in Tables 2.4 and 2.5) of the second target (though, there is an access near the intended target at 10/14 12:58), and only one target which has the eye of the storm in view. It is noted that, while the times of each access for each target are the same for both McGrath's and the author's solutions, there is around a +/- 10km difference or less for the distances to the targets. McGrath's solution was propagated using a

Table 2.5: Non-maneuvering satellite results for Typhoon Megi Case Study by Morgan

Target	Non-maneuvering					
	Date	Time UTCG	Eye Latitude (deg)	Eye Longitude (deg)	Distance from center of FOV to eye (km)	Eye in View?
1	10/12/2010	13:20	11.9	141.4	84	No
2	-	-	-	-	-	-
3	10/17/2010	22:01	17.5	123.6	86	No
4	10/19/2010	21:38	17.1	117.4	83	No
5	10/23/2010	19:10	25.0	118.0	78	Yes

Table 2.6: Non-maneuvering satellite results for Typhoon Megi Case Study by STK [6]

Target	Non-maneuvering					
	Date	Time UTCG	Eye Latitude (deg)	Eye Longitude (deg)	Distance from center of FOV to eye (km)	Eye in View?
1	10/12/2010	13:20	11.9	141.4	78	Yes
2	-	-	-	-	-	-
3	10/17/2010	22:01	17.5	123.6	99	No
4	10/19/2010	21:38	17.1	117.4	98	No
5	10/23/2010	19:10	25.0	118.0	92	No

numerical solution, rather than the general perturbation formulas, which could be the cause for these differences. Additionally a different time step was used (the author used 10 seconds, while McGrath's numerical integrator used 1 second) which could contribute to the exact timings (i.e. the precise second of each access) and distances. This can be compared to results generated from STK in Table 2.6. These results were computed using the Astrogator propagator in STK, which uses a numerical integration propagator (high precision orbit propagator using Runge-Kutta-Fehlberg of order 7-8 or similar integration methods) including only J2 effects (secular only) [7].

Again, the only difference here is a slight difference in the recorded distances (<10km overall). So, overall, these methods of problem solving produce similar results with this slight difference in exact distances remaining.

Now, the maneuvering solution will be shown from each source in Table 2.7 and

Table 2.7: Maneuvering satellite results for Typhoon Megi case study by McGrath [50]

Target	Maneuvering					
	Date	Time UTCG	Time from Non-Maneuvering (mins)	Delta-V (m/s)	Minimum Access Distance (km)	Eye in View?
1	10/12/2010	13:20	0	1	83	No
2	-	-	-	-	-	-
3	10/17/2010	21:55	-6	5	2	Yes
4	10/19/2010	21:32	-6	0.5	5	Yes
5	10/23/2010	19:08	-2	7	58	Yes

Table 2.8: Maneuvering satellite results for Typhoon Megi case study by Morgan

Target	Maneuvering					
	Date	Time UTCG	Time from Non-Maneuvering (mins)	Delta-V (m/s)	Minimum Access Distance (km)	Eye in View?
1	10/12/2010	13:20	0	0.5 (raise)	79	Yes
2	-	-	-	-	-	-
3	10/17/2010	22:01	0	0.5 (lower)	88	No
4	10/19/2010	21:38	0	0.5 (raise)	87	No
5	10/23/2010	19:10	0	0.5 (raise)	80	No

Table 2.8. Both have been generated exploring possible maneuver options from 0 to 15 m/s at 0.5 m/s steps. However, as mentioned previously, these are generated with a slightly different problem set-up, where the maneuvers from McGrath have a fixed end SSP in some time frame, and the results generated in this thesis have a fixed maneuver duration.

The results overall are similar, but clearly different maneuver options are chosen. The solution presented by McGrath uses a total of 13.5 m/s delta-V and, across the targets accessed, flyovers are a mean of 37 km away. The solution found by the author uses a total of 2 m/s delta-V and, across all time steps that the storm is in view, flyovers are a mean of 88 km away. The second target is also viewed outside of the viewing window, not in the chart above. As one can see, these two solutions were found differently; the solution presented by the author only just hits the 100km

Table 2.9: Maneuvering satellite results for Typhoon Megi case study by McGrath (Eye in View) [50]

Target	Maneuvering					
	Date	Time UTCG	Time from Non -Maneuvering (mins)	Delta-V (m/s)	Minimum Access Distance (km)	Eye in View?
1	10/12/2010	13:21	1	0.5	68	Yes
2	-	-	-	-	-	-
3	10/17/2010	21:54	-7	7	19	Yes
4	10/19/2010	21:31	-7	1	19	Yes
5	10/23/2010	19:09	-1	12	70	Yes

Table 2.10: Maneuvering satellite results for Typhoon Megi Case Study by Morgan (Eye in View)

Target	Maneuvering					
	Date	Time UTCG	Time from Non -Maneuvering (mins)	Delta-V (m/s)	Minimum Access Distance (km)	Eye in View?
1	10/12/2010	13:20	0	0.5 (raise)	79	Yes
2	-	-	-	-	-	-
3	10/17/2010	22:00	-1	4 (lower)	79	Yes
4	10/19/2010	21:38	0	0.5 (raise)	78	Yes
5	10/23/2010	19:09	-1	0.5 (lower)	70	Yes

requirement, and utilizes low delta-V. The solution presented by McGrath includes much closer passes, due to the requirement that the satellite must pass over the target within the time frame. The solutions presented in this thesis are more dependent on the minimum required distance to access.

This maneuvering result can be further restricted to only include only results that allow for full view of the eye of the storm. Therefore, for the following results, solutions will only be shown where the distance to the target is restricted from the natural FOV, 100km, to 80km. These results are shown in Table 2.9 and Table 2.10.

The results overall are similar, but clearly different maneuver options are chosen. The solution presented by McGrath uses a total of 20.5 m/s delta-V and, across the targets accessed, flyovers are a mean of 44 km away. The solution found by the

author of this thesis uses a total of 5.5 m/s delta-V and, across the targets accessed, flyovers are a mean of 79 km away. Again, the second target is also viewed outside of the viewing window, not in the chart above. As shown before, the solutions are different, with the author's solution showing flyovers just under the required 80km, but consuming significantly less of the total delta-V budget due to the aforementioned difference in approach. Closer passes can be found with the author's solution as well with more priority given to the closeness of the passes rather than the delta-V used.

So overall, the results found by McGrath appear reasonable, verified by the similar solutions found by the author. In addition to this validation of McGrath's work, the potential for a greedy solution approach of searching the graph solution were briefly explored. This would involve taking the closest passing flyover option for each target. The result for this method included a large initial maneuver to view the first target. As this problem is analogous to a time-varying traveling salesman problem, a greedy solution produces poor results. As described briefly above, aggressive initial maneuvers can severely restrict options for maneuvers to future targets if these are not taken into account. This emphasizes the need for addressing future maneuvers.

As discussed by McGrath et al. [49] the order of nodes generated in the graph (essentially a tree graph) will depend up on the depth and number of the individual branches. The order of nodes produced will be $O(b^d)$ where b is the branching factor, the maximum number of children generated at any node in the tree and d is the search depth of the tree, the length of the longest path from the root to the leaf of the tree. The depth of the tree will depend upon the number of targets, and the branching factor will depend upon maximum delta-V and delta-V interval used. Therefore, the time for tree generation can be found by multiplying the time taken to calculate the search from each node by this b^d term [49]. In the case of multiple satellites, this factor will additionally be multiplied by the number of satellites s. This means the number of targets and the delta-V step will have a larger (power law) impact on the time of tree generation than increasing the number of satellites in this search method (multiplication factor) [49]. Additionally, if the time step is shorter, the time for each node calculation will take longer. If a different delta-V step is used, the

number of potential solutions will increase, however better solutions may exist in this expanded space. For example if a delta-V step of 0.25 m/s is used rather than 0.5 m/s, approximately 2× more nodes will be generated, but a smaller delta-V solution can be found. In conclusion, while the graph theory approach is suitable for an initial exploration of the solution space, the inherent discretization involved creates undue constraints on possible performance of solutions. In addition there is no guarantee of global optimality due to the discretization of the search space itself.

2.1.3 Conclusions

A more continuous exploration of the solution space will allow for the possibility of finding niche solutions which may have better performance characteristics. Therefore, exploring the space of possible sequential maneuvers in a continuous way may be reveal other solutions. Additionally, it was noted in initial exploration that a greedy solution which selected the 'best' maneuver (e.g. closest pass or lowest delta-V without considering the overall solution) for each target typically had poor results overall, as this mobile target tracking problem is akin to a traveling salesman problem.

2.2 Extensions of McGrath's Method

2.2.1 Optimization

With the inclusion of an optimizer, the problem set up changes to fit the mold of an optimization problem. The problem set-up is shown in Figure 2-4. The optimizer was given control of the delta-V used by each satellite for each maneuver. This means there are nt design variables where n represents the number of satellites and t represents the number of targets along the hurricane track. These design variables are bound by a maximum delta-V limited by the fixed maneuver duration. The optimization had the objectives to minimize the overall mean distance to each target each time an access occurred, minimize total delta-V used, and maximize the amount of time each target was in view. Note that no distinction was made between longer continual

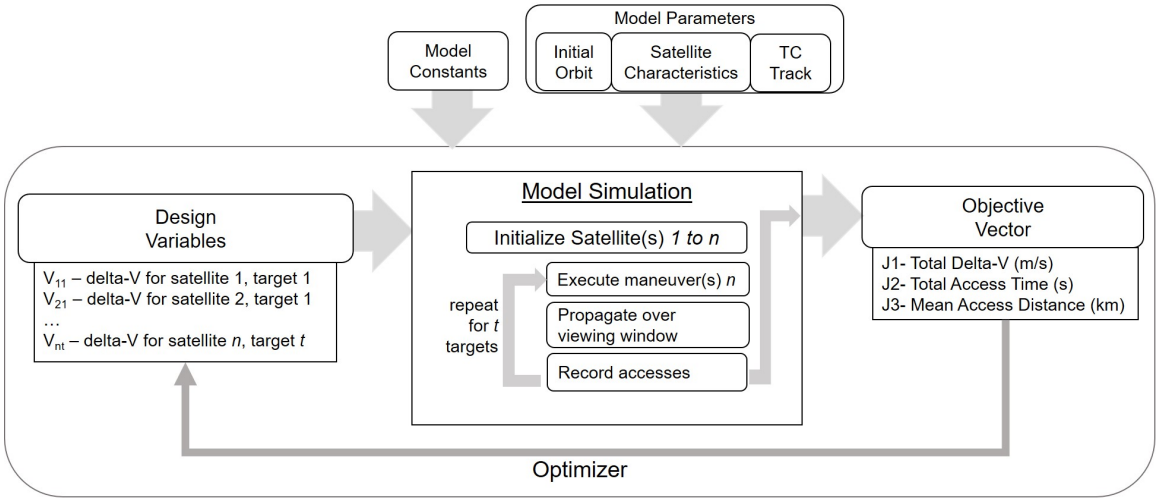

Figure 2-4: Optimization process.

accesses and shorter frequent accesses, which should be further explored.

By computing these three objectives, more trade-offs may be apparent than through the graph search methodology. Additionally, it should be noted that these objectives are cumulative, representing the performance of the satellite(s) over the entire series of maneuvers, discouraging greedy maneuvers that may prohibit future accesses, as discussed in [50].

Optimization Selection

Given the previous success of genetic algorithms exploring similar problems (aforementioned satellite constellations and coverage), genetic algorithms were selected for use. Like many other heuristic techniques, genetic algorithms work to avoid getting trapped in a local optimum. The optimization mimics natural selection and mutation throughout the population of potential solutions, and possible designs are assessed by a fitness function based upon the objective function. A genetic algorithm was selected from possible options run through pymoo, a Python-based package that can conduct multi-objective optimization. Specifically a BRKGA (Biased Random Key Genetic Algorithm), was used for this exploration, which utilized both elitism (breeding the best performing solutions) and random restarts [12]. Both of these techniques work to avoid getting trapped in local optima and push for optimal solutions. A brief design of

Table 2.11: Genetic Algorithm Parameters

Parameter	Description	Value
Number of Elites	number of elite individuals	250
Number of Offsprings	number of offpsrings to be generated through mating of an elite and a non-elite individual	800
Number of mutants	number of mutations to be introduced each generation	100
Bias	chance of an offspring inheriting the allele of its elite parent	0.3

experiments of the algorithm parameters was conducted to obtain good convergence performance with this algorithm, resulting in the parameters shown in Table 2.11.

Essentially the algorithm generates a random initial population of solutions (individuals) and evaluates the performance of each individual. Elite individuals, those that perform well, are noted from the rest of the population (in this case, the top 250 individuals). The next generation of solutions are then created with carrying over the elite solutions, adding random solutions (the number of mutants), and mating the elite solutions with another random solution in the population. Whether or not the offspring takes on the allele (design variable) of the elite parent is a chance based upon the bias parameter. In this case, the randomization appears to offer more effective ways to search the space, and a lower bias parameter tends to perform better. Because of this process of introducing random solutions and caring forward parameters of non-elite solutions, the optimizer can avoid local optima.

2.2.2 Multiple Satellites

When evaluating solutions for multiple satellites, the problem set up remains largely the same. Adding n satellites to the solution space simply means exploring n times more options. When fed to the optimizer, this adds $t(n-1)$ more design variables (delta-V options), where t is the number of targets. When 2- or 3- satellite cases were evaluated, these were placed in the same orbits, only shifting the initial RAAN by 20 degrees and 40 degrees respectively. Including the optimizer in this multiple satellite evaluation does greatly reduce the complexity of the problem set up when compared

to the graph theoretical case [49]. For example, if a 2-satellite case is considered, each satellite could maneuver or both could maneuver, greatly increasing the number of options at each branch. In the case of including the optimizer, nt more design variables must simply be added, with no major changes to the model itself. This is represented in the optimization flowchart shown in Figure 2-5.

2.2.3 Inclusion of Forecasted Data

The above problem description implies that a mobile target track is known apriori. However, in the case of realistic mobile targets such as TCs, the exact path cannot be known in advance. Instead, the satellite must work only based upon forecasted data and plan maneuvers including that uncertainty. This introduces a complication to the previously presented planning process for a sequence of maneuvers. In this case, maneuvers may only be planned so far in advance rather than all at once since future target locations are partially uncertain or, further down the line, completely unknown.

Therefore, an adjusted version of the methodologies described above will be included in the case studies to follow in Chapter 3. To include predicted data in maneuver planning, a subset of maneuvers are planned ahead of time. For example, two maneuvers will be planned based upon predicted data for the next two targets. The best performing solution of those options will be selected. Then the satellite will conduct only one of these maneuvers, and updated data will be used to plan the following two maneuvers. This ensures that a greedy solution is not selected, and some consideration is made to the next required maneuver while basing the actual executed maneuvers upon more certain data. Thus, one of the contributions of this thesis is the introduction of adaptive maneuver planning for reconfigurable satellite constellations.

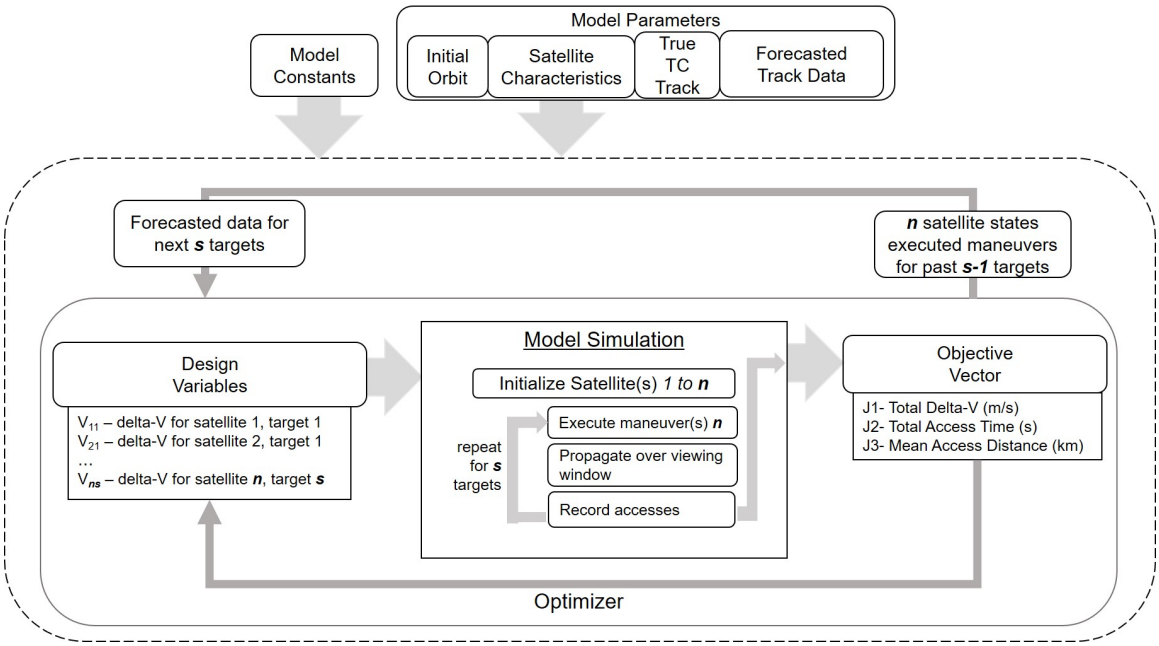

Figure 2-5: Optimization process with forecasted data.

Chapter 3

Case Studies

The methodology described in Chapter 2 will now be applied to two different TC case studies. One is Typhoon Megi, selected to provide a point of comparison between these results and those originally produced in Chapter 2. As mentioned previously, these results for Typhoon Megi have been explored in a prior paper [53]. The other is Hurricane Harvey, a TC in the Atlantic with a different track pattern when compared to Typhoon Megi. Both were destructive TCs that could have benefited from more data gathering to better inform intensity forecasting. The results shown will include the solutions found with the optimizer, as well as multiple satellite solutions, using the methodology described in Chapter 2. These solutions will be compared to the original results by McGrath as well as the non-maneuvering result in each case. Additionally, a single-satellite solution utilizing the forecasted track data of each TC will be included.

3.1 Case Study: Typhoon Megi

Typhoon Megi, also known as Typhoon Juan, was the most significant typhoon in 2010 and one of the most intense TCs on record [34]. The storm was first classified as a tropical disturbance on October 12th, 2010 [83]. It became a typhoon around October 14th and early on October 18th, it made landfall over the Philippines [83]. It was classified as a super typhoon, the only storm to be given that categorization that year, and severely impacted the islands, affecting nearly 700,000 people [78]. The

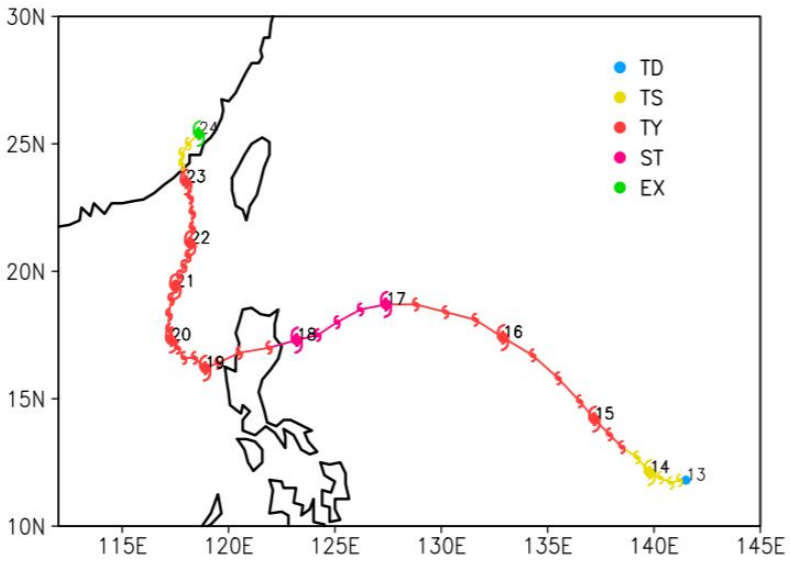

Figure 3-1: Typhoon Megi track with marked intensity [11]

.

actual track (which was only known aposteriori) is shown in Figure 3-1. The storm is a case study in rapid intensification, this period occurring just before landfall in the Philippines [83]. After crossing the islands, the typhoon made a sharp turn northward, but weakened to a tropical storm before making its second landfall in China [83].

The same five targets were used as in 2.3 for the purposes of this simulation. The multi-objective optimization as described in Section 2.2 was carried out for a single satellite as well as 2- and 3- satellite constellations. The non-dominated solution sets will be displayed for each case, and sample solutions will be discussed to describe the nature of the solutions.

3.1.1 Results

Single Satellite Case

Non-dominated solution sets for each of these cases are shown in Figure 3-2. These solutions represent essentially the best performing solutions found by the optimizer - those which cannot improve in one objective without degrading in another as previously described. This allows for an exploration of trade-offs within the solution space. Sample solutions are also included from these non-dominated sets to demonstrate

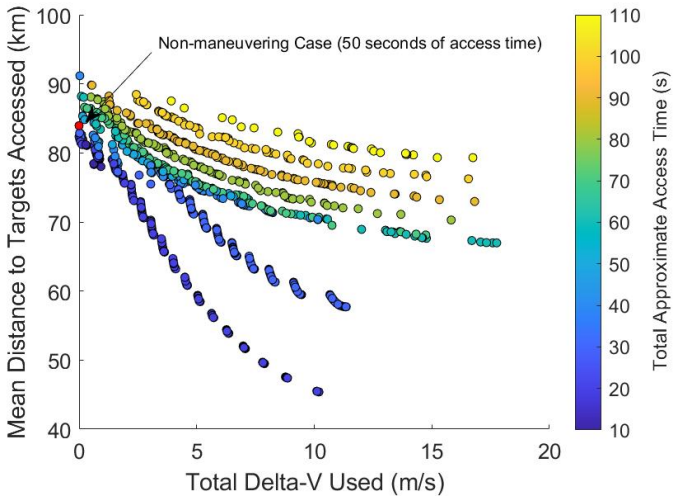

Figure 3-2: Non-dominated set of solutions for single satellite case.

specific performance characteristics. These particular solutions will be compared to non-maneuvering satellites to show the advantage of maneuverability in specific use cases.

As shown in Figure 3-2, there are a multitude of possible solutions. The non-dominated set resulting from optimization is shown with the non-maneuvering solution labeled. Broad trade-offs from this can be identified from this. Clearly, increased delta-V is required to have increased accesses of the targets from the same mean distances. Additionally, greater delta-V is required to get closer to the targets for the same number of accesses. This is indicated by downward curving series of points made across the plot. These trade-offs should all be considered when evaluating possible maneuver options. Displaying the possible options in this manner makes trade-offs more apparent in the solution space; for example, one may desire closer passes rather than greater access time for the same total delta-V.

A sample maneuvering solution is shown in Table 3.1 compared to the non-maneuvering case. This includes a summary of the accesses over all targets, including the total access time, the mean distance to the eye of the storm over all accesses for each target, delta-V used, and whether the eye is in view for any of the accesses. The maneuver type used is shown next to the delta-V used (raising or lowering maneuver). As discussed in Chapter 2 and by McGrath et al., there is no solution available

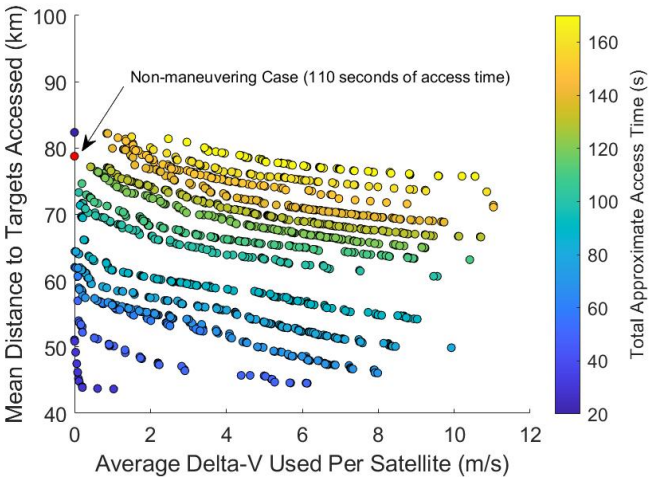

Figure 3-3: Non-dominated set of solutions for 2-satellite constellation.

within the solution space, with the thrust available, no maneuver combination enables a flyover of the second target [50]. Therefore, the satellite simply propagates through this maneuver period for the second target. This approach can be adjusted to fit a user's needs; for example, if one prioritized a full view of the eye of the storm, the solution space could be further constrained to only include passes closer than 80km. The graph theory result, presented in Chapter 2 Table 2.8, had a mean access distance of around 89 km, using 2 m/s delta-V, and had 70 seconds of total access time. This solution produced by the optimization uses slightly more delta-V than the graph theory approach, but with greater total access time and a slightly closer mean distance.

Multiple Satellite Case

The same analysis was conducted for a two-satellite case. The non-dominated set of solutions is shown in Figure 3-3. Similar trade-offs to those shown in Figure 3-2 exist, and it is clear that a multiple satellite case inherently has better performance, including naturally closer passes. Note that the x-axis displays the average delta-V usage across the satellites rather than the total usage.

Again, a sample solution is shown in Table 3.2. The maneuver type, as well as which satellite is maneuvered (1 or 2, beginning at 0 deg RAAN and 20 deg RAAN

Table 3.1: Sample comparison between non-maneuvering and maneuvering single satellites.

Target	Non-maneuvering			
	Delta-V (m/s)	Total Access Time (s)	Mean Access Distance (km)	Eye in View?
1	-	10	83.96	No
2	-	-	-	-
3	-	10	86.28	No
4	-	10	83.15	No
5	-	20	82.37	Yes
Summary	0 m/s	50 s	83.94 km	-

Target	Maneuvering			
	Delta-V (m/s)	Total Access Time (s)	Mean Access Distance (km)	Eye in View?
1	0.87 (lower)	20	96.39	No
2	-	-	-	-
3	1.11 (lower)	20	86.98	Yes
4	0.04 (lower)	30	88.45	Yes
5	0.40 (lower)	30	82.03	Yes
Summary	2.43 m/s	100 s	88.46 km	-

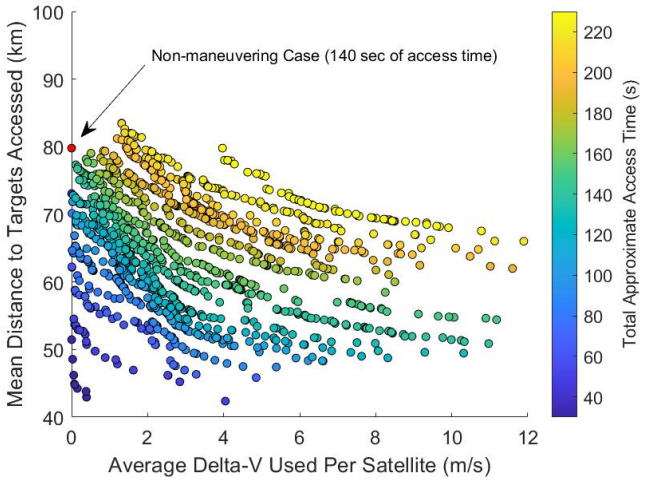

Figure 3-4: Non-dominated set of solutions for 3-satellite constellation.

respectively) is shown next to the delta-V. If multiple satellites are maneuvered, the delta-V for each satellite is shown along with the maneuver type for each satellite. As mentioned for the single satellite case, a pass of the second target is still not achieved, and a pass within 80km of the first target is still not possible in the constraints. Again, the best possible performance of this case includes viewing 4 targets, and achieving at least one view of the eye for 3 of those targets. However, the two satellite case shows heavily increased accesses of the third, fourth, and fifth target due to the addition of the second satellite.

Finally, the optimization was conducted with three satellites, and the non-dominated set of solutions is shown in Figure 3-4. As is clear in the figure, three satellites inherently perform better than the 1- or 2-satellite case, having a greater number of chances of accesses. Closer passes of the targets naturally occur, with greater total access time possible. With increasing satellites though, there is a sense of diminishing returns. the improvement from a single-satellite case to the 2-satellite case is much more significant than the performance between the 2- and 3- satellite case (in terms of closer accesses in particular), as shown in Figure 3-5. There is still a large improvement in the total approximate access time, increasing across all three cases, so depending on user priorities, an increase in number of satellites may still be desirable.

With the addition of the third satellite, all targets are in view in both maneuvering

Table 3.2: Sample comparison between non-maneuvering and maneuvering constellation of 2 satellites.

Target	Non-maneuvering			
	Delta-V (m/s)	Total Access Time (s)	Mean Access Distance (km)	Eye in View?
1	-	10	83.96	No
2	-	-	-	-
3	-	10	86.28	No
4	-	40	59.16	Yes
5	-	50	76.75	Yes
Summary	0 m/s	110 s	78.77 km	-

Target	Maneuvering			
	Total Delta-V (m/s)	Total Access Time (s)	Mean Access Distance (km)	Eye in View?
1	0.90 (lower, 1)	20	96.48	No
2	-	-	-	-
3	1.88 (lower, 1)	30	89.23	Yes
4	1.93 (1.69, lower, 1) (0.28, raise, 2)	60	63.56	Yes
5	0.23 (0.15, lower, 1) (0.08, lower, 2)	60	76.34	Yes
Summary	4.94 m/s	170 s	81.40 km	-

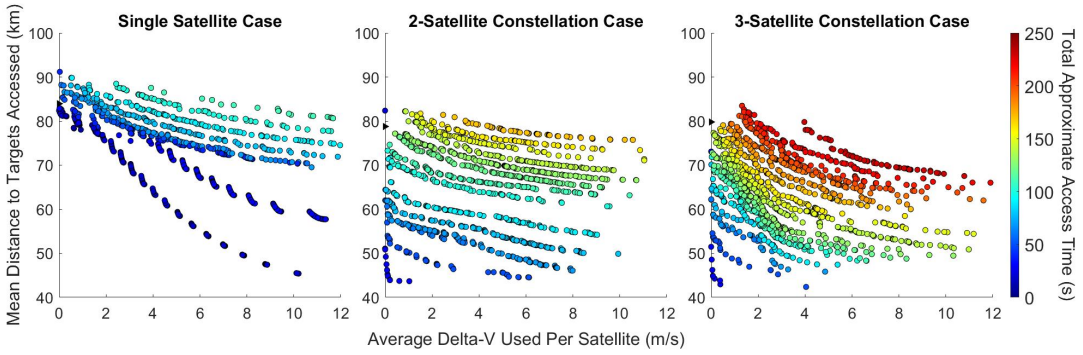

Figure 3-5: Non-dominated sets of solutions for all evaluated cases.

and non-maneuvering cases, as shown by the sample solution in Table 3.3. Again, the total delta-V is broken down into the delta-V used for each satellite and the maneuver type for each is listed. The third satellite added (at 40 deg RAAN) achieves an access of the first target late in the viewing window, and achieves access of the second target as well. In the non-maneuvering case, all targets are in view, and only the fourth and fifth target are viewed within 80km. However, in the sample maneuvering case shown below, a view of the eye is possible at all five target locations within the desired time window.

In summary, this exploration has confirmed that this method of optimization can be used, with single- or multiple-satellite cases, to find low delta-V solutions for increased access time and closer passes of targets along a mobile target track are possible. In the case of a single satellite, less than 2.5 m/s delta-V doubled the total approximate access time in comparison to a non-maneuvering case. This method of exploring the space through multiple objectives has also exposed distinct trade-offs in the design space of mobile target tracking through low thrust maneuvers. The trade between access time and distance to the target is one example.

Figure 3-5 displays the solutions across single- and multiple- satellite cases. This clearly demonstrates a trade-off between choosing increased maneuverability and increased numbers of satellites. More coverage is naturally possible with increased number of satellites. So, there is a sense of diminishing returns and the advantage of maneuverability fades. Legge [39] has explored this in part, and more exploration is needed for the particular case of mobile target tracking.

Table 3.3: Sample comparison between non-maneuvering and maneuvering constellation of 3 satellites.

Target	Non-maneuvering			
	Delta-V (m/s)	Total Access Time (s)	Mean Access Distance (km)	Eye in View?
1	-	30	85.55	No
2	-	10	83.54	No
3	-	10	86.28	No
4	-	40	59.16	Yes
5	-	50	76.75	Yes
Summary	0 m/s	140 s	79.96 km	-

Target	Maneuvering			
	Delta-V (m/s)	Total Access Time (s)	Mean Access Distance (km)	Eye in View?
1	2.06 (0.90, lower, 1) (1.17, raise,3)	50	90.51	Yes
2	0.24 (lower, 3)	30	91.23	Yes
3	4.97 (lower, 1)	30	84.88	Yes
4	4.17 (3.93, lower, 1) (0.24, raise, 2)	60	59.47	Yes
5	0.47 (0.12, lower, 1) (0.34, lower, 2)	60	71.88	Yes
Summary	11.91 m/s	230 s	79.79 km	-

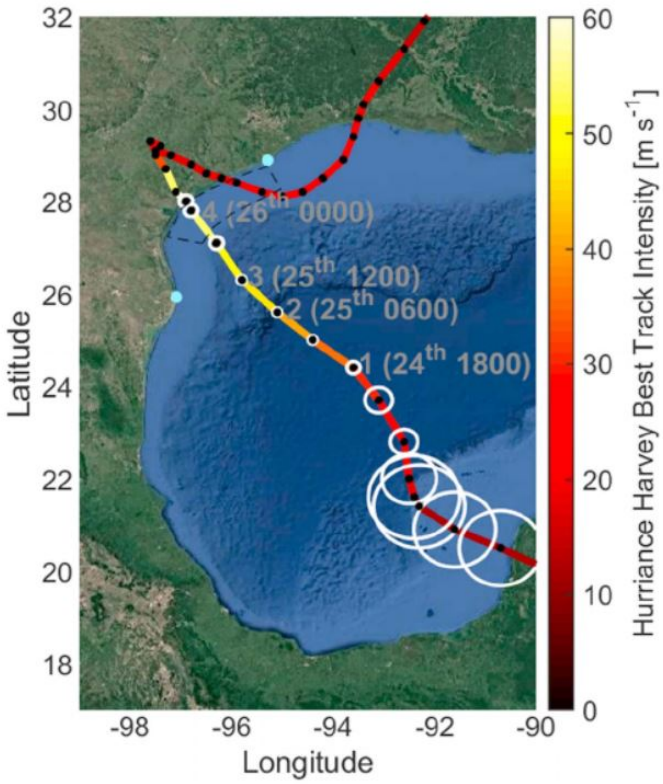

Figure 3-6: Hurricane Harvey track. The black dots show Harvey's location and the white circles show the radius of maximum wind (the distance between the center of a TC and the strongest wind band) every 6 hr [62].

3.2 Case Study: Hurricane Harvey

Hurricane Harvey was one of the deadliest hurricanes in recent times, making landfall on August 26th, 2017 [71, 62]. The storm track is shown in Figure 3-6. The storm started forming as a tropical depression, weakened, and then was reclassified as a tropical depression and on August 24th, strengthened to a category 1 [62]. Over the next 30 hours, the storm rapidly intensified, and continued intensification until it reached a category 4 storm [62]. It made landfall on the 26th of August 2017 in Texas, and maintained high windspeeds for around 6 hours, after which it dropped in intensity [62].

Five targets were selected along the hurricane track as shown in Table 3.4 [57]. Note that this sets the first target prior to its official classification as a tropical depression or tropical storm. In reality, this first target may be more likely placed

Table 3.4: Hurricane Harvey eye locations at 2.5 day intervals. [57]

Date and Time	Days Since Epoch	Latitude (deg)	Longitude (deg)
16 Aug 2017 06:00 UTCG	2.5	13.7	-45.8
18 Aug 2017 18:00 UTCG	5	13.2	-62.2
21 Aug 2017 06:00 UTCG	7.5	15.7	-80.5
23 Aug 2017 18:00 UTCG	10	21.6	-92.4
26 Aug 2017 06:00 UTCG	12.5	28.2	-97.1

around the 18th or so, when TC was categorized as a tropical storm. The succeeding weakening and then rapid intensification of the TC presents an interesting topic for future analysis - at what time are these TCs considered a significant threat, such that a maneuverable satellite should begin utilizing resources to monitor them?

The epoch time for the satellites was set at 8/13 18:00 UTC. As before, the same multi-objective optimization as described in Section 2.2 was carried out for a single satellite as well as 2- and 3- satellite constellations. Again, the non-dominated solution sets will be displayed for each case, and sample solutions will be discussed to describe the nature of the solutions.

3.2.1 Results

Single Satellite Case

Initially, the Hurricane Harvey single satellite results appear much more sparse than those shown for Typhoon Megi. As can be seen in Table 3.5, the non-maneuvering satellite only can view the third target. The low-thrust maneuvers can only adjust so much from this initial state, and therefore, only few opportunities for better performance can be identified in Table 3-7. As mentioned, a 'complete' pass of a target, following along the diameter of the FOV, has a duration of less than 30 seconds. Therefore, in a simulation with a 10 second time step, a single access duration for a single satellite and single target will at most be 30 seconds.

Some potential solutions, lowest in the plot, maintain the original 20 second access of the third target but offer a closer flyover of the target. The next line of solutions of 30 second total access time again shift this slightly to achieve a longer flyover.

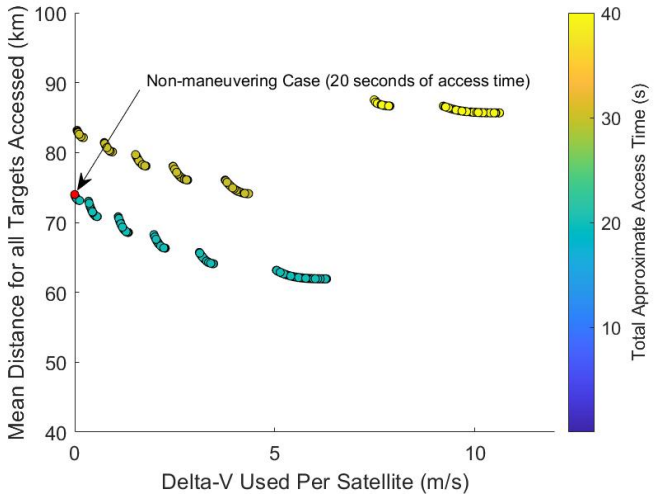

Figure 3-7: Non-dominated set of solutions for single satellite case.

The upper most family of solutions in the upper right of the plot display an option of achieving two target accesses (the third and fifth target), but with much greater delta-V required. One of these is chosen as a sample solution displayed in Table 3.5.

Multiple Satellite Case

Next, a second and third satellite will be introduced. First, the solutions from the 2-satellite case will be shown. This includes an additional satellite initiated at epoch, shifted by +20 degrees RAAN, with all other orbital elements held constant.

As seen in Table 3.6, a second satellite offers more opportunities for target accesses. The second satellite offers natural accesses of the fifth and first target in addition to what is shown by the original satellite. All accesses available allow the satellite to have the full eye of the storm in view.

While maneuvering solutions increase possible access time and offer ways to decrease the mean distance to all targets, there are still no accesses of the second or fourth target available. So, if one only desired having accesses of the eye of the storm, there is not significant improvement available through maneuvering for the two satellite case.

Finally, a 3-satellite case is considered. The non-maneuvering case as shown in Figure 3-9 performs fairly well in comparison to the surrounding maneuvering solutions,

Table 3.5: Sample comparison between non-maneuvering and maneuvering single satellites.

Target	Non-maneuvering			
	Delta-V (m/s)	Total Access Time (s)	Mean Access Distance (km)	Eye in View?
1	-	-	-	-
2	-	-	-	-
3	-	20	73.88	Yes
4	-	-	-	-
5	-	-	-	-
Summary	0 m/s	20 s	73.88 km	-

Target	Maneuvering			
	Delta-V (m/s)	Total Access Time (s)	Mean Access Distance (km)	Eye in View?
1	-	-	-	-
2	-	-	-	-
3	4.44 (lower)	30	74.15	Yes
4	-	-	-	-
5	5.62 (lower)	10	97.32	No
Summary	10.06 m/s	40 s	85.73 km	-

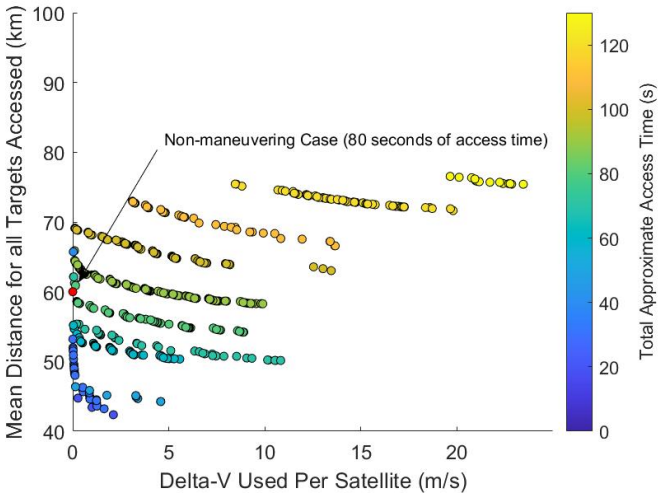

Figure 3-8: Non-dominated set of solutions for 2-satellite case.

Table 3.6: Sample comparison between non-maneuvering and maneuvering constellation of 2 satellites.

Target	Non-maneuvering			
	Delta-V (m/s)	Total Access Time (s)	Mean Access Distance (km)	Eye in View?
1	-	30	52.71	Yes
2	-	-	-	-
3	-	20	73.88	Yes
4	-	-	-	-
5	-	30	58.66	Yes
Summary	0 m/s	80 s	61.75 km	-

Target	Maneuvering			
	Delta-V (m/s)	Total Access Time (s)	Mean Access Distance (km)	Eye in View?
1	2.86 (raise, 2)	30	46.52	Yes
2	-	-	-	-
3	3.48 (0.17, lower, 1) (3.31, raise, 2)	30	88.17	Yes
4	-	-	-	-
5	0.24 (lower, 2)	30	73.39	Yes
Summary	6.58 m/s	110 s	69.85 km	-

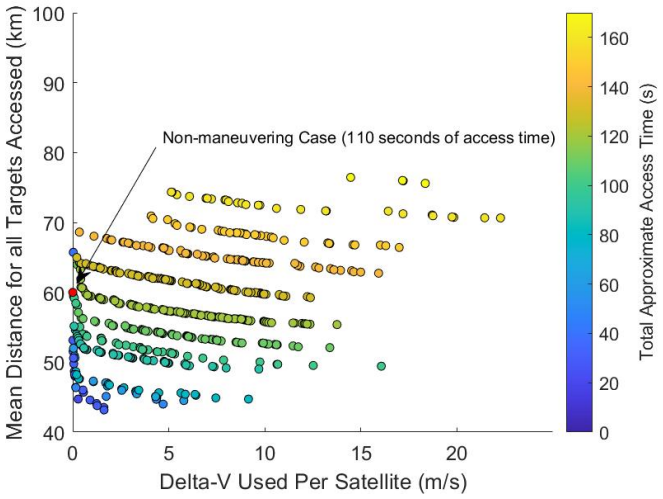

Figure 3-9: Non-dominated set of solutions for 3-satellite case.

as in Figure 3-8, with a fairly long total access time and close passes. Maneuvering solutions which perform better offer increased access time at the sacrifice of longer distances to the targets.

This is reflected in Table 3.7, as the sample solution with only a few m/s delta-V only increases the total access time without offering closer accesses. The addition of the third satellite allows for accesses of the fourth target, but the second target still remains unavailable within the maneuver constraints.

3.2.2 Forecasted Model: Single Satellite Case

Finally, the use of forecasted data will be discussed. As described in Chapter 2, this will be conducted by feeding the forecast track to the model every two days. This data is sourced from a number of different models, averaged together, all represented from the THORPEX Interactive Grand Global Ensemble (TIGGE) Model Tropical Cyclone Track Data [4]. This creates a singular set of possible latitude and longitude points to represent expected storm track locations. Collapsing this dataset for use here is a rather large assumption, as there is an associated uncertainty with each individual point in the model, and therefore with averaged set as well. However, this can offer a first glance at how one may use this mobile target tracking method in true operations, and offer insight into how the method should be adjusted for use with

Table 3.7: Sample comparison between non-maneuvering and maneuvering constellation of 3 satellites.

Target	Non-maneuvering			
	Delta-V (m/s)	Total Access Time (s)	Mean Access Distance (km)	Eye in View?
1	-	30	52.71	Yes
2	-	-	-	-
3	-	20	73.89	Yes
4	-	30	52.86	Yes
5	-	30	58.66	Yes
Summary	0 m/s	110 s	59.53 km	-

Target	Maneuvering			
	Total Delta-V (m/s)	Total Access Time (s)	Mean Access Distance (km)	Eye in View?
1	0.29 (lower, 2)	40	66.37	Yes
2	-	-	-	-
3	2.78 (lower, 2)	30	76.11	Yes
4	0.17 (lower, 3)	40	67.53	Yes
5	0.71 (lower, 2)	30	56.20	Yes
Summary	3.94 m/s	140 s	66.55 km	-

Table 3.8: Non-maneuvering satellite results for Typhoon Megi Case Study by Morgan

Target	Non-maneuvering (True Storm Track)					
	Date	Time UTCG	Eye Latitude (deg)	Eye Longitude (deg)	Distance from center of FOV to eye (km)	Eye in View?
1	10/14/2010	12:58	13.2	138.5	86.57	Yes
2	-	-	-	-	-	-
3	-	-	-	-	-	-
4	-	-	-	-	-	-
5	10/23/2010	19:10	25.0	118.0	62.07	Yes

this forecasted data.

The same general process as with the true storm track described in Chapter 2 will be followed, with the nondominated set being examined for each maneuver option for the next series of targets. This will reveal possible families of solutions and then a solution will be selected from these results. Now, for this particular case of Typhoon Megi, the model will begin at 10/13/2010 0:00 UTC, the first date and time at which the forecast is available. This will mark the beginning of the first maneuvering period. Initially, targets will be set 2 and 4 days out from this time, at 10/15/2010 0:00 UTC and 10/17/2010 0:00 UTC. A solution will be selected from these results, and the satellite will maneuver through the time of the first target, at which point a new set of forecast data will be used to generate the next target locations. This hypothetically ensures the first maneuver is chosen with consideration for where the storm may be in the future, as far out as forecasts typically provide with relative confidence.

In the case of the non-maneuvering satellite, only the first and fifth of these planned targets are available for possible accesses. This is true across the predicted and true storm track, as shown in Table 3.8 and Table 3.9; this is not a consequence of a poor forecast. So, this does not necessarily indicate promising target viewings when maneuverability is added.

Some solutions were found for the first maneuver, which began at the model start time. From this state, only the first of the two targets evaluated can be successfully accessed within the constraints of the optimizer. Notably, this means that something

Table 3.9: Non-maneuvering satellite results for Typhoon Megi Case Study by Morgan

Target	Non-maneuvering (Predicted Storm Track)					
	Date	Time UTCG	Eye Latitude (deg)	Eye Longitude (deg)	Distance from center of FOV to eye (km)	Eye in View?
1	10/14/2010	12:58	13.6	137.8	29.2	Yes
2	-	-	-	-	-	-
3	-	-	-	-	-	-
4	-	-	-	-	-	-
5	10/23/2010	19:10	23.4	118.5	37.7	Yes

similar to the 'greedy solution' as described in Chapter 2 is approached. With only one target of the next two available to the satellite, the optimizer simply provides the best-performing solutions for this target, and propagates through the second target period. While the multi-objective nature of the optimization does offer a range of possible solutions in comparison to the originally discussed 'greedy solution', it still eliminates consideration for future storm location.

From this non dominated set shown in Figure 3-11a, a solution was selected and the first maneuver in this set was executed, with the viewing window for the satellite concluding a bit after 10/15/2010 0:00 UTC. Then, the next set of solutions was generated from that point. In this case, no solutions were found for the second or third maneuver period (starting at 10/15 and 10/17 respectively), and so the satellite simply propagated forward for these cases. Options exist for the fourth and fifth maneuver period, as shown in Figure 3-11b and Figure 3-10c, resulting in a possible access of the fifth target. So, in this case, the added maneuverability does not result in increased number of target accesses, but provides possible options for future alternative accesses.

Ultimately, this optimization alone may not perform well in this particular case. There are several ways to address this. One option is to adjust the possible targets; as forecasted data is updated every 12 hours, one can simply determine if a non-maneuvering satellite would have an access or a near-access at each update, rather than having evenly spaced targets. Target selection could be included as a part of

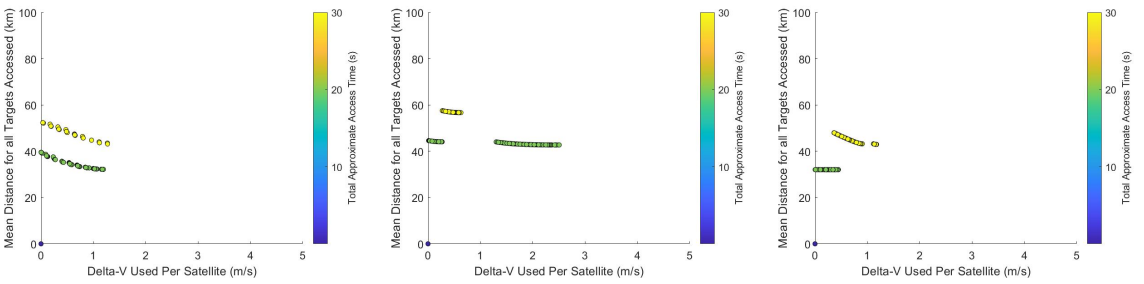

(a) First maneuver options (10/13/2010 0:00 UTC)

(b) Fourth maneuver options (10/19/2010 0:00 UTC)

(c) Fifth maneuver options (10/21/2010 0:00 UTC)

Figure 3-10: Non-dominated sets for single satellite case using forecasted track, start dates of simulations shown in parentheses.

an outer optimization, determined internally to the model rather than an external input. This would create a more adaptive approach, suitable for uncertain targets, and offers another level of control to a future user. This is a rich area for potential future work.

Alternatively, if these evenly space targets are desired, this can be used to set requirements for the satellite system. This could require an increase in number of satellites to achieve better possible accesses, or increasing propulsion system performance. In this case, with the closest non-maneuvering pass for targets 2-4 being around 250km, the propulsion system would need to produce an order of magnitude more thrust (increasing from around 0.35mN to 7mN) to allow target accesses.

Finally, it is important to note that, in general, this method of optimization may not be the most suitable for use with forecasted data. This is due to the fact that the optimization is being performed upon little data; essentially maneuvers involving only 30 second passes are being optimized as though there is complete certainty in the results, when in reality there is a level of uncertainty present in each storm location.

To mitigate some of these issues present with using precise optimization for an uncertain set of targets, robustness should be included in the analysis. A robust solution is defined as "one that performs well across a variety of possible future states of a system" [10]. However, there is an associated price of robustness, as any robust solution is not typically ideal for any particular individual scenario [10]. Robust decision making practices in general involve testing solution alternatives over

a number of plausible scenarios, attempting to account for the uncertainty present in the model [10].

There are a variety of levels of uncertainty; a forecasted storm with models from multiple sources would likely fall under a so-called 'Level 4' uncertainty, where a multiplicity of possible future exist [82]. This would be what is called a 'deep uncertainty' which may result from uncertain future events that cannot be well-characterized [73]. There are different methods of incorporating robustness against these uncertainties into optimization. Many-objective robust decision making (MORDM) and generally robust optimization techniques may be useful for the variety of problem at hand[73]. MORDM involves the same kind of multi-objective search of the solution space as described prior, with additional evaluation of possible solutions under deep uncertainty [73] [10]. There are many different ways to characterise robustness of solutions generated, through robustness metrics, measuring system performance over a set of future states of the system in a number of different ways [52]. For example, in this particular case, the mean predicted storm track could be used as the nominal future state, and then predicted tracks from individual models could be used to test this result.

3.3 Conclusions

It is confirmed through this preliminary exploration that for relatively low amounts of delta-V, satellites can be slightly maneuvered to gain better quality and quantity of accesses along a hurricanes track, as proposed by McGrath et al. This particular methodology of utilizing multi-objective optimization reveals particular tradeoffs, as an enhancement to [50]. This evaluation of the design space can be especially useful to decision makers; for example, a greater number of accesses may be more vital in certain applications like early in a hurricane's lifetime [1] but a closer pass may be more important for high resolution data-gathering. This difference between shorter passes and longer passes, is demonstrated in Figure 3-11. This prioritization can be used in conjunction with the non-dominated sets of solutions to select an ideal set of

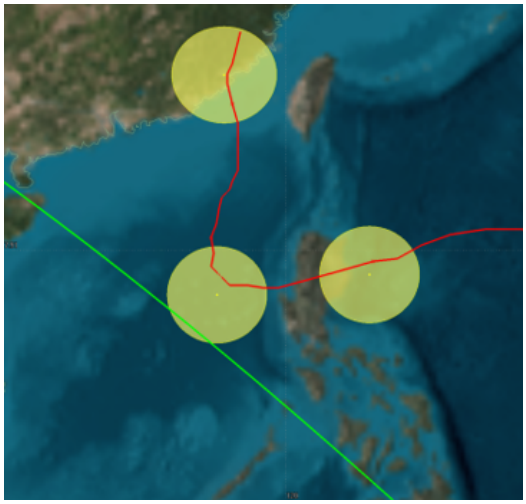

(a) A shorter pass with the target along the of edge of the field of view.

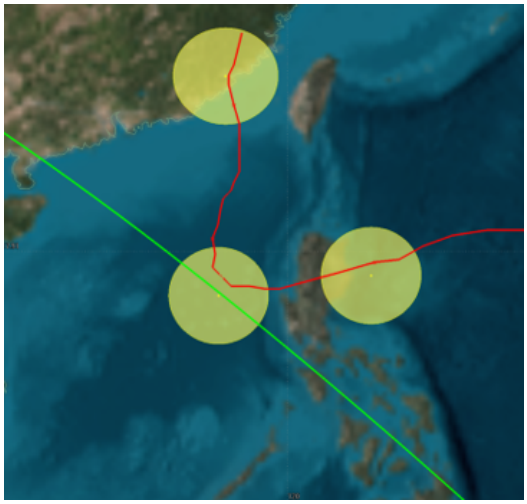

(b) A longer pass with the target along the center of the field of view.

Figure 3-11: Different possible target accesses, with the targets shown in yellow with a 200km access distance and satellite passes shown in green.

maneuvers.

It is also clear in the non-dominated sets that particular families of solutions exist, as shown by the groupings of designs in each plot. Additionally, the continuous design space exploration allows for other maneuver opportunities not otherwise seen in the graph theory formulation. By displaying the success of this low-thrust maneuver methodology on an additional case study, the validity of the method is further confirmed.

One significant note to make is that the orbit used for the Typhoon Megi case was preselected as a relatively convenient orbit, allowing for some storm accesses in the non-maneuvering case [50]. In the event that a satellite is completely out of phase with desired targets (i.e. not having some accesses in the non-maneuvering case), successful solutions may require a significantly greater amount of delta-V, or may simply be unachievable within the constraints given. For example, both in the Typhoon Megi and Hurricane Harvey case, at least one target was inaccessible in the time constraints of the problem in the single satellite case. Multiple were unavailable in the Hurricane Harvey case. Therefore, it is important to consider the initial orbit of the satellites as the low-thrust maneuvers over the short time scales considered

can only adjust the expected SSP by so much. Ideally, this would fit into the larger ReCon concept as an additional adjustment to a ROM orbit.

The two hurricane case studies discussed offer an initial insight into the usefulness of this mobile target tracking method with optimization and some tradeoffs of the resulting solutions. There is an opportunity to further explore this with different mission scenarios (satellite initial conditions, hurricane tracks, etc.) and different objectives. For example, one might desire simply more targets to be visited rather than the total access time. There are numerous areas yet to be explored in this solution space. Throughout the work involved with this thesis, the code required to perform this mobile target tracking method with optimization for different mission scenarios has been compiled and is publicly available (Appendix B). A tool form of this code can be developed to streamline future testing, allowing a user to input mission scenarios and view the nondominated set of solutions as the output. A potential tool set-up is displayed in Figure 3-12, and the development of this tool is likewise stored as referenced in Appendix B.

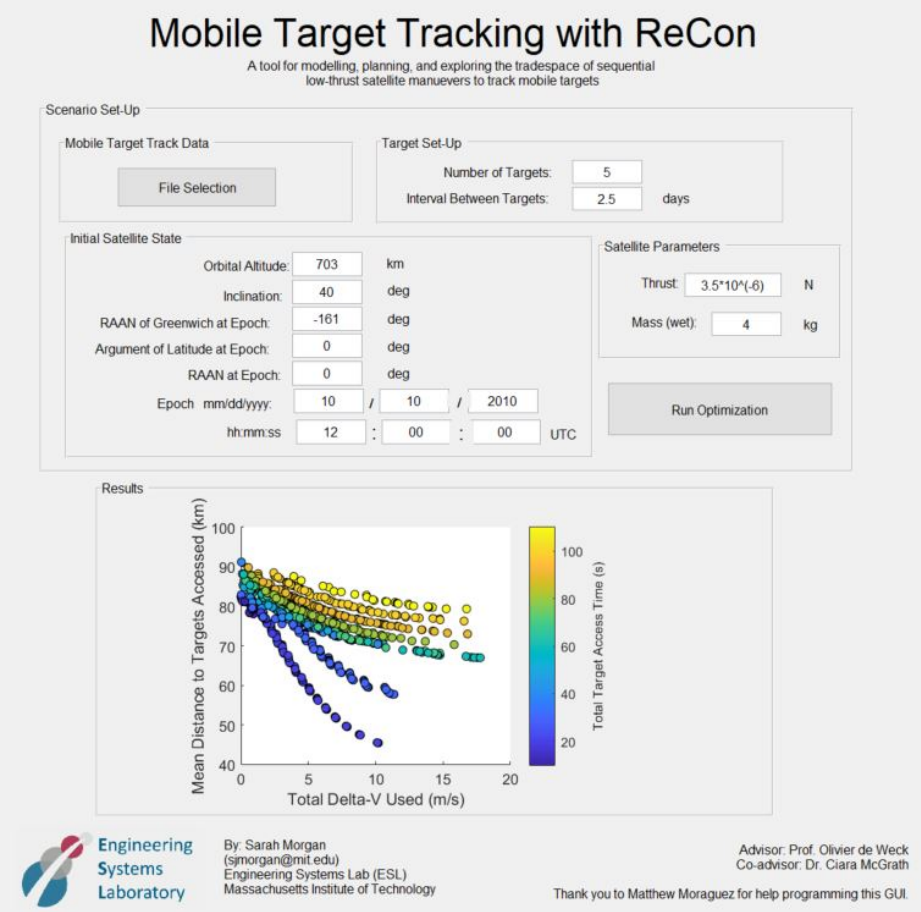

Figure 3-12: Tool GUI mock-up.

Chapter 4

ReCon Demonstrator (ROAMS) Considerations

4.1 ROAMS Mission Summary and Considerations

4.1.1 ROAMS Mission Motivations

There is an effort currently ongoing at MIT to explore the reality of the ReCon concept and propose intermediate de-risking missions before fully implementing an entire 20-30 satellite constellation. A couple of intermediate missions have been identified, all under the larger category of a ROAMS (Reconfigurable On-orbit Adaptive and Maneuverable Spacecraft). First, a propulsive payload would be used on a shared Cube Satellite (CubeSat) mission. This payload version of ROAMS would allow for the proving-out of the reconfiguration in a relatively inexpensive and low-risk manner. Then, a larger mission of several ROAMS satellites, building off of the ROAMS payload, could demonstrate coordinated reconfiguration among a small 'constellation' and emphasize the findings of the payload mission. These two concepts of increasing scope has been developed throughout the MIT 16.851 and 16.89 courses and are ongoing projects. The ROAMS payload mission has been the most developed thus far, with initial design and prototyping performed. This payload mission will be the focus of the following section, and further references made to the ROAMS mission are to

this preliminary demonstrator payload.

Overall the proposed ROAMS mission places the ReCon concept in the real world, by testing out the main principles of the concept on a small, inexpensive scale with a single CubeSat demonstrator; this can enable future missions to utilize the ReCon concept with lower risk. It also allows for the exploration of key concepts ignored in the ideal environment of simulation, where the ReCon concept has been largely explored until now. This presents new challenges. Certain orbits can be rather crowded, especially in LEO where the ReCon concept has been explored and where most inexpensive and convenient launch opportunities are available. Therefore, hurdles include maneuver planning in the context of other satellites and debris which may lead to less-than-ideal maneuver opportunities impacting performance. Additionally, maneuvers will not be exact; considerations must be made for the precision of propulsion systems available including maneuver timing and accuracy. This can lead to the satellite arriving in a slightly different orbit than originally intended as well, which will impact performance and future maneuver options. In the following sections, the existing mission design will be discussed and existing uses of CubeSat propulsion will be explored to better contextualize this demonstrator. The chosen propulsion system presented will then be evaluated for a potential mission involving RGT orbits and then a mobile target tracking mission will be planned using this proposed ROAMS demonstrator.

4.1.2 ROAMS Mission Design

One of the primary methods to de-risk this variety of mission is prove the ability of a small satellite to perform the maneuvers described in an RGT ReCon architecture. This would involve moving from one orbit to an RGT (or simply another orbit) within a certain tolerance, achieving better localized revisit for a ground target for a time period in the RGT, and being able to return to the original orbit. This would simulate the GOM to ROM and ROM to GOM return of a larger constellation. The proposed design reference mission involves a launch to the ISS, deployment and transferring into a 'GOM'-type nominal orbit, calibration, observation, and then maneuvering into

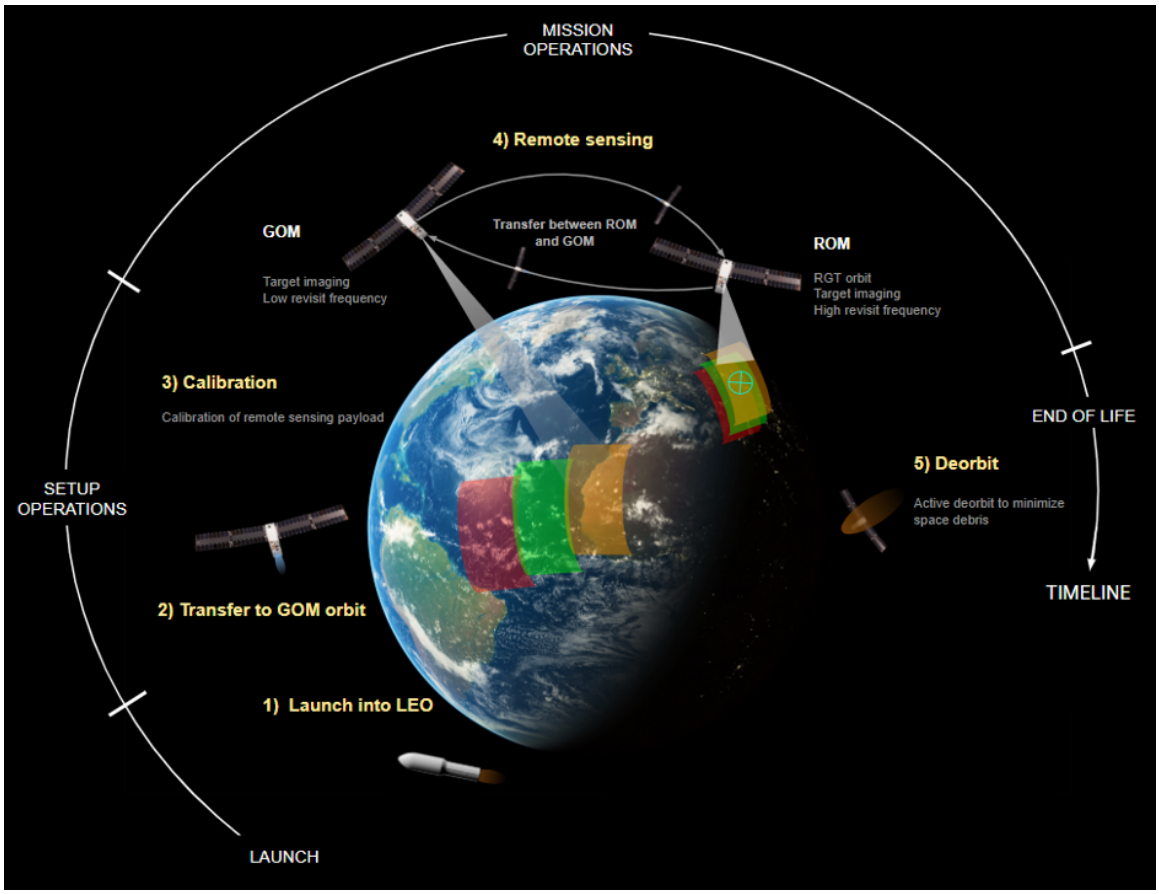

Figure 4-1: ROAMS concept of operations *[MIT 16.89 Students (Spring 2021 PDR)]*.

an RGT orbit (simulating ROM) over a target of interest, as shown in Figure 4-2.

Similar to the ReCon concept, this maneuver to an RGT may utilize the relative RAAN drift of a third orbital altitude. The spacecraft would return to the original nominal orbit and the maneuver, observation, and return process would repeat throughout the mission duration until the satellite runs out of fuel. The target of interest would not be planned ahead of launch, meaning that the spacecraft would have to respond in real time, simulating a ReCon-type response; however, given the low amount of delta-V available on a payload of a CubeSat, the target possibilities may be restricted by feasibility.

The payload is nominally 2U (20cm x 10cm x 10cm) in volume, and would include a propulsion module, a remote sensing module, and the necessary on board computer to control each. Possible remote sensing options are under consideration for various

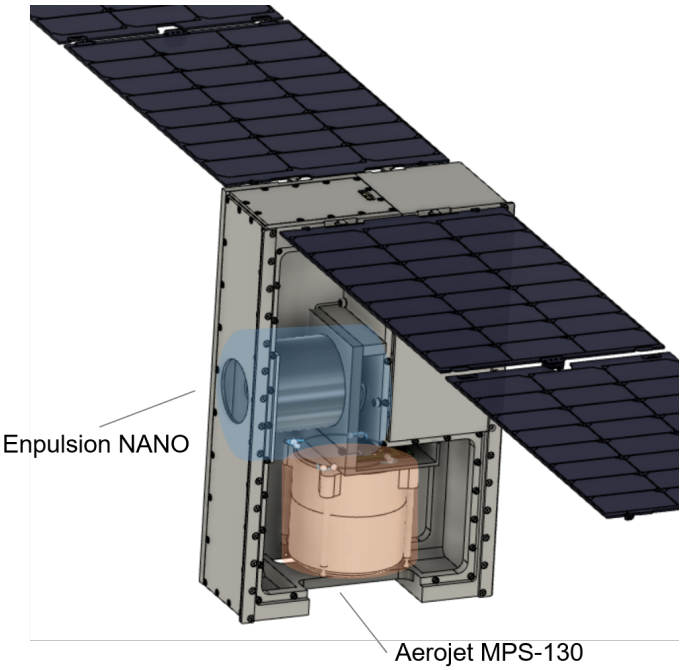

Figure 4-2: ROAMS CubeSat configuration *[MIT 16.89 Students (Spring 2021)]*.

mission stakeholders (microwave for TC tracking, VIS/IR for wildfire tracking, etc), however requirements of the mission emphasize ability to prove the maneuver process and improved data gathering over the targets of interest rather than the quality or variety of data itself. Based upon the requirements of the mission, the propulsion module is to include both a low-thrust and high-thrust propulsion system, meaning that both a chemical and electric propulsion system will be included on board. This approach is deemed a requirement to demonstrate hybrid capability on a small satellite. The relatively low volume of the payload ensures a wide range of potential launch opportunities in the future, assuming it will share space on a 6U (30cm x 20cm x 10cm) CubeSat, but this also severely limits the amount of delta-V available. A potential system design, determined at the time of the preliminary design review (PDR), by the students in the 16.89 course, includes the following propulsion systems in Table 4.1.

While the final system configuration has not been set in stone, assumptions can be made and system requirements can be set out to enable the planning of potential specific maneuvers for the vehicle. For example, for the above delta-V capability

Table 4.1: Propulsion System Selection *[MIT 16.89 Students (Spring 2021)]*

Propulsion System	Enpulsion Nano [77]	Aerojet MPS130 [67]
Physical Characteristics		
Dry Mass (g)	680	1060
Wet Mass (g)	900	1660
Dimensions (cm^3)	$10 \times 10 \times 8.25$	$10 \times 10 \times 10$
Propellant	Indium	ASCENT Green Propellant
System Performance		
I_{sp} (s)	2000-6000	206-235
Thrust (N)	330×10^{-6}	1
Delta-V Capability (m/s)	363-1088	104-118

calculation, an 12kg CubeSat was assumed. Throughout the courses 16.851 and 16.89, a comprehensive list of system requirements were generated based upon these preliminary design assumptions and stakeholder meetings. For example, it can be assumed that the MIT ground station will be sufficient for downlink and maneuvers can be planned around this ground station access. However, other assumptions must be considered carefully; for example, it cannot be readily assumed that thrusters can be oriented such that the thrust vector is perfectly directed through the center of mass of the spacecraft. With the small volume constraint on a 6U satellite, the positioning and orientation of these thrusters must be considered carefully, as well as any residual torques that might be introduced by thrust maneuvers about the spacecraft center of mass.

4.2 Small Satellite Propulsion Systems Background

Generally, CubeSats are very constrained in mass and volume. A 6U satellite must be 30cm x 20cm x 10cm and weigh around 8kg or so [30]. There has been a large increase in the number of CubeSats launched since the early 2000s, with an increasing number created to address needs like remote sensing and technology development [81]. However, largely these missions have not included propulsion systems [40]. As of 2017, only two missions had featured propulsion systems for technology demonstration (for uses other than attitude control) [40]. More missions have been conducted since

then, including one testing the high-thrust system the team intends on using [51]. Overall, though, there is only a small amount of flight history one can draw from when considering CubeSat propulsion options, and this generally restricts the TRL of available products. Additionally the kind of propulsion systems that may be used may be restricted by the launch system used; for example the P-POD developed by CalPoly restricts any use of solid propulsion and the amount of stored chemical energy that may be stored on board (i.e. amount of propellant) [40]. Finally, while electric propulsion systems are attractive for their higher Isp, offering higher delta-V for the same propellant storage, these systems can require high power consumption which is not easily achievable in the mass and volume constraints of CubeSats, especially in the ROAMS case where spacecraft power may be shared across multiple payloads.

Due to the low amount of available flight heritage, overall the TRL of most available systems is 8 or less, as they have only been flown at most a few times in orbit [14]. Each of the systems chosen by the MIT team (in collaboration with the Aerospace Corporation Slingshot program) have previously been flown, and performance has at least in part been validated. The Aerojet MPS-130 system, with 1N thrusters was tested on the GPIM (Green Propellant Infusion Mission) in 2019 [51]. The thrusters successfully performed perigee altitude changes with results within about 20km of the target altitude [51]. The thrusters were also successfully used for momentum management (despinning reaction wheels) and detumbling demonstrations [51]. The Enpulsion Nano, a FEEP (Field Emission Electric Propulsion) system, has also been tested in orbit, with 37 units launched by mid-2020 [77]. One of these was a 3U CubeSat, with observed change in semi-major axis aligning with the expected change based on thruster telemetry [35]. So, the ROAMS mission presents an opportunity for emphasizing the capability of these systems on-orbit but also presents a risk to overall mission performance with reduced confidence in system performance. The ROAMS mission also faces unique challenges in utilizing a couple of these propulsion systems in tandem. As this is planned to be a shared mission as well, containing other distinct modular payloads, resources will have to be shared. Particularly, power and energy management will be a concern as the electric propulsion system will take the

majority of the system power. Thermal management is a concern as well, as both propulsion systems will produce heat which could possibly affect surrounding payloads if they are not completely thermally isolated. Especially as the FEEP thruster requires heating to melt the indium fuel, the heat produced by each system requires consideration. Finally, considerations must be made for the ADACS as well; if there is an off-axis thrust, some of this may be compensated for by reaction wheels on board. Likewise, ADACS will be responsible for slewing the spacecraft for target viewing. The performance of this system will impact required performance of the propulsion system. With all of these aspects, iteration between the bus provider, other payloads, and the ROAMS team will be required to ensure the ROAMS payload is compatible and sufficiently capable to meet the larger system requirements.

4.3 Logistics of Maneuver Planning

There are several challenges to conducting the kinds of maneuvers planned for the ROAMS mission. First, these maneuvers have thus far been planned and executed in simulation with exact accuracy under particular assumptions; the errors present in maneuver execution (i.e. errors in thrust direction or magnitude) have not yet been considered. These maneuvers have assumed to be timed ideally as well. However, in an actual LEO orbit, some maneuvers may have to be delayed due to available communication windows (depending on the autonomy level of the satellite), available power levels or needs of other payloads on board (as a result of being on a shared satellite), and possibility of collision with other space debris or satellites in the planned maneuver path.

4.3.1 Error Tolerances

First, the errors within the spacecraft system itself must be considered. This system includes the ground station communicating to the satellite and the satellite itself including receiver, ADCS (attitude determination and control system), thrusters, and transmitters [72]. It is assumed that the calculations for maneuvers will be conducted

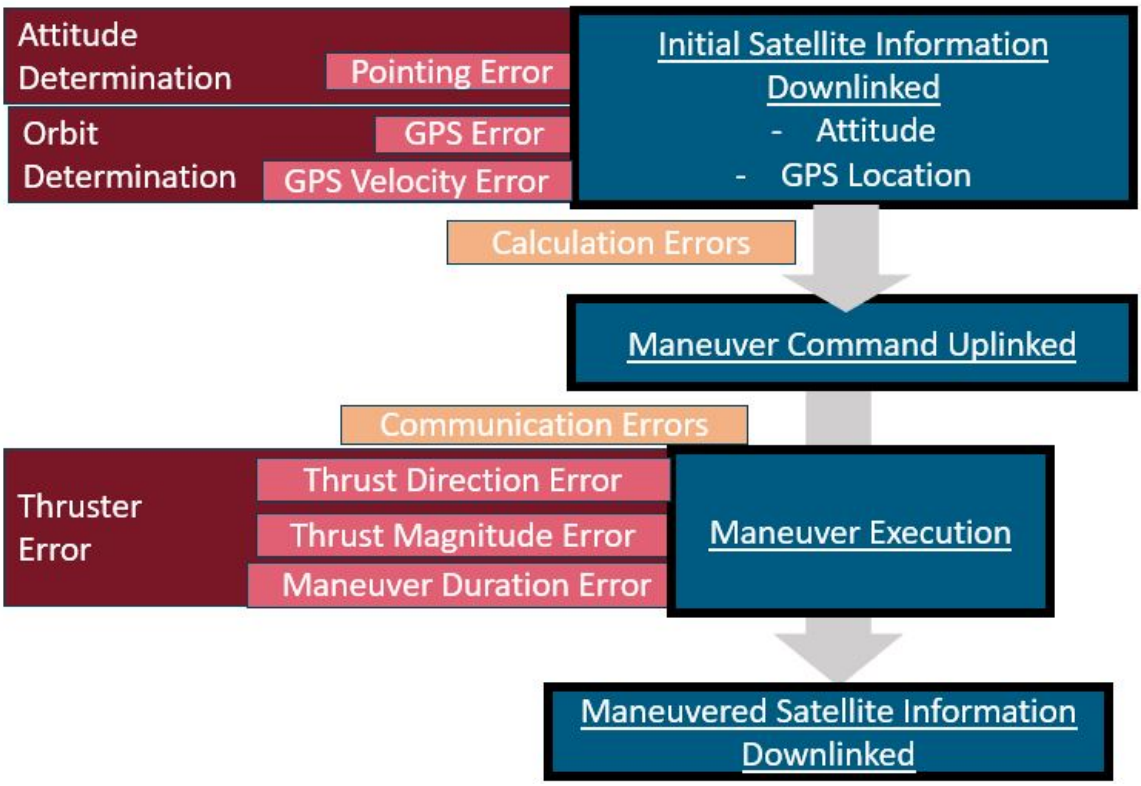

Figure 4-3: Sources of maneuver error.

on the ground and relayed to the satellite, meaning that the satellite will not be able to execute these larger decisions having a relatively low level of autonomy. Figure 4-3 shows the sequence of possible maneuver errors throughout this process- each of these sources of error should be evaluated.

First there are attitude and orbital determination issues. This relates to the pointing error and the location and velocity error of the ADCS. For example, in the case of the BeaverCube mission, where the ADCS system is comprised of a 3-axis magnetometer and a GPS receiver, the pointing error in azimuth and elevation of the satellite will be derived from the errors of the magnetometer reading, and the errors in the location and velocity will be derived from the errors in the GPS readings [72]. Both these GPS readings and magnetometer data must be downlinked to the ground station [72]. The accuracy of these measurements is based upon the exact components used and their integration. The data received can also be further processed. For example, an Extended Kalman Filter (EKF) can be used to process received measurements to

reduce statistical noise and other inaccuracies [75]. Different data sources can also augment the knowledge obtained through data downlink. Frequently TLEs (two-line elements, which describe position and velocity of the spacecraft) provided by a Combined Space Operations Center (JSpOC) shortly after deployment are used to assist CubeSat acquisition and orbit determination [66] [72]. For example, IceCube, a 3U CubeSat with the mission to obtain data on cloud ice was deployed from the ISS in 2017 and used the provided TLEs to aid in spacecraft acquisition [75]. However, the spacecraft lost contact after initial acquisition and there were persistent issues with locating the spacecraft [75]. Some issues include that the TLEs received did not line up with the GPS states downlinked and unknown spacecraft attitude, which made it difficult to predict the influence of drag on the spacecraft [75]. Depending on the needs of missions, TLEs may not be sufficient on their own. Errors in TLE generated locations can be around 4.5 km (median), and from 2 km up to 20 km (from the first to third quartile) [66]. The error varies between the direction of tracking, with the largest error in the in-track direction (when considering the local vertical local horizontal frame), and smaller error in the cross-track direction [66].

From there, the maneuver required is calculated and then this command is uplinked to the satellite. Finally the command will be executed on the satellite itself, whereby the computer and thrust determination errors must be taken into account. The thrust magnitude, direction, and duration will all have an associated error, whether derived from the thruster itself or the computer directing these commands. Errors carried throughout this sequence of operations will result in a slightly different final satellite orbit than originally intended. As seen in Chapter 3, some of these access times for target imaging are only on the order of 20-30 seconds, so that a maneuver execution timing error on the order of 10 seconds could be significant.

The thrust determination errors will be derived from the system installed. In the case of the ROAMS mission, there will be two different sets of thrust determination errors derived from each of the systems installed. Also, the method of installation and configuration of these components may influence the error. Additionally, the timing of the maneuvers as controlled by the on-board computer can also influence possible

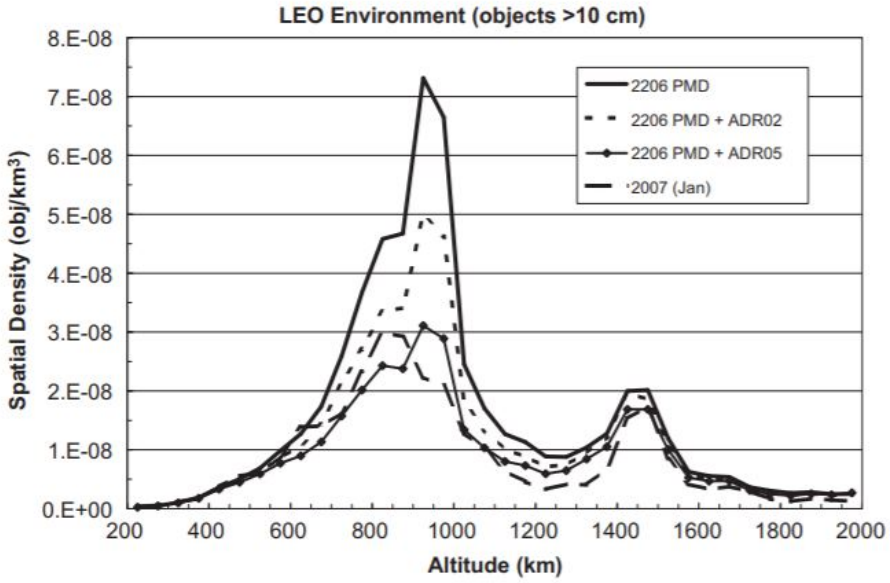

Figure 4-4: Comparison of spatial density distributions from 2007 to those projected for 2206, considering the addition of post-mission disposal (PMD) of all objects and two varieties of active debris removal (ADR02 and ADR05). [42]

thrust duration.

4.3.2 External Factors

Aside from the errors possible within the spacecraft system, the environment in LEO also influences maneuver planning. For example, when changing orbits, probability of collision with space debris and active satellites in LEO must be considered. The amount of debris is only projected to increase in coming years, however, the altitudes planned for the ROAMS mission (400km-500km range) are relatively low-risk in comparison to higher (900km or so) LEO altitudes, as shown in Figure 4-4 [41]. Broadly, the capacity of LEO is important to considered as evaluated in [8]. Multiple spacecraft may be used in future iterations of ROAMS as well, and the slotting method discussed in [8] to fix constellation spacing is noted as worthwhile for future exploration.

A simple probabilistic calculation can be performed for a rough estimate of collision probability over the satellite lifetime. Based on what has been determined for

the mission thus far, a mission lifetime of two years will be assumed. The following formula from [86] can be used

$$P_c = 1 - \exp^{-SPD \cdot A \cdot t \cdot v_{rel}} \tag{4.1}$$

where SPD refers to the spatial density of objects (m^-3), A refers to the collision cross-sectional area (m^2), t refers to mission time (s), and v_{rel} refers to the relative velocity between the satellite and object (m/s). Assuming a worst-case cross sectional area of 0.14 m^2 [28], and head-on collision at 500km altitude (15.2 km/s impact velocity and an SPD of around 0.5^{-8} objects/km^3) this results in a collision probability of $6.7 \cdot 10^{-5}$ %. Note that this is for objects greater than $10cm$. If objects greater than 3mm are considered, the SPD increases by about 300× (as projected by the MASTER-2009 space debris model for 2017) [37], so the probability of collision increases to 0.02%. It is also important to note that if higher altitude is used in LEO, this SPD could dramatically increase (Figure 4-4). One final note is that probability of collision depends, to a lesser extent, on orbit inclination [15]. Typically, collision probability is worsened for orbits with inclinations supplementary to inclinations that are crowded by debris. Highly trafficked near-polar orbits and SSO retrograde orbits therefore cause higher collision probability in higher inclinations. Therefore, orbits with inclinations lower than 60 degrees or so (such as the ISS orbit) have relatively lower collision risk.

While the probability of collision is overall low throughout a mission lifetime of one year from this evaluation, this is a non-zero threat that must be addressed. In addition, in reality, given the uncertainty of the location of each object in orbit, close passes (so called conjunctions) must be considered as well as collisions. These individual conjunction events must be considered in operations. Once the satellite is deployed in orbit, the US Combined Space Operations Center will perform conjunction assessments for active satellites and objects, so informed collision avoidance maneuvers can be conducted as necessary [79]. Any threats will be communicated

to the spacecraft operators (through a service such as SOCRATES (Satellite Orbital Conjunction Reports Assessing Threatening Encounters in Space) [86]), so satellite operators must be on-call to analyze and address these [36]. Hundreds of alerts for possible conjunctions are issued each week for typical LEO satellites, but in most cases, the risk of collision for each possible conjunction decreases as more orbital information is gathered [23]. For example for ESA satellites in LEO, about two alerts per week per satellite require a follow-up, and analysis must be conducted to fully evaluate the risk; if the probability is greater than 0.01%, action must be taken typically in the from of collision avoidance maneuvers [23]. Ultimately, for this fleet of ESA satellites, about one maneuver per year must be conducted [23]. Therefore, for the ROAMS mission, some propellant must be reserved for conducting these avoidance maneuvers, similar to reserving some propellant for deorbit at the end of satellite lifetime [79]. The currently selected propulsion systems, both having flight heritage, will likely be considered sufficiently reliable to conduct these maneuvers [79]. Depending on the exact maneuver required, ROAMS intended observations and maneuver plans will have to be reevaluated from the new satellite location.

4.4 Evaluation

Given all of this information, an evaluation will now be performed to demonstrate the projected performance of a simulated ROAMS mission. First, the currently planned CONOPS of a satellite moving from the starting (ISS) orbit to the nearest RGT orbit will be evaluated for the low-thrust system, including the uncertainty relevant to these maneuvers. This will first be conducted assuming Keplerian orbits without a RAAN change requirement, then assuming J2 perturbations and a RAAN change requirement via drift orbit (utilizing McGrath's formulas [46]). Then, the potential performance of the ROAMS mission for mobile target tracking applications will be examined; the delta-V capability of the system will be compared to what is required for the low-thrust maneuvers for mobile target tracking as discussed in Chapter 3.

As mentioned previously, there are several parameters of the spacecraft that influ-

ence the possible errors in maneuvers, including parameters of the propulsion systems, timing capabilities of the computer on board, and parameters of the ADCS system. In the case of the ROAMS mission, a 6U bus is being planned. Currently, it is assumed this bus will roughly have the characteristics of the Blue Canyon Technologies 6U bus so these bus parameters will be assumed. The aforementioned Nano Enpulsion and Aerojet MSP-130 propulsion systems are being used. The relevant characteristics of these components are included in Table 4.1.

For a preliminary evaluation, errors in communication to the satellite and the commands executed on board will be ignored. Only errors in the propulsion system (thrust timing, duration, direction, and magnitude) will be considered. Of course, in the consideration of a circular to circular orbit transfer with static targets, the precise timing of the maneuver will not have an impact on the final orbit, simply the exact location of the satellite in the final orbit. This, however, could have an adverse effect when observing mobile targets as previously discussed, as the mean anomaly shift caused by imprecise timing may cause future passes to be poorly timed.

If the satellite is maneuvering with the low thrust system, a spiral transfer from the ISS orbit (440km altitude) to that of the RGT (497 km) will be conducted. Based upon the in-flight results of [35], the average thrust recorded for the 30 minute operation of the propulsion system was around 0.2212+/- 0.0033 mN. In this test as well, the attitude control system did not maintain attitude during the burn, leading to only 82% of the total thrust force being used or about a 35 degree off-axis angle. Assuming the spacecraft will have operational ADACS throughout system burns, and that the spacecraft will have at least the performance level of the aforementioned BeaverCube (another student-led project at MIT), a worst-case 15 degree pointing error will be assumed [72] with the off-axis thrust produced compensated for by ADACS. So, in this case, an error range of +/- 15 degrees thrust direction, +/-60 seconds thrust duration, and +/- 0.0033 mN thrust magnitude (0.2212 mN nominal) will be considered. These are simply sample errors; the exact range of these will depend upon the bus used and exact component configuration and installation which at this time is not certain. The impact of these errors independently on final orbit

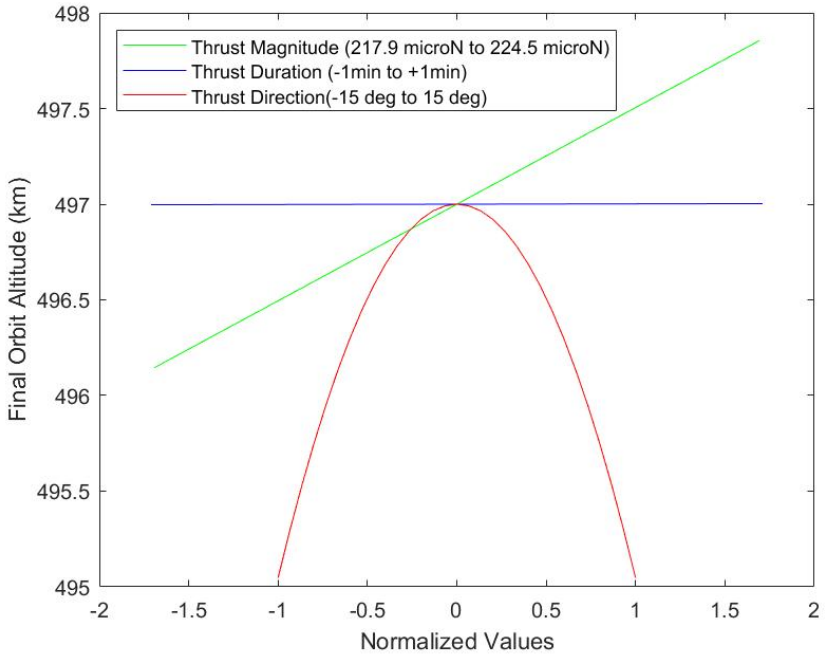

Figure 4-5: Final orbit altitude resulting from various individual errors.

altitude are shown in Figure 4-5.

It is clear the angle difference has the largest impact, but ultimately, from each factor individually, the difference in final altitude is only off by $2km$. Of course, in reality these factors may compound. A random sampling of errors from each of these factor ranges leads to the final altitude as shown in the histogram of 100,000 runs in Figure 4-6, with a mean value of 496.35km, just a bit below the intended altitude.

A worst case scenario is ending up at around 494km, or only about 3km off the nominal altitude. This is close to the uncertainty in GPS measurements (+/- 5km) [35] so depending on the orbit determination, this difference may not even be apparent. When looking at the ground track resulting from this slight altitude difference in Figure 4-7, it is clear the ground track does not quite repeat as intended. The impact of this difference will depend upon the FOV of the satellite, target size, and viewing duration. Additionally, if the target is being viewed for a sufficiently long period, such that the reliability of the ground track can be evaluated, a small correction maneuver could be executed to rectify the orbit altitude. For further analysis, effects of drag and J2 perturbations should be included.

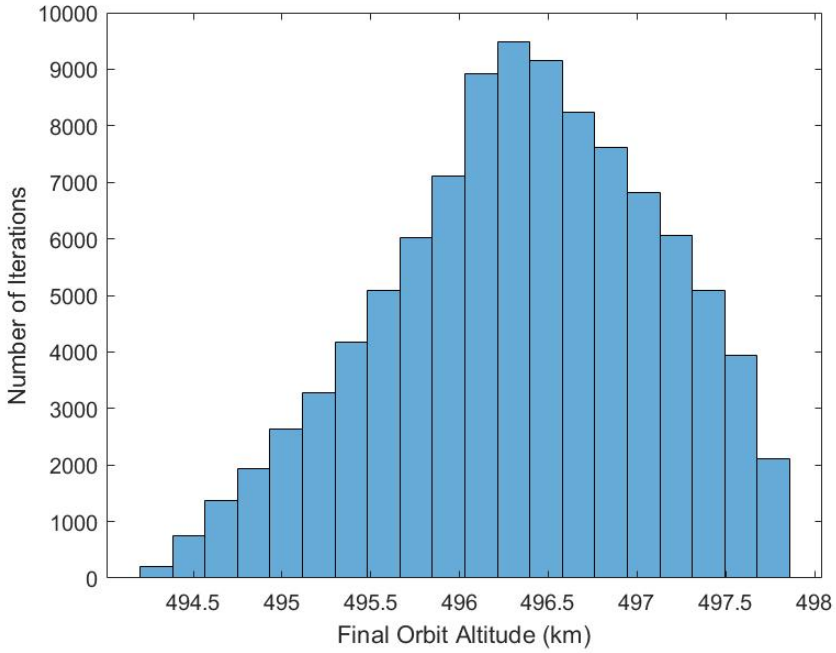

Figure 4-6: Final Orbit Altitude Resulting from Various Errors Combined.

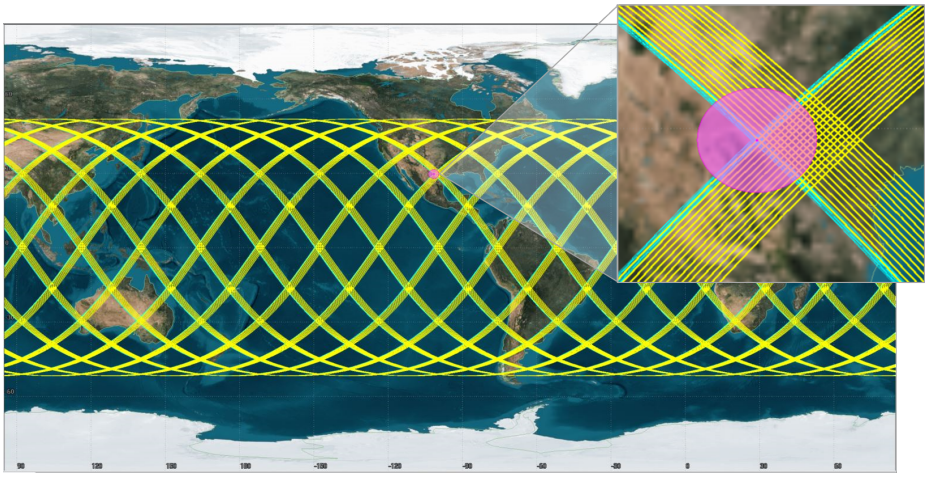

Figure 4-7: Ground tracks resulting from intended altitude (497km, blue) and a potential altitude (494km, yellow) over a 2-week period. A sample ground target is shown in with a 200km diameter area (pink).

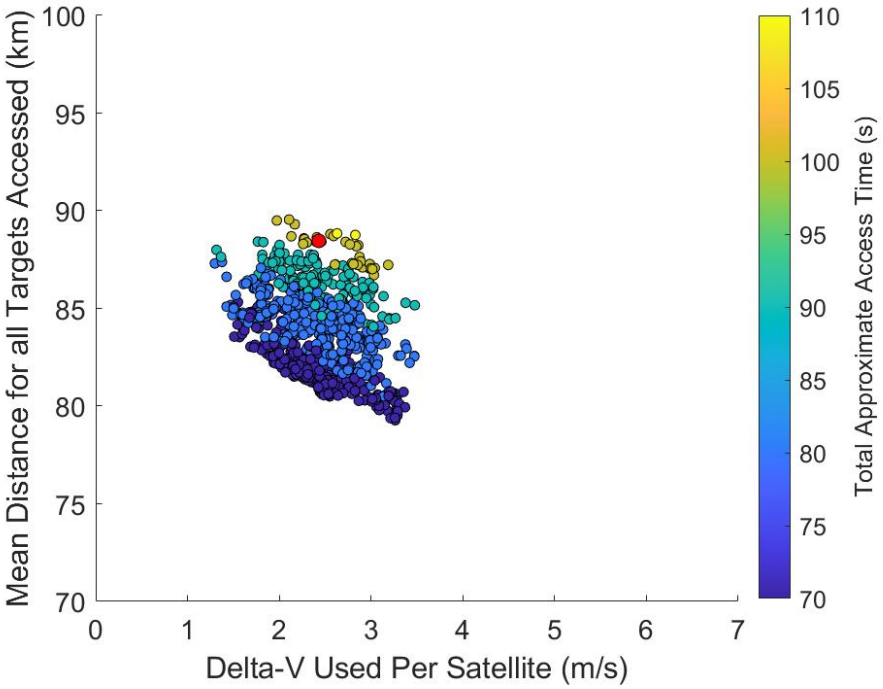

Figure 4-8: Performance of a random sampling of maneuver options with up to 50% error in delta-V magnitude.

When compared to the prior work presented in Chapter 3, it is clear that the low-thrust system would have the delta-V capability to perform the maneuvers required for target viewing the Megi or Harvey case studies. These maneuvers required on the order of 10 m/s per satellite or less, and the propulsion system is capable of up to 1 km/s as shown in Table 4.1. However, precision will be important to conduct these maneuvers as well. The same random sampling of the errors conducted above was performed for a maneuver of similar duration (in the worst case), the errors can result in a corresponding difference in intended delta-V of just below 0.1 m/s, or about 5 % of the intended delta-V. In the context of the majority of the mobile target tracking solutions, this translates to a few kilometers shift in distance to ground target. In the case of the sample solution for a single satellite for Megi as in Table 3.1, this does not significantly change accesses; however, depending on how close the accesses are to the edge of satellite field of view, this could create a larger impact, due to the sharp cutoff in FOV visibility. This can be further extended by evaluating the impact of larger errors. A random sampling of potential error in delta-V, up to 50 % error, results in

the objectives shown in Figure 4-8. This reveals relatively a variety of performance, with the majority of potential results performing worse than the intended results. Depending on the desired performance of a future satellite performing mobile target tracking, one could set ADACS and propulsion system requirements based upon this variety of evaluation. It is likewise important to consider how this system may change with time; low-thrust systems, including FEEP thrusters, tend to have worse performance with time, and initial mission requirements should be determined based upon the end-of-life characteristics to ensure conservative design.

4.5 Summary

Overall, the ROAMS mission effort is vital to place the ReCon concept in the real world, and ensure considerations are made for non-ideal circumstances. The challenges faced by this effort include dealing with these non-ideal circumstances and ensuring maneuvers can be conducted such that the desired ground track and target flyovers can occur despite errors inherent to realistic payload design. As the team continues to develop this concept, they will also face the challenges of working with a hybrid propulsion system on a small Cubesat; this has not yet been tested.

Chapter 5

Conclusions and Future Work

5.1 Summary and Contributions

This thesis has validated and extended work by McGrath et al. [50] in an effort to present an adjusted methodology to track mobile targets. By utilizing a series of low-thrust maneuvers, satellite orbits can be adjusted to obtain improved passes of targets than could otherwise be achieved. This application can allow for better quality and quantity of data gathered over a hurricane's track, which can lead to improved hurricane forecasting; this is especially vital as increasing hurricane intensity continues. For example, the next hurricane season in the US (2021) is projected to include more hurricanes than average, with a nearly 70% chance of a major hurricane to hit the US coastline (in comparison the past century average was a 52% probability of such an event occurring) [32].

Overall, this thesis has validated McGrath's method as described in [50] and has further explored the tradeoffs in this space; the major contribution of this thesis is adding to this concept of adaptive reconfigurable maneuver planning. The method has been extended through the addition of an optimizer; the output from this multi-objective optimization has allowed for an exploration of the solution space in a new way. Key tradeoffs include trading higher delta-V use for closer passes or longer access time. Access time can likewise be traded for closer passes; for example, a few targets could be accessed with closer passes or many targets could be accessed at

further passes. All of these various trades would be worthwhile for a future user to understand.

Additionally, this method has been implemented with multiple satellites. The increase in natural accesses with RAAN-shifted additional satellites has been apparent in both case studies explored. There is a clear sense of diminishing returns on maneuverability as more satellites are added to the constellation; depending on the particular case explored, a greater number of static satellites can be considered equivalent to fewer maneuverable satellites. Finally, the use of forecasted data was considered to create a more realistic model of this mobile-target tracking method. In both case studies explored, the use of multi-objective optimization revealed interesting possible solutions. Both revealed maneuvering options that offered closer accesses or longer access times than otherwise achievable in the non-maneuvering case with low amounts of required delta-V (typically on the order of 10 m/s or less).

Finally, while there have been many prior investigations into potential ReCon applications and uses, the ROAMS mission offers an opportunity to take a step toward actualizing this concept. Potential errors in maneuvers that must be considered were explored, and serve as a jumping off point for future mission planning and operations.

5.2 Future Work

There are a number of areas yet to be explored in this work. One simple area for growth is simply applying this method to a larger swath of hurricane tracks. This could be explored through the tool described at the end of Chapter 3 and the code developed from this work. Other initial conditions can be used with more satellites and different overall mission scenarios. For example, one could explore having multiple satellites in the same plane rather than shifted by RAAN, which can help decrease hypothetical launch costs. Alternatively, one could look into beginning in an RGT orbit, to examine if this has any benefit for these mobile target tracking observations. Further exploration into incorporating uncertainty into the optimization through approaches like MORDM can aid in producing improved results for maneuver planning

with forecasted tracks. It would likewise be worthwhile to gather more information from the potential users of this kind of maneuverable satellite or constellation; considerations from the users including desires for greater number of accesses at particular time in the TC track or simply a closer passes overall would greatly inform how the solution space can be explored in the future and what objectives need to be taken into account. This can help inform what may be best used for optimization, as there are numerous objectives one could use.

There are many areas that are yet to be explored within this topic of mobile-target tracking and applied ReCon. Other adjacent applications such as oil spills and wildfires may benefit from similar explorations as those described in this thesis. These are targets of changing area unlike this thesis' exploration of tracking a TC eye, but the same methodology could be applied to slightly shift SSPs to more readily obtain data for particular vital points within the target area. Further aspects of target viewing such as prioritizing particular solar illumination angles for constructing stereoscopic imagery are currently being explored. Additionally, this work assumes an effective field of view of each satellite but does not take into account the slewing maneuvers that may be required by the satellite. This could be combined with the work presented by Straub [76] for the collection of imagery to prioritize maneuvers based on their ease of access from both a delta-V and a slewing capability perspective.

The ROAMS mission work will be continuing forward, in the effort to create a payload capable of performing maneuvers and bring the research done thus far on ReCon into the real world. This effort will help prove the validity of this concept and derisk a larger mission including multiple satellites, bringing a full ReCon mission one step closer to reality.

Appendix A

Three-Phase Raising and Lowering Equations [46]

Available here: https://doi.org/10.5281/zenodo.4452979 [45]

$$\Delta\Omega_1 = \frac{1}{7560\sqrt{2}AJ_2R_e^2}\cot(i)\csc^7(i)\left\{\frac{1}{(3\gamma-2a_0^2)^3}\sqrt{\frac{\mu}{a_0^3}}a_0\sqrt{\frac{\mu\csc^6(i)a_0^3}{(2\csc^2(i)a_0^2-3J_2R_e^2)^3}}[432\gamma(129-236\cos(2i)+171\cos(4i))a_0^6\right.$$
$$-64(129-236\cos(2i)+171\cos(4i))a_0^8-2268(57-108\cos(2i)+83\cos(4i))\gamma^2a_0^4+2835(43-84\cos(2i)+73\cos(4i))\gamma^3a_0^2$$
$$+102,060(1+3\cos(2i))\gamma^4\sin^2(i)]+\frac{1}{\beta\{[32\mu^2\csc^2(i)a_0^2/\beta^2]-3J_2R_e^2\}^3}4\mu\csc^6(i)\sqrt{\frac{\beta^3}{\mu^2a_0^3}}a_0\sqrt{\frac{\mu^4a_0^3}{\beta^3[-3\gamma+(32\mu^2a_0^2/\beta^2)]^3}}$$
$$-\frac{419,4304\mu^8(129-236\cos(2i)+171\cos(4i))a_0^8}{\beta^8}-\frac{580,608\mu^4(57-108\cos(2i)+83\cos(4i))a_0^4\gamma^2}{\beta^4}$$
$$\left.+\frac{45,360\mu^2(43-84\cos(2i)+73\cos(4i))a_0^2\gamma^3}{\beta^2}+102,060(1+3\cos(2i))\gamma^4\sin^2(i)+\frac{1,769,472\gamma\mu^6(129-236\cos(2i)+171\cos(4i))a_0^6}{\beta^6}\right]\right\}$$

$$\Delta\Omega_2 = -\frac{3\cos(i)J_2R_e^2}{2[(4\mu a_0/\beta)-(3\gamma\beta/8\mu a_0)]^2}\left\{\frac{\sqrt{\mu}[-640a_0^2(\mu a_0/\beta)^{5/2}+96(-2+3\sin^2(i))(\mu a_0/\beta)^{5/2}J_2R_e^2+a_0^{5/2}(320\mu^2a_0^2/\beta^2)+3(2-3\sin^2(i))J_2R_e^2)]}{640Aa_0^{5/2}(\mu a_0/\beta)^{5/2}}\right.$$
$$\left.-\frac{\sqrt{\mu}[-(320\mu^2a_0^2a_3^{5/2}/\beta^2)+3(-2+3\sin^2(i))a_3^{5/2}J_2R_e^2+32(\mu a_0/\beta)^{5/2}(20a_3^2+3(2-3\sin^2(i))J_2R_e^2)]}{640A(\mu a_0/\beta)^{5/2}a_3^{5/2}}+t_t\right\}$$
$$\times\sqrt{\frac{\mu}{[(4\mu a_0/\beta)-(3\gamma\beta/8\mu a_0)]^3}}\left[1+\frac{3\{1-[3\sin^2(i)/2]\}J_2R_e^2}{2(4\mu a_0/\beta)-(3\gamma\beta/8\mu a_0)^2}\right]$$

$$\Delta\Omega_3 = -\frac{1}{7560\sqrt{2}AJ_2R_e^2}\cot(i)\csc^7(i)\left\{\frac{1}{(2\csc^2(i)a_3^2-3J_2R_e^2)^3}\csc^6(i)\sqrt{\frac{\mu}{a_3^3}}a_3\sqrt{\frac{\mu a_3^3}{(-3\gamma+2a_3^2)^3}}[432\gamma(129-236\cos(2i)\right.$$
$$+171\cos(4i))a_3^6-64(129-236\cos(2i)+171\cos(4i))a_3^8-2268(57-108\cos(2i)+83\cos(4i))a_3^4\gamma^2$$
$$+2835(43-84\cos(2i)+73\cos(4i))a_3^2\gamma^3+102,060(1+3\cos(2i))\sin^2(i)\gamma^4]$$
$$+\frac{1}{\beta[3\gamma-(32\mu^2a_0^2/\beta^2)]^3}4\mu\sqrt{\frac{\beta^3}{\mu^2a_0^3}}a_0\sqrt{\frac{\mu^4\csc^6(i)a_0^3}{\beta^3\{[32\mu^2\csc^2(i)a_0^2/\beta^2]-3J_2R_e^2\}^3}}\left[-\frac{4,194,304\mu^8(129-236\cos(2i)+171\cos(4i))a_0^8}{\beta^8}\right.$$
$$-\frac{580,608\mu^4(57-108\cos(2i)+83\cos(4i))a_0^4\gamma^2}{\beta^4}+\frac{45,360\mu^2(43-84\cos(2i)+73\cos(4i))a_0^2\gamma^3}{\beta^2}$$
$$\left.\left.+102,060(1+3\cos(2i))\sin^2(i)\gamma^4+\frac{1,769,472\gamma\mu^6(129-236\cos(2i)+171\cos(4i))a_0^6}{\beta^6}\right]\right\}$$

$$\Delta u_1 = -\frac{1}{918,540\sqrt{2}A\sqrt{(\mu/a_0^3)}a_0^7J_2^6R_e^{12}}\csc^{12}(i)\left[\frac{\mu a_0^3}{(-3\gamma+2a_0^2)^3}\right]^{3/2}\{18,600,435(1+3\cos(2i))\sin^{18}(i)J_2^{10}R_e^{20}$$
$$+229,635\sin^{12}(i)a_0^2J_2^6R_e^{12}[-216\gamma^3+3(1+3\cos(2i))J_2R_e^2(-180\gamma^2+3\gamma\kappa)]-2835\sin^6(i)a_0^4J_2^3R_e^6[3(1+3\cos(2i))J_2R_e^2$$
$$\times(9\zeta\gamma^2+432\kappa\gamma^3-25920\gamma^4)-216\gamma^3(144\gamma^2+3\gamma\kappa)]+2268\sin^4(i)a_0^6J_2^2R_e^4[3(1+3\cos(2i))J_2R_e^2(9\zeta\gamma^2+459\kappa\gamma^3-25920\gamma^4)$$
$$-6\gamma(5184\gamma^4+108\gamma^3\kappa+9\gamma^2\zeta)]\quad+64a_0^{10}[3(1+3\cos(2i))J_2R_e^2(18\zeta\gamma^2+918\kappa\gamma^3-51435\gamma^4)-6\gamma(13203\gamma^4+351\gamma^3\kappa+18\gamma^2\zeta)]$$
$$-432\gamma a_0^8[-6\gamma(10368\gamma^4+351\gamma^3\kappa+18\gamma^2\zeta)+3(1+3\cos(2i))J_2R_e^2(-51435\gamma^4+918\gamma^3\kappa+18\gamma^2\zeta)]\})$$
$$+\frac{1}{3,674,160\sqrt{2}A\mu^7\sqrt{(\beta^3/\mu^2a_0^3)}a_0^7J_2^6R_e^{12}}\beta^7\csc^{12}(i)\left[\frac{\mu^4a_0^3}{\beta^3[-3\gamma+(32\mu^2a_0^2/\beta^2)]^3}\right]^{3/2}\{18,600,435(1+3\cos(2i))\sin^{18}(i)J_2^{10}R_e^{20}$$
$$+\frac{3,674,160\mu^2\sin^{12}(i)a_0^2J_2^6R_e^{12}[-216\gamma^3+3(1+3\cos(2i))J_2R_e^2(-180\gamma^2+3\gamma\kappa)]}{\beta^2}-\frac{1}{\beta^4}725,760\mu^4\sin^6(i)a_0^4J_2^3R_e^6$$
$$[3(1+3\cos(2i))J_2R_e^2(9\zeta\gamma^2+432\kappa\gamma^3-25920\gamma^4)-216\gamma^3(144\gamma^2+3\gamma\kappa)]+\frac{1}{\beta^6}9,289,728\mu^6\sin^4(i)a_0^6J_2^2R_e^4$$
$$[3(1+3\cos(2i))J_2R_e^2(9\zeta\gamma^2+459\kappa\gamma^3-25920\gamma^4)-6\gamma(5184\gamma^4+108\gamma^3\kappa+9\gamma^2\zeta)]+\frac{1}{\beta^{10}}67,108,864\mu^{10}$$
$$a_0^{10}[3(1+3\cos(2i))J_2R_e^2(18\zeta\gamma^2+918\kappa\gamma^3-51435\gamma^4)-6\gamma(13203\gamma^4+351\gamma^3\kappa+18\gamma^2\zeta)]$$
$$\left.-\frac{28,311,552\gamma\mu^8a_0^8[-6\gamma(10368\gamma^4+351\gamma^3\kappa+18\gamma^2\zeta)+3(1+3\cos(2i))J_2R_e^2(-51435\gamma^4+918\gamma^3\kappa+18\gamma^2\zeta)]}{\beta^8}\right\}$$

$$\Delta u_2 = \left\{\sqrt{\frac{\mu}{[-(3\beta\gamma/8\mu a_0)+(4\mu a_0/\beta)]^3}}\left[1+\frac{3[1-(3\sin^2(i)/2)]J_2R_e^2}{2[-(3\beta\gamma/8\mu a_0)+(4\mu a_0/\beta)]^2}\right]\right.$$
$$\left.+\frac{3[2-(5\sin^2(i)/2)]\sqrt{\frac{\mu}{[-(3\beta\gamma/8\mu a_0)+(4\mu a_0/\beta)]^2}}J_2R_e^2(1+(3[1-(3\sin^2(i)/2)]J_2R_e^2/2[-(3\beta\gamma/8\mu a_0)+(4\mu a_0/\beta)]^2))}{2[-(3\beta\gamma/8\mu a_0)+(4\mu a_0/\beta)]^2}\right\}$$
$$\left\{-\frac{1}{2A}\left[-\frac{9\gamma\sqrt{\mu}}{10a_0^{5/2}}+\frac{2\sqrt{\mu}}{\sqrt{a_0}}+\frac{9\gamma\sqrt{\mu}}{320(\mu a_0/\beta)^{5/2}}-\frac{\sqrt{\mu}}{\sqrt{(\mu a_0/\beta)}}+\frac{3\sqrt{\mu}J_2R_e^2}{5a_0^{5/2}}-\frac{3\sqrt{\mu}J_2R_e^2}{160(\mu a_0/\beta)^{5/2}}\right]\right.$$
$$\left.+\frac{1}{2A}\left[-\frac{9\gamma\sqrt{\mu}}{320(\mu a_0/\beta)^{5/2}}+\frac{\sqrt{\mu}}{\sqrt{(\mu a_0/\beta)}}+\frac{9\gamma\sqrt{\mu}}{10a_3^{5/2}}-\frac{2\sqrt{\mu}}{\sqrt{a_3}}+\frac{3\sqrt{\mu}J_2R_e^2}{160(\mu a_0/\beta)^{5/2}}-\frac{3\sqrt{\mu}J_2R_e^2}{5a_3^{5/2}}\right]+t_t\right\}$$

$$
\begin{aligned}
\Delta u_3 = &-\frac{1}{918{,}540\sqrt{2}A\sqrt{(\mu/a_3^3)}a_3^7J_2^6R_e^{12}}\csc^{12}(i)\left[\frac{\mu a_3^3}{(-3\gamma+2a_3^2)^3}\right]^{3/2}\{18{,}600{,}435(1+3\cos(2i))\sin^{18}(i)J_2^{10}R_e^{20}\\
&+229,635\sin^{12}(i)a_3^2J_2^6R_e^{12}[-216\gamma^3+3(1+3\cos(2i))J_2R_e^2(-180\gamma^2+3\gamma\kappa)]\\
&-2835\sin^6(i)a_3^4J_2^3R_e^6[3(1+3\cos(2i))J_2R_e^2(9\zeta\gamma^2+432\kappa\gamma^3-25920\gamma^4)-216\gamma^3(144\gamma^2+3\gamma\kappa)]\\
&+2268\sin^4(i)a_3^6J_2^2R_e^4[3(1+3\cos(2i))J_2R_e^2(9\zeta\gamma^2+459\kappa\gamma^3-25920\gamma^4)-6\gamma(5184\gamma^4+108\gamma^3\kappa+9\gamma^2\zeta)]\\
&+64a_3^{10}(3(1+3\cos(2i))J_2R_e^2(18\zeta\gamma^2+918\kappa\gamma^3-51435\gamma^4)-6\gamma(13203\gamma^4+351\gamma^3\kappa+18\gamma^2\zeta))\\
&-432\gamma a_3^8[-6\gamma(10368\gamma^4+351\gamma^3\kappa+18\gamma^2\zeta)+3(1+3\cos(2i))J_2R_e^2(-51435\gamma^4+918\gamma^3\kappa+18\gamma^2\zeta)]\}\\
&+\frac{1}{3{,}674{,}160\sqrt{2}A\mu^7\sqrt{(\beta^3/\mu^2a_0^3)}a_0^7J_2^6R_e^{12}}\beta^7\csc^{12}(i)\left[\frac{\mu^4a_0^3}{\beta^3[-3\gamma+(32\mu^2a_0^2/\beta^2)]^3}\right]^{3/2}\{18{,}600{,}435(1+3\cos(2i))\sin^{18}(i)J_2^{10}R_e^{20}\\
&+\frac{1}{\beta^2}3{,}674{,}160\mu^2\sin^{12}(i)a_0^2J_2^6R_e^{12}[-216\gamma^3+3(1+3\cos(2i))J_2R_e^2(-180\gamma^2+3\gamma\kappa)]\\
&-\frac{1}{\beta^4}725{,}760\mu^4\sin^6(i)a_0^4J_2^3R_e^6[3(1+3\cos(2i))J_2R_e^2(9\zeta\gamma^2+432\kappa\gamma^3-25920\gamma^4)-216\gamma^3(144\gamma^2+3\gamma\kappa)]\\
&+\frac{1}{\beta^6}9{,}289{,}728\mu^6\sin^4(i)a_0^6J_2^2R_e^4[3(1+3\cos(2i))J_2R_e^2(9\zeta\gamma^2+459\kappa\gamma^3-25920\gamma^4)-6\gamma(5184\gamma^4+108\gamma^3\kappa+9\gamma^2\zeta)]\\
&+\frac{1}{\beta^{10}}67{,}108{,}864\mu^{10}a_0^{10}[3(1+3\cos(2i))J_2R_e^2(18\zeta\gamma^2+918\kappa\gamma^3-51435\gamma^4)-6\gamma(13203\gamma^4+351\gamma^3\kappa+18\gamma^2\zeta)]\\
&-\frac{28{,}311{,}552\gamma\mu^8a_0^8[-6\gamma(10368\gamma^4+351\gamma^3\kappa+18\gamma^2\zeta)+3(1+3\cos(2i))J_2R_e^2(-51435\gamma^4+918\gamma^3\kappa+18\gamma^2\zeta)]}{\beta^8}\}
\end{aligned}
$$

where

$$\gamma = J_2R_e^2\sin^2(i)$$

$$\zeta = 72J_2^2R_e^4\sin^4(i) + 9J_2^2R_e^4\left(7\sin^2(i)-2\right)\left(9\sin^2(i)-4\right)$$

$$\kappa = 3J_2R_e^2\left(7\sin^2(i)-2\right) + 3J_2R_e^2\left(9\sin^2(i)-4\right)$$

and, for the case where the satellite altitude is lowered in Phase 1,

$$\beta = a_0\left(\sqrt{\frac{\mu}{a_3}}+\Delta V_{alt}\right)\left(2\sqrt{\frac{\mu}{a_0}}+\sqrt{\frac{\mu}{a_3}}+\Delta V_{alt}\right)+\mu$$

while for the case in which the satellite altitude is raised in Phase 1

$$\beta = a_0\left(\sqrt{\frac{\mu}{a_3}}-\Delta V_{alt}\right)\left(2\sqrt{\frac{\mu}{a_0}}+\sqrt{\frac{\mu}{a_3}}-\Delta V_{alt}\right)+\mu$$

where

A is the acceleration of the satellite

for lowering maneuvers, a negative acceleration should be used

for raising maneuvers, a positive acceleration should be used

a_0 is the initial mean semi-major axis

a_3 is the final mean semi-major axis

ΔV_{alt} is the total delta-V required for altitude change

i is the inclination of the orbit

μ is the gravitational parameter of the Earth

J_2 is the coefficient of Earth's gravitational zonal harmonic (2nd degree)

R_e is the mean Earth radius

Appendix B

Mobile Target Tracking Code and GUI Framework

The following Github URL contains the code used for the analysis in this thesis, including both code for the graph theory analysis and optimization analysis. A description of the code is included.

https://github.com/sjmorgan6/Mobile-Target-Tracking

Contact: sjmorgan@mit.edu

Bibliography

[1] The Role of Satellite Data in the Forecasting of Hurricane Sandy. 142.

[2] Tropical Storm Harvey in the Gulf of Mexico, August 2017.

[3] Ossama Abdelkhalik and Daniele Mortari. Orbit Design for Ground Surveillance Using Genetic Algorithms. *Journal of Guidance, Control, and Dynamics*, 29(5):1231–1235, September 2006.

[4] Japan Meteorological Agency/Japan, Meteorological Service Of Canada/Environment Canada, European Centre For Medium-Range Weather Forecasts, National Centers For Environmental Prediction/National Weather Service/NOAA/U.S. Department Of Commerce, Meteo-France/France, Korea Meteorological Administration/Republic Of Korea, China Meteorological Administration/China, and Met Office/Ministry Of Defence/United Kingdom. THORPEX Interactive Grand Global Ensemble (TIGGE) Model Tropical Cyclone Track Data, 2008. Artwork Size: 359.960 Gbytes Medium: CXML Pages: 359.960 Gbytes type: dataset.

[5] Jeremy Agte, Olivier de Weck, Jaroslaw Sobieszczanski-Sobieski, Paul Arendsen, Alan Morris, and Martin Spieck. MDO: Assessment and direction for advancement-an opinion of one international group. *Structural and Multidisciplinary Optimization*, 40:17–33, January 2009.

[6] Incorporated Analytical Graphics. Systems Tool Kit 11, 2019.

[7] Systems Tool Kit Analytical Graphics Inc. STK - HPOP: Technical Notes, 2016.

[8] David Arnas, Miles Lifson, Richard Linares, and Martin Avenda. Low Earth Orbit Slotting for Space Traffic Management Using Flower Constellation Theory. In *AIAA Scitech 2020 Forum*, Orlando, FL, January 2020. American Institute of Aeronautics and Astronautics.

[9] E.P.W. Attema, G. Duchossois, and G. Kohlhammer. ERS-lI2 SAR Land Applications: Overview and Main Results. In Institute of Electrical and Electronics Engineers, editor, *IGARSS '98: sensing and managing the environment: 1998 IEEE International Geoscience and Remote Sensing Symposium proceedings: Seattle, 6-10 July, 1998, Sheraton Seattle, Seattle, WA, USA*. IEEE, Piscataway, N.J, 1998. Meeting Name: International Geoscience and Remote Sensing Symposium.

[10] Erin Bartholomew and Jan H. Kwakkel. On considering robustness in the search phase of Robust Decision Making: A comparison of Many-Objective Robust Decision Making, multi-scenario Many-Objective Robust Decision Making, and Many Objective Robust Optimization. *Environmental Modelling & Software*, 127:104699, May 2020.

[11] Mingyu Bi, Tim Li, Melinda Peng, and Xinyong Shen. Interactions between Typhoon Megi (2010) and a Low-Frequency Monsoon Gyre. *Journal of the Atmospheric Sciences*, 72(7):2682–2702, July 2015.

[12] J. Blank and K. Deb. Pymoo: Multi-Objective Optimization in Python. *IEEE Access*, 8:89497–89509, 2020.

[13] Daniel Casanova, Martin Avendano, and Daniele Mortari. Optimizing Flower Constellations for Global Coverage. In *AIAA/AAS Astrodynamics Specialist Conference*, Minneapolis, Minnesota, August 2012. American Institute of Aeronautics and Astronautics.

[14] The Aerospace Corporation. Propulsion Technologies Survey: Micro, Nano, Pico, and Cube-Satellites (CubeSat), October 2018 For Public Release, Version 1.11 Approved for public release. OTR 2019-00005., 2018.

[15] National Research Council. *Orbital Debris: A Technical Assessment*. National Academies Press, Washington, D.C., June 1995. Pages: 4765.

[16] Howard D. Curtis. *Orbital mechanics for engineering students*. Elsevier Aerospace engineering series. Elsevier/Butterworth-Heinemann, Amsterdam, 1. ed., reprinted edition, 2008. OCLC: 552116374.

[17] Jeremy John Davis. *Constellation Reconfiguration: Tools and Analysis*. Thesis, October 2011. Accepted: 2011-10-21T22:02:59Z.

[18] Olivier de Weck, L., Maha Haji, N., and Johannes Norheim, J. MIT Course Notes, 16.888/EM.428/IDS.338 Multidisciplinary Design Optimization, 2020.

[19] Olivier L. de Weck, Richard de Neufville, and Mathieu Chaize. Staged Deployment of Communications Satellite Constellations in Low Earth Orbit. *Journal of Aerospace Computing, Information, and Communication*, 1(3):119–136, March 2004.

[20] Mark DeMaria, John A. Knaff, and Raymond Zehr. Assessing Hurricane Intensity Using Satellites. In John Qu, Alfred Powell, and M.V.K. Sivakumar, editors, *Satellite-based Applications on Climate Change*. Springer Netherlands, Dordrecht, 2013.

[21] E. W. Dijkstra. A note on two problems in connexion with graphs. *Numerische Mathematik*, 1:269–271, December 1959.

[22] Maxx Dilley. *Natural disaster hotspots: a global risk analysis*. Number no. 5 in Disaster risk management series. World Bank, Washington, D.C, 2005. OCLC: ocm56834544.

[23] ESA. Automating collision avoidance, October 2019.

[24] Matthew P. Ferringer. *GENERAL FRAMEWORK FOR THE RECONFIGURATION OF SATELLITE CONSTELLATIONS*. Doctor of Philosophy, The Pennsylvania State University, 2009.

[25] Matthew P. Ferringer and David B. Spencer. Satellite Constellation Design Tradeoffs Using Multiple-Objective Evolutionary Computation. *Journal of Spacecraft and Rockets*, 43(6):1404–1411, November 2006.

[26] Aric Hagberg, Dan Schult, and Pieter Swart. NetworkX — NetworkX documentation, 2021.

[27] Xiangyue He, Haiyang Li, Luyi Yang, and Jian Zhao. Reconfigurable Satellite Constellation Design for Disaster Monitoring Using Physical Programming. *International Journal of Aerospace Engineering*, 2020:e8813685, September 2020. Publisher: Hindawi.

[28] Dan Hegel. FlexBus – A 6U Cubesat Platform for Any Mission, 2016.

[29] SeungBum Hong, Hyungho Na, and Jaemyung Ahn. Assessment of architectural options for a dual-mode disaster monitoring constellation supported by on-orbit propellant depots. *Proceedings of the Institution of Mechanical Engineers, Part G: Journal of Aerospace Engineering*, 228(11):2108–2122, September 2014. Publisher: IMECHE.

[30] NASA CubeSat Launch Initiative. CubeSat 101: Basic Concepts and Processes for First-Time CubeSat Developers, October 2017.

[31] Asanobu Kitamoto. *Digital Typhoon: Typhoon 201013 (MEGI) - Detailed Track Information*. National Institute of Informatics (NII), December 2012. Publication Title: Digital Typhoon.

[32] Philip J. Klotzbach, Michael M. Bell, and Jhordanne Jones. EXTENDED RANGE FORECAST OF ATLANTIC SEASONAL HURRICANE ACTIVITY AND LANDFALL STRIKE PROBABILITY FOR 2021. *Department of Atmospheric Science, Colorado State University*, April 2021.

[33] Thomas Knutson, Suzana J. Camargo, Johnny C. L. Chan, Kerry Emanuel, Chang-Hoi Ho, James Kossin, Mrutyunjay Mohapatra, Masaki Satoh, Masato Sugi, Kevin Walsh, and Liguang Wu. Tropical Cyclones and Climate Change Assessment: Part I: Detection and Attribution. *Bulletin of the American Meteorological Society*, 100(10):1987 – 2007, October 2019. Place: Boston MA, USA Publisher: American Meteorological Society.

[34] Dong Shan Ko, Shenn-Yu Chao, Chun-Chieh Wu, and I.-I. Lin. Impacts of typhoon megi (2010) on the South China Sea. *Journal of Geophysical Research: Oceans*, 119(7):4474–4489, 2014. _eprint: https://agupubs.onlinelibrary.wiley.com/doi/pdf/10.1002/2013JC009785.

[35] David Krejci, Alexander Reissner, Bernhard Seifert, David Jelem, Thomas Hörbe, Florin Plesescu, Pete Friedhoff, and Steve Lai. DEMONSTRATION OF THE IFM NANO FEEP THRUSTER IN LOW EARTH ORBIT. 2018.

[36] Francois Laporte and Eloy Sasot. Operational Management of Collision Risks for LEO Satellites at CNES. In *SpaceOps 2008 Conference*, Heidelberg, Germany, May 2008. American Institute of Aeronautics and Astronautics.

[37] S. Le May, S. Gehly, B.A. Carter, and S. Flegel. Space debris collision probability analysis for proposed global broadband constellations. *Acta Astronautica*, 151:445–455, October 2018.

[38] Jacqueline Le Moigne, John Carl Adams, and Sreeja Nag. A New Taxonomy for Distributed Spacecraft Missions. *IEEE Journal of Selected Topics in Applied Earth Observations and Remote Sensing*, 13:872–883, 2020.

[39] Robert S. Legge, Jr. *Optimization and valuation of recongurable satellite constellations under uncertainty*. Thesis: Ph. D., Massachusetts Institute of Technology, 2014.

[40] Kristina Lemmer. Propulsion for CubeSats. *Acta Astronautica*, 134:231–243, May 2017.

[41] J.-C Liou, A K Anilkumar, B Bastida, T Hanada, H Krag, H Lewis, M X J Raj, M M Rao, A Rossi, and R K Sharma. STABILITY OF THE FUTURE LEO ENVIRONMENT – AN IADC COMPARISON STUDY. 2013. Publisher: Unpublished.

[42] J.-C. Liou, N.L. Johnson, and N.M. Hill. Controlling the growth of future LEO debris populations with active debris removal. *Acta Astronautica*, 66(5-6):648–653, March 2010.

[43] Becky Little. How the Galveston Hurricane of 1900 Became the Deadliest U.S. Natural Disaster, April 2019.

[44] Ciara Mcgrath and Malcolm Macdonald. IAC-15.C1.9.4 Design of a Reconfigurable Satellite Constellation. 2015.

[45] Ciara McGrath and Malcolm Macdonald. Equations for General Perturbation Method for Satellite Constellation Reconfiguration Using Low-Thrust Maneuvers. July 2019. Publisher: Zenodo.

[46] Ciara Mcgrath and Malcolm Macdonald. General Perturbation Method for Satellite Constellation Reconfiguration Using Low-Thrust Maneuvers. *Journal of Guidance, Control, and Dynamics*, 42:1–17, July 2019.

[47] Ciara McGrath, Malcolm Macdonald, Paulo Lozano, David Miller, and David Krejci. Applications of responsive small satellites with MIT TILE electrospray propulsion. page 14, GBR, October 2017. University of Strathclyde Technology & Innovation Centre.

[48] Ciara N. McGrath. *Analytical Methods for Satellite Constellation Reconfiguration and Reconnaissance using Low-Thrust Manoeuvres*. Doctor of Philosophy (PhD) in Mechanical and Aerospace Engineering, University of Strathclyde, 2018.

[49] Ciara N. McGrath, Ruaridh A. Clark, and Malcolm Macdonald. Novel concept of satellite manoeuvre planning using graph theoretical techniques. *Advances in Space Research*, June 2020.

[50] Ciara N. McGrath, Ruaridh A. Clark, Astrid Werkmeister, and Malcolm Macdonald. Small satellite operations planning for agile disaster response using graph theoretical techniques. Washington, D.C., October 2019.

[51] Christopher H. McLean. Green Propellant Infusion Mission: Program Construct, Technology Development, and Mission Results. In *AIAA Propulsion and Energy 2020 Forum*, VIRTUAL EVENT, August 2020. American Institute of Aeronautics and Astronautics.

[52] C. McPhail, H. R. Maier, J. H. Kwakkel, M. Giuliani, A. Castelletti, and S. Westra. Robustness Metrics: How Are They Calculated, When Should They Be Used and Why Do They Give Different Results? *Earth's Future*, 6(2):169–191, February 2018.

[53] Sarah J. Morgan, Ciara McGrath, and Olivier L. De Weck. Mobile Target Tracking Using a Reconfigurable Low Earth Orbit Constellation. In *ASCEND 2020*, Virtual Event, November 2020. American Institute of Aeronautics and Astronautics.

[54] Mary Morris and Christopher S. Ruf. Determining Tropical Cyclone Surface Wind Speed Structure and Intensity with the CYGNSS Satellite Constellation. *Journal of Applied Meteorology and Climatology*, 56(7):1847 – 1865, July 2017. Place: Boston MA, USA Publisher: American Meteorological Society.

[55] D. Mortari and M.P. Wilkins. Flower constellation set theory. Part I: Compatibility and phasing. *IEEE Transactions on Aerospace and Electronic Systems*, 44(3):953–962, July 2008.

[56] Isabelle Nann, Dario Izzo, and Roger Walker. Reconfigurable Mars Constellation for Radio Occultation Measurements and Navigation, 2005.

[57] NOAA. HURDAT Re-analysis: Hurricane Database, 2019.

[58] Sung Paek, Sangtae Kim, and Olivier de Weck. Optimization of Reconfigurable Satellite Constellations Using Simulated Annealing and Genetic Algorithm. *Sensors*, 19(4):765, February 2019.

[59] Sung Wook Paek. *Reconfigurable satellite constellations for geo-spatially adaptive Earth observation missions*. Thesis: S.M., Massachusetts Institute of Technology, 2012.

[60] Sung Wook Paek, Olivier de Weck, and M.W. Smith. Concurrent design optimization of earth observation Satellites and reconfigurable constellations. *Journal of the British Interplanetary Society*, 70:19–35, 2017.

[61] S.W. Paek, S. Kim, L. Kronig, and O. de Weck. Sun-synchronous repeat ground tracks and other useful orbits for future space missions. *The Aeronautical Journal*, 124(1276):917–939, June 2020.

[62] Henry Potter, Steven F. DiMarco, and Anthony H. Knap. Tropical Cyclone Heat Potential and the Rapid Intensification of Hurricane Harvey in the Texas Bight. *Journal of Geophysical Research: Oceans*, 124(4):2440–2451, 2019. _eprint: https://agupubs.onlinelibrary.wiley.com/doi/pdf/10.1029/2018JC014776.

[63] M. Pritt. Deep Learning for Recognizing Mobile Targets in Satellite Imagery. In *2018 IEEE Applied Imagery Pattern Recognition Workshop (AIPR)*, pages 1–7, 2018.

[64] John E. Prussing and Bruce A. Conway. *Orbital mechanics*. Oxford University Press, New York, second edition edition, 2013.

[65] Edward N. Rappaport, James L. Franklin, Lixion A. Avila, Stephen R. Baig, John L. Beven, Eric S. Blake, Christopher A. Burr, Jiann-Gwo Jiing, Christopher A. Juckins, Richard D. Knabb, Christopher W. Landsea, Michelle Mainelli, Max Mayfield, Colin J. McAdie, Richard J. Pasch, Christopher Sisko, Stacy R. Stewart, and Ahsha N. Tribble. Advances and Challenges at the National Hurricane Center. *Weather and Forecasting*, 24(2):395–419, April 2009.

[66] Kathleen Riesing and Kerri Cahoy. Orbit Determination from Two Line Element Sets of ISS-Deployed CubeSats. In *SSC15-VIII-5*, Utah State University, UT, US, 2015.

[67] Aerojet Rocketdyne. MPS-130 Datasheet.

[68] C. Ruf, M. Unwin, J. Dickinson, R. Rose, D. Rose, M. Vincent, and A. Lyons. CYGNSS: Enabling the Future of Hurricane Prediction [Remote Sensing Satellites]. *IEEE Geoscience and Remote Sensing Magazine*, 1(2):52–67, 2013.

[69] Christopher Ruf, Shakeel Asharaf, Rajeswari Balasubramaniam, Scott Gleason, Timothy Lang, Darren McKague, Dorina Twigg, and Duane Waliser. In-Orbit Performance of the Constellation of CYGNSS Hurricane Satellites. *Bulletin of the American Meteorological Society*, 100(10):2009–2023, October 2019.

[70] Mario Rüttgers, Sangseung Lee, Soohwan Jeon, and Donghyun You. Prediction of a typhoon track using a generative adversarial network and satellite images. *Scientific Reports*, 9(1):6057, April 2019.

[71] Sudipta Sarkar, Ramesh P. Singh, and Akshansha Chauhan. Anomalous changes in meteorological parameters along the track of 2017 Hurricane Harvey. *Remote Sensing Letters*, 9(5):487–496, February 2018.

[72] M. Schröder, Christopher Womack, and Amelia Gagnon. SSC20-VII-02 Maneuver Planning for Demonstration of a Low-Thrust Electric Propulsion System. 2020.

[73] Lake A. Singh, Jose J. Guzman, Christopher G. Lorenz, Stephanie L. Martin, Christopher L. Ranieri, Demyan V. Lantukh, and Gregory Fruth. Investigating the Impacts of Electric Propulsion on Constellation Replenishment Using a Many-Objective Evolutionary Approach IEPC-2017-127. Georgia Institute of Technology, October 2017.

[74] Adam B. Smith. U.S. Billion-dollar Weather and Climate Disasters, 1980 - present (NCEI Accession 0209268), 2020. type: dataset.

[75] Alexander Smith. Assessment of TLE-based Orbit Determination and Prediction for Cubesats, 2019.

[76] Alexandra Straub. *Expanded Tradespace Analysis and Operational Considerations for Reconfigurable Satellite Constellations*. PhD thesis, May 2020.

[77] Enpulsion Spacecraft Technology. Enpulsion Spacecraft Technology Product Portfolio October 2020, 2020.

[78] UNICEF. UNICEF responds to the devastation of Typhoon "Juan" (Megi) in north eastern province of Isabela, Philippines, October 2010.

[79] Joost Vanreusel. Launching a CubeSat: Rules, laws, and best practice. In *Cubesat Handbook*, pages 391–414. Elsevier, 2021.

[80] C. Velden, J. Simpson, W. Timothy Liu, J. Hawkins, K. Brueske, and R. Anthes. The Burgeoning Role of Weather Satellites. In Robert H. Simpson, Richard A. Anthes, and Michael Garstang, editors, *Hurricane! coping with disaster: progress and challenges since Galveston, 1900*. American Geophysical Union, Washington, DC, 2003.

[81] Thyrso Villela, Cesar A. Costa, Alessandra M. Brandão, Fernando T. Bueno, and Rodrigo Leonardi. Towards the Thousandth CubeSat: A Statistical Overview. *International Journal of Aerospace Engineering*, 2019:1–13, January 2019.

[82] Warren E. Walker, Robert J. Lempert, and Jan H. Kwakkel. Deep Uncertainty. In Saul I. Gass and Michael C. Fu, editors, *Encyclopedia of Operations Research and Management Science*, pages 395–402. Springer US, Boston, MA, 2013.

[83] Hui Wang and Yuqing Wang. A Numerical Study of Typhoon Megi (2010). Part I: Rapid Intensification. *Monthly Weather Review*, 142(1):29–48, January 2014. Publisher: American Meteorological Society Section: Monthly Weather Review.

[84] Astrid Werkmeister, Hans Graber, Ralph Foster, and Roland Romeiser. Tropical cyclone boundary layer rolls derived from SAR. In *2015 IEEE International Geoscience and Remote Sensing Symposium (IGARSS)*, pages 2526–2528, Milan, Italy, July 2015. IEEE.

[85] J. Wertz. Coverage, Responsiveness, and Accessibility for Various "Responsive Orbits". 2005.

[86] James Richard Wertz, David F. Everett, and Jeffery John Puschell, editors. *Space mission engineering: the new SMAD*. Number v. 28 in Space technology library. Microcosm Press : Sold and distributed worldwide by Microcosm Astronautics Books, Hawthorne, CA, 2011. OCLC: ocn747731146.

[87] H. E. Willoughby, E. N. Rappaport, and F. D. Marks. Hurricane Forecasting: The State of the Art. *Natural Hazards Review*, 8(3):45–49, August 2007.